UNIVERSITÀ ITALO FRANCESE

THESIS IN JOINT-SUPERVISION

with

UNIVERSITY OF LIMOGES

PhD school in Science and Engineering in Materials, Mechanics, Energy and Aeronautics

and

UNIVERSITY OF MODENA AND REGGIO EMILIA

PhD school in Multiscale Modelling, Computational Simulations and Characterization in Material and Life Sciences, XXV cylce

Director: Maria Cristina Menziani

presented by

Andrea CATTINI

in partial fulfillment of the requirements for the degree of

DOCTOR OF PHILOSOPHY

in: *Multiscale Modelling, Computational Simulations and Characterization in Material and Life Sciences,* and *Ceramic Materials and Surface Treatments*

COATINGS OF BIOACTIVE GLASSES AND HYDROXYAPATITE AND THEIR PROPERTIES

Discussion: February 22, 2013

Advisors:	Valeria CANNILLO:	Professor, DIEF, Modena
	Lech PAWŁOWSKI:	Professor, SPTCS, Limoges
Examinators:	Alain DENOIRJEAN:	Director of Research, SPTCS, Limoges
	Luca LUSVARGHI:	Researcher, DIEF, Modena
Reviewers:	Igor Yu SMUROV:	Professor, ENISE, Saint-Etienne
	Didier CHICOT:	Professor, USTL, LML, Lille
	Thomas LAMPKE:	Professor, TU, Chemnitz

UNIVERSITÀ ITALO FRANCESE

THÈSE EN CO-TUTELE

avec

UNIVERSITÉ DE LIMOGES

Ecole Doctorale de Sciences et Ingénierie en Matériaux, Mécanique, Energétique et Aéronautique

et

UNIVERSITÉ DE MODENA ET REGGIO EMILIA

Ecole Doctorale de Modélisation et Simulation Multi-Echelle et de Caractérisation pour la Sciences des Matériaux et de la Vie, XXV cylce

Directeur: Maria Cristina Menziani

présentée par

Andrea CATTINI

pour obtenir le grade de

DOCTEUR

en: *Matériaux Céramiques et Traitements de Surface*

REVÊTEMENTS DE VERRES BIOACTIFS ET D'HYDROXYAPATITE ET LEURS PROPRIÉTÉS

Soutenance: 22 Février 2013

Directeurs de thèse:	Valeria CANNILLO:	Professeur, DIEF, Modena
	Lech PAWŁOWSKI:	Professeur, SPTCS, Limoges
Examinateurs:	Alain DENOIRJEAN:	Directeur de Recherche, SPTCS, Limoges
	Luca LUSVARGHI:	Chercheur, DIEF, Modena
Rapporteurs:	Igor Yu SMUROV:	Professeur, ENISE, Saint-Etienne
	Didier CHICOT:	Professeur, USTL, LML, Lille
	Thomas LAMPKE:	Professeur, TU, Chemnitz

UNIVERSITÀ ITALO FRANCESE

TESI IN CO-TUTELA

tra

UNIVERSITÀ DI LIMOGES

Scuola di dottorato in Scienza ed Ingegneria in Materiali, Meccanica, Energia ed Aereonautica

e

UNIVERSITÀ DEGLI STUDI DI MODENA E REGGIO EMILIA

Scuola di dottorato di ricerca in Modellistica, simulazione computazionale e caratterizzazione multiscala per le scienze dei materiali e della vita, XXV ciclo

Direttore: Maria Cristina Menziani

presentata da

Andrea CATTINI

per conseguimento del titolo di

DOTTORE DI RICERCA

in: *Modellistica, simulazione computazionale e caratterizzazione multiscala per le scienze dei materiali e della vita*

PRODUZIONE E CARATTERIZZAZIONE DI RIVESTIMENTI IN BIOVETRI E IDROSSIAPATITE

Discussione: 22 Febbraio 2013

Relatori:	Valeria CANNILLO:	Professore, DIEF, Modena
	Lech PAWŁOWSKI:	Professore, SPTCS, Limoges
Esaminatori:	Alain DENOIRJEAN:	Direttore di Ricerca, SPTCS, Limoges
	Luca LUSVARGHI:	Ricercatore, DIEF, Modena
Revisori:	Igor Yu SMUROV:	Professore, ENISE, Saint-Etienne
	Didier CHICOT:	Professore, USTL, LML, Lille
	Thomas LAMPKE:	Professore, TU, Chemnitz

Acknowledgement

Foremost, I would like to express my sincere gratitude to my advisors Prof. Valeria Cannillo and Prof. Lech Pawłowski for their guide and continuous support. They both gave me important advice and shared with me their vast knowledge.

Besides my advisors, I'd like to thank all the numerous colleagues who have helped me over these years.

My sincere thanks goes to Dr. Leszek Łatka and Alain Grimaud, they taught me all the practical aspects of plasma spraying.

I'd like to thank all the members of Axe 2 in SPCTS for their willingness. In particular, I thank Geoffroy Rivaud and Dr. Simon Goutier for their continous help in the laboratory. Moreover I'd like to apologize to them for all the times I bothered them. I also thank all the labmates who helped me during the coatings production: Joanna, Achraf, Denys, and particularly Pablo.

I'd like to thank all the members of DIMA, especially Dr. Giovanni Bolelli and Dr. Luca Lusvarghi for many fruitful discussions. A special thanks to Dr. Antonella Sola and Dr. Devis Bellucci, they always pushed me to work better, and they helped me so much with a huge amount of corrections. I also thank my office mate, Elena, for many suggestions, but mainly for putting up with me during these years.

A dutiful thanks to the Università Italo-Francese, which has incurred great part of the Italy-France mobility costs through the Capitolo II of “Bando Vinci 2011”.

Finally I thank all the friends with whom I spent good times in the last years. I would like to thank especially my old friends, but also all the friends I've met along the way.

Last but not the least, I thank my family: my parents for supporting me throughout my life, and my brother on which I can always count.

Index:

List of figures:

List of tables:

Abstract

Over the last decades, biomedical research has acquired a growing importance. Moreover, the progressive population ageing, with related musculoskeletal disorders, is driving the development of innovative materials for bone implants. Though the production of prosthetic implants is nowadays a mature and well-established practice, the scientific research is constantly evolving with the aim of improving the reliability and effectiveness of the available prostheses, thus increasing their life expectancy.

The purpose of the present study is the production of new-generation coatings to support the adhesion between prosthetic implants and bone tissues. Bioactive materials, which are ones that elicit a specific biological response at their interface, were selected as coating materials.

The new coatings were produced with hydroxyapatite and/or bioactive glass, two bioactive materials which are able to bond to bone. In particular, hydroxyapatite is a ceramic material whose composition and structure are very similar to those of the mineral component of bones. Moreover hydroxyapatite is highly stable in biological environment. For these reasons, this ceramic is currently the most widely used bioactive material to produce coatings for orthopaedic implants. Bioactive glasses, instead, are special glasses which exhibit a great bioactivity.

Unfortunately, the use of hydroxyapatite and bioactive glasses in structural applications is limited by their mechanical properties, in particular their brittleness. To solve this problem, hydroxyapatite and bioactive glasses can be successfully used as coatings on metal prostheses. In this way the bone-bonding ability of bioactive materials is combined with the high mechanical properties of metals.

Plasma spray is an established technique to produce bioactive coatings. In this study, a recent evolution of this process has been used i.e. the suspension plasma spray. The main difference between the new technique and the conventional one resides in the feedstock materials. In fact, the new process uses suspensions instead of dry powders which makes it possible to process sub-micrometric or nanometric particles and therefore to obtain coatings with an extremely fine and controlled microstructure.

In the first part of this work, bulk bioactive glasses with different compositions were studied in order to select the most promising one for the coatings production. Specifically, a study to compare their *in vitro* bioactivity was carried out. Following, the deposition parameters to produce bioactive glass coatings were optimized. The coatings were characterized from a

microstructural and mechanical point of view; also preliminary *in vitro* tests were carried out to assess the reactivity in physiological media.

Then, a bioactive glass topcoat was applied on traditional hydroxyapatite coatings to increase their bioactivity. Since the topcoat showed the ability to promote coatings *in vitro* reactivity, the study progressed with the realization of specific composite systems using the hydroxyapatite and bioactive glasses.

Accordingly, composite bioactive glass/hydroxyapatite coatings were produced and analysed. Three different microstructures were produced: conventional composite coatings (the constituent phases were evenly and randomly distributed); bi-layer coatings (the coatings included a hydroxyapatite bond coat and a bioactive glass topcoat); functionally graded coatings (the composition gradually changed from pure hydroxyapatite, in contact with the metal substrate, to pure bioactive glass, on the working surface). The basic goal was to merge the high bioactivity of bioactive glasses with the stability of hydroxyapatite.

On account of the results of an introductory characterization, the graded structure was selected for further optimizations. New graded coatings were produced and analysed; in particular, their microstructure and mechanical properties were investigated before and after *in vitro* tests. In this way, both the bioactivity and the stability of the coatings could be estimated.

Résumé

Dans les dernières décennies, la recherche biomédicale est devenue de plus en plus important. En outre, le vieillissement progressif de la population, avec leurs troubles musculo-squelettiques, est le moteur du développement de matériaux innovants pour les implants osseux. Bien que la production d'implants prothétiques est aujourd'hui une pratique éprouvée et bien établie, la recherche scientifique est en constante évolution dans le but d'améliorer la fiabilité et l'efficacité des prothèses disponibles, augmentant ainsi leur espérance de vie.

Le but de ce travail est la production de revêtements de nouvelle génération pour les prothèses dont l'objectif est l'augmentation de l'adhérence entre les implants prothétiques et les tissus osseux. Pour la réalisation des revêtements des matériaux bioactifs ont été pris en considération, nommément matériel spéciaux qui provoquent une réponse biologique spécifique à leur interface.

Les nouveaux revêtements ont été produits avec l'hydroxyapatite et/ou du bioverre, deux matériaux bioactifs qui sont capables de se lier avec les tissus osseux. En particulier, l'hydroxyapatite est un matériau céramique dont la composition et la structure sont très semblables à ceux de la fraction minérale des os.

Les bioverre sont des verres spéciaux qui sont caractérisés par une bioactivité tres élevée.

Malheureusement, l'utilisation d'hydroxyapatite et bioverre dans des applications structurelles est limitée par leurs propriétés mécaniques, notamment de leur fragilité. Pour résoudre ce problème, bioverres et hydroxyapatite peuvent être appliqués comme revêtements sur des prothèses métalliques; ainsi la capacité de se lier à les tissus osseux des matériaux bioactifs est combinée à les élevées propriétés mécaniques typiques des métaux.

Le procédé de production actuellement le plus utilisé pour le revêtements bioactifs est la projection au plasma. Dans cette étude une récente évolution de cette technique a été utilisée: projection au plasma de suspension. La différence entre cette nouvelle technique et la projection au plasma classique réside dans les matières premières utilisées. En fait, le nouveau procédé utilise des suspensions au lieu de poudres sèches qui permet de traiter les particules sub-micrométriques ou nanométriques et donc d'obtenir des revêtements avec une microstructure très fine et contrôlée.

Dans la première partie de ce travail des bioverres ayant des compositions différentes ont été étudiés afin de choisir le plus prometteur pour la production de revêtements. Plus précisément, une étude visant à comparer leur bioactivité *in vitro* en a été réalisée.

Après, les paramètres de dépôt pour produire des revêtements de bioverre ont été optimisés. Les revêtements ont été caractérisées d'un point de vue microstructurale et mécanique; également, des tests préliminaire *in vitro* ont été réalisées afin d'évaluer la réactivité des revêtements dans les liquide physiologiques.

Ensuite, une couche superficiel en bioverre a été appliqué sur des revêtements traditionnels d'hydroxyapatite pour augmenter leur bioactivité. Depuis cette couche a montré la capacité de promouvoir la réactivité *in vitro* des revêtements, l'étude a évolué avec la réalisation de systèmes composites qui ont été produits avec bioverres et hydroxyapatite.

Par conséquent, des revêtements composites bioverre/hydroxyapatite ont été produites et analysées. Trois différentes microstructures ont été produits: revêtements composites conventionnels (les phases constitutives sont réparties de façon aléatoire d'une manière uniforme); revêtements bicouches (composée d'une couche d'hydroxyapatite et d'une couche de surface en bioverre); revêtements avec un gradient de composition (dans laquelle la composition varie graduellement à partir de l'hydroxyapatite pure, en contact avec le substrat métallique, jusqu'à bioverre pur, sur la surface extérieure). L'objectif de ces systèmes est de joindre l' élevé bioactivité du bioverre avec la stabilité de l'hydroxyapatite.

Les échantillons ainsi obtenus ont été caractérisés, et le revêtement à gradient a été choisi pour une optimisation ultérieure. Des nouveaux revêtements à gradient ont été produites et analysées et, en particulier, la leur microstructure et les leur propriétés mécaniques ont été analysés avant et après les tests *in vitro*. De cette façon, la bioactivité et aussi la stabilité des échantillons ont été évalués.

Riassunto

Negli ultimi decenni la ricerca in campo biomedico ha acquisito un'importanza sempre maggiore. Inoltre, il progressivo invecchiamento della popolazione, con i relativi disturbi muscolo-scheletrici, sta guidando lo sviluppo di materiali innovativi per impianti ossei. Nonostante la realizzazione di impianti protesici sia una pratica già matura e consolidata, la ricerca è in continua evoluzione con lo scopo di aumentare sia la compatibilità delle protesi con i tessuti ospiti che l'aspettativa di vita delle protesi stesse.

Scopo di questo lavoro di tesi è la produzione di rivestimenti per protesi di nuova generazione che siano in grado di aumentare l'adesione tra impianti protesici ed i tessuti ossei. Per la realizzazione dei rivestimenti sono stati presi in considerazione dei materiali bioattivi, ossia speciali materiali in grado sia di favorire la formazione di nuovi tessuti ossei sia di legarsi con essi. In particolare, questo studio si è occupato di due tipologie di materiali bioattivi: l'idrossiapatite ed i biovetri. L'idrossiapatite è il materiale ceramico bioattivo attualmente più utilizzato in campo biomedico, sia per la sua composizione molto simile a quella della componente minerale delle ossa, sia per la sua elevata stabilità in ambiente biologico. I biovetri sono invece vetri speciali caratterizzati da una elevatissima bioattività.

Purtroppo l'utilizzo di l'idrossiapatite e biovetri in impieghi strutturali è precluso dalle loro proprietà meccaniche, in particolare dalla loro fragilità. Una soluzione a questo problema è l'utilizzo dei materiali bioattivi per la realizzazione di rivestimenti su protesi metalliche; in tal modo la peculiare capacità di legarsi ai tessuti ossei dei materiali bioattivi viene abbinata alle elevate proprietà meccaniche tipiche dei metalli. Il metodo di produzione di rivestimenti bioattivi attualmente più utilizzato è il plasma spray, in particolare in questo studio si è utilizzato una recente evoluzione di questa tecnica: il plasma spray da sospensione. La differenza tra questa tecnica ed il tradizionale plasma spray risiede nell'utilizzo di materie prime in forma di sospensione invece che di polveri secche; ciò consente di processare particelle sub-micrometriche o nanometriche e quindi di ottenere rivestimenti dalla microstruttura più fine.

Nella prima parte di questo lavoro si sono studiati dei biovetri massivi di diversa composizione, al fine di selezionare le composizioni più promettenti per la produzione di rivestimenti. Nello specifico si è effettuato uno studio *in vitro* per comparare la bioattività dei diversi biovetri. In seguito sono stati studiati i parametri di deposizione ottimali per la

produzione di rivestimenti in biovetro. I rivestimenti sono poi stati caratterizzati da un punto di vista microstrutturale, meccanico e ne è stata testata la bioattività.

In seguito, il vetro bioattivo è stata utilizzato per produrre un *topcoat* su tradizionali rivestimenti di idrossiapatite allo scopo di aumentarne la bioattività. Poiché il *topcoat* ha mostrato la capacità di promuovere la reattività *in vitro* dei rivestimenti, si è poi proceduto producendo dei rivestimenti con strutture composite in biovetro e idrossiapatite.

Pertanto, compositi bioattivi vetro / idrossiapatite rivestimenti sono stati prodotti e analizzati.

Nella fattispecie si sono realizzati dei rivestimenti con tre microstrutture composite: rivestimenti compositi convenzionali (le fasi costituenti sono distribuite casualmente in modo uniforme), rivestimenti a doppio strato (composti da uno strato di idrossiapatite a contatto con il substrato ed uno strato superficiale di biovetro); rivestimenti a gradiente (nei quali la composizione varia gradualmente passando da idrossiapatite pura, a contatto con il substrato metallico, a puro biovetro, sulla superficie esterna). L'obbiettivo di questi sistemi è quello di fondere l'elevata bioattività dei biovetri con la stabilità dell'idrossiapatite. I campioni così ottenuti sono stati caratterizzati, e il composito a gradiente di composizione è stato selezionato per un'ulteriore ottimizzazione dei i parametri di processo. E' stato quindi prodotto un rivestimento con gradiente di composizione il quale è stato analizzato dal punto di vista microstrutturale e meccanico sia prima che post test *in vitro*. In tal modo ne sono state valutate sia la bioattività che la stabilità.

Introduction

Hydroxyapatite, (HA), is a calcium phosphate ceramic which has a composition and a structure very similar to those of the mineral component of bones. It is osteoconductive, and it has an excellent bioactivity which allows bone cells to grow on its surface. For this reason HA has been successfully used in orthopaedics and dentistry for many years. Since HA is brittle, its use in structural applications is limited. A way to overcome this problem is the application of HA as a coating on metal implants, since this ceramic enhances the fixation of the prosthesis to human bone.

The plasma spray technique is currently the standard method to produce HA coatings. This technology makes it possible to achieve a high deposition rate, which results in fast coating production; moreover plasma sprayed HA coatings generally have a good adhesion to the substrate. Although this production process has been thoroughly studied and optimized in recent years, isolated cases of implant failure are still reported and revision surgeries are sometimes necessary. Moreover the bone-bonding effect of HA takes place after several hours and therefore HA coatings are not the optimal solution in those applications which require a fast fixation.

Accordingly, numerous studies are addressed to develop new bioactive coatings. The research is focused on both innovative deposition techniques and alternative materials.

Bioactive glasses are an emerging family of biomedical materials. They are particularly interesting, because they possess the highest degree of bioactivity. Unfortunately Bioactive glasses, like HA, are fragile and therefore they are not suitable for load-bearing applications. As a consequence, they are mainly used in the production of bioactive coatings. Moreover, bioactive glasses may be applied in composite coatings, combined with HA in order to adjust the reactivity in a physiological environment.

Nowadays plasma spraying is the most widely used process to deposit bioactive coatings, but recently many innovations have been proposed, such as, for example, the so-called Suspension Plasma Spray (SPS). In this process, a liquid suspension is used as feedstock instead of a dry powder. This technique makes it possible to work on sub-micrometric powders which otherwise would have an inadequate rheology in dry form. The sub-micrometric feedstock results in coatings having a finer microstructure if compared with conventional plasma sprayed ones.

Objective of the Thesis

The primary intention of the present research project is the production of innovative coatings for biomedical applications.

With this aim, bioactive glasses and HA were selected as coating materials, while the innovative SPS process was employed as production technology.

Summary and general outline

Chapter 1: it consists in a review of the current state of the art and it is divided into three parts: the first one examines the available thermal spray techniques, with a particular emphasis on the SPS process and on the parameters that affect it; the second one proposes a general discussion on materials for biomedical use, especially bioactive glasses and HA, the two materials which are used in this study; the last part analyses in detail the coatings for biomedical applications, and it investigates their characteristics and properties. Although this study is mainly focused on bioactive glass coatings, HA ones are widely discussed since they are the current state of the art of bioactive coatings.

Chapter 2: it introduces the experimental activity of the research. The study is divided into various sections, each of which corresponds to one step of the procedure followed to obtain the final bioactive coatings.

Section 2.1 consists of an in situ study of the reactivity of bulk bioactive glasses immersed in a physiological medium. In this way, several bioactive glasses of different composition were compared in order to select a candidate for the coatings deposition.

Section 2.2 analyses the production of bioactive glass coatings via SPS. In this section the deposition parameters are carefully discussed.

Section 2.3 reports the production of a SPS bioactive glass topcoat on a traditional HA coating. The previously analysed spray parameters are optimized to achieve a bioactive glass layer having high bioactivity. The topcoat shows to be effective for increasing the *in vitro* bioactivity of the HA coating. Accordingly, to better combine the high bioactivity of bioactive glasses with the stability of HA, specific composite coatings are produced via SPS.

Section 2.4 shows the production and characterization of the composite coatings. Three different microstructures were produced and compared: conventional composite coatings (HA and bioactive glass zones randomly distributed throughout the coating); bi-layer coatings (a

bioactive glass topcoat and a HA bond coat); functionally graded coatings (the composition varies gradually from HA on the substrate to bioactive glass on the surface).
Since the functionally graded microstructure seems the optimal one, a second series of graded coatings is produced.
Section 2.5 reports the spraying of optimized composite coating with a graded composition. The coating is mechanically and *in vitro* tested and its adhesion to substrate is evaluated before and after SBF tests.

Finally, the conclusions drawn from this research work are outlined in Chapter 3; in addition, future perspectives are proposed.

Chapter 1:

State of the Art.

1.1 *Thermal Spray*

Thermal spray is a generic term for a “family” of coating processes used to deposit metallic or non-metallic coatings. It is based on the production of a flame or a plasma into which the material to deposit is injected, usually in powder form. The flame/plasma melts and accelerates the particles towards the substrate. The impact of molten or semi molten particles at high speed on the substrate causes them to flatten and solidify; as a result a typical lamellar structure composed of thin slices, called “splats”, is obtained.

The history of thermal spray dates back to the late 19th century, when M.U. Schoop deposited the first patents. In 1911 Schoop started to spray tin and lead on metal substrates to enhance their corrosion resistance, using a technique analogous to the modern flame spraying [1]. Starting From those early studies many innovations have been made, and several new techniques have been developed such as: Plasma Spraying (PS), Arc Spraying, Detonation-Gun Spraying, High-Velocity Oxy-Fuel (HVOF) Spraying and Cold-Gas Spraying.

1.1.1 Plasma spray

Plasma spraying (PS) torches are based on the Gerdien-type plasma generator dating back to the 1922, but they were first used to produce coatings in the early ’60s. In fact, the process was patented by Giannini and Ducati in 1960 and by Gage et al. in 1962 [2].

Since the first torches were introduced, several evolutions have been developed, such as multi-cathode torches, radio frequency (RF) plasma torches, controlled atmosphere plasma spray, vacuum plasma spray, and water-stabilized torches [3-5].

The main components of a standard plasma torch are the cathode and the anode between which an electrical arc forms, thus creating a plasma. Usually the anode is a circular nozzle made of high purity copper, while the cathode is an electrode of thoriated tungsten [2]. When a DC potential is applied to the cathode, a current discharges across to the anode creating an electric arc. Plasma forming gases, such as Argon or Nitrogen, are fed inside the torch, and they are excited by the arc to high energy levels forming a plasma. Usually gases are inserted

by means of a distribution ring which surrounds the cathode and, in this way, the stability of the arc is increased [6]. However the plasma is unstable and it recombines to form gases again, thus releasing a large amount of thermal energy. Due to the high temperature, gases expand and form a jet, which has a speed and momentum adequate to drag powders. A feedstock powder, suspended in a carrier gas, is injected into the jet. Inside the plasma, the particles are melted and accelerated towards the substrate. The particles then flatten and solidify, forming the coating [2, 7].

Several parameters are involved in the formation of the plasma; among them, the geometry of the electrodes, the composition of the gases, and the electrical power are the most important ones [2].

Geometry:

The shape of the cathode tip influences the arc voltage, while the geometry of the anode/nozzle controls the velocity, flow pattern, and temperature of the plasma. The internal geometry should be tailored to the employed gases.

Some commercial torches can be equipped with many sets of electrodes, having different geometries, to achieve plasmas with different properties; for example different geometries for sub-sonic jets and for supersonic ones.

To conclude, the electrodes undergo heavy wear processes from the plasma, which involves two problems: the pollution of the coatings due to the metal particles abraded from the electrodes, and the modification of the internal geometry of the torch during its use. For this reason, the consumption of the elements should be carefully monitored to preserve the quality of the produced coatings.

Gases:

Gases employed in plasma spray technology must meet certain requirements: they should be easily ionised and dissociated, and they should protect the electrodes from oxidation. The four main gases used in plasma spray are argon, nitrogen, hydrogen and helium.

1) Argon is the most common primary plasma gas and it is often used with a secondary plasma gas to increase its energy. Argon can be ionized easily and, since it is a noble gas, it tends to be completely inert to all materials and it is not aggressive towards the electrodes. Most plasmas are started up using pure argon.
2) Nitrogen is the cheapest plasma gas, and it is a general-purpose primary gas which

may be used alone or associated with hydrogen secondary gas. Nitrogen in its turn may be used as the secondary gas for Argon since it has a higher ionization energy, and thus it increases the enthalpy of the plasma. Nitrogen tends to be inert to most feedstock materials.

3) Hydrogen is mainly used as a secondary gas. Hydrogen dramatically affects the heat transfer properties and plasma temperatures; in particular, it highly increases the melting ability of the plasma. Hydrogen also acts as an anti-oxidant, but it reduces the arc stability.
4) Helium is mainly used as a secondary gas with argon. Helium imparts good heat transfer properties and gives high sensitivity for control of plasma energy. This gas is preferred for high velocity plasma spraying. Helium drawbacks are the cost and low availability.

Electric power:

The electric power is the energy provided to the system, and therefore it controls the temperature and the speed of the plasma. High levels of energy involve a high electric current resulting in a faster deterioration of the electrodes. In commercial torches electric power is up to 80 kW.

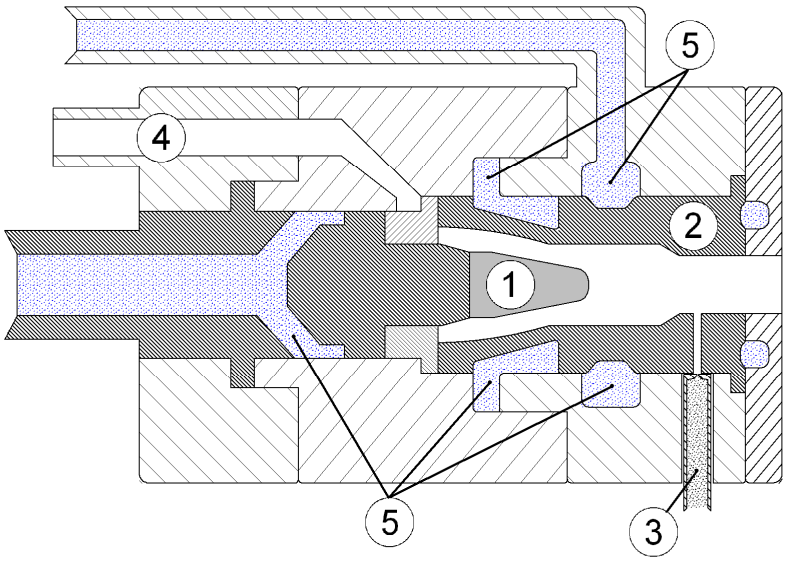

***Figure 1.1**:* Scheme of a DC plasma torch with internal injection.
1: cathode, 2: anode, 3: injector, 4: gases input, 5: cooling water.

Generally speaking, more than 50 non-independent parameters are known to affect the thermo-mechanical or service properties of plasma sprayed coatings [7]. Moreover, powders characteristics and their injection into the plasma play a key role. In fact, the granulometry and the morphology of the powders govern their interaction with the plasma. On the other hand, the thermal history of a particle is determined by its momentum and trajectory. Accordingly, the geometry and the speed of the powder injection must be properly set. Other parameters, such as the flow rate of the carrier gas, should be considered as well. In particular, the flow must be strong enough to drag the powders, but it must not be excessive in order to avoid any alteration of the plasma.

Furthermore, all the parameters concerning the relative movement between the torch and substrate affect the coatings microstructure. Probably the distance between torch and substrate is the most important parameter, but also the scan speed and scan-step between adjacent lines should be optimized.

1.1.2 Coatings with submicrometric and nanometric structure.

In the last few decades, the interest towards materials with submicrometric or nanometric grain sizes has increased constantly due to their excellent properties when compared to conventional microstructured materials. Accordingly, also the production of nanostructured coatings has gained great interest. This kind of structure is commonly realized through thin film technologies, but the production of nanostructured coatings thicker than a few tens of microns is particularly difficult when traditional techniques are employed. Thermal spray processes are widely used to produce coatings in this thickness range, but the direct use of nanometric or submicrometric powders is difficult to apply in practice. The main problems related to the use of very fine powders in thermal spray are:

1) the poor flowability of these particles, which involves agglomeration, clogging and discontinuities in the powder feeding
2) the low mass, and thus inertia, of sub-micrometric powders, which makes very difficult their penetration within the core of the plasma/flame [7].

To solve the latter drawback, for example, Su et al. [8] introduced a special powder injection system, which allowed to process particles having a diameter of about ten microns. This method, called small-particle-plasma-spraying, improved the control over the particle temperature and trajectory. Unfortunately, this technique does not allow to manage sub-micrometric or nanometric powders [8].

An alternative approach, which is currently available for industrial applications, relies on the deposition of coarse powders composed by nanometric grains [9]. As a rule, these powders are produced by spray-drying a nano-powder based slurry, and they have a size of 10-100 microns. Therefore they can be handled like ordinary micrometer-sized powders. The disadvantage of this method is that the deposition parameters must be carefully designed to control the sintering/melting of the particles in flight. In fact an excessive heat treatment can completely melt the aggregates, thus nullifying the use of nanostructured powders. Moreover, even if the parameters are properly monitored, the coatings obtained in this way usually show a nonuniform microstructure, in which nanostructured zones are surrounded by highly fused areas [9].

An alternative approach in order to face these drawbacks is the use of a liquid (instead of a gas) as a carrier fluid. In fact, if a liquid suspension is injected, the rheological problems associated with the dry powder are overcome, since the fluid can drag the low mass particles into the plasma/flame. Moreover, the use of liquids instead of dry powders makes it easy to manage different suspensions/raw materials at the same time. In this way, layered coating with a compositional gradient may be produced varying the flow rate of the suspensions during spray [10]. On the other hand, the use of a suspension implies some drawbacks. First, the suspension must be carefully prepared to reduce the formation of aggregates, which may cause defects in the coating and/or occlude the injector. In addition, the injection of the suspension into the plasma/flame becomes a crucial part of the process, as discussed in the following paragraphs. The use of suspensions has been applied to many types of torches: flame spray, HVOF, D-gun, and plasma spray.

1.1.3 Suspension plasma spray (SPS)

The first attempts to use suspensions in plasma spray (SPS) were probably made with RF torches in the ’90s to synthesize powders [11, 12]; instead the extension of suspension-based processes to traditional plasma torches to produce coatings dates back to the early 2000s [13, 14].

Obviously, one of key elements in SPS is the suspension. Usually the suspensions are prepared by simple dispersion of the nanometric or sub-micrometric powder in the fluid. In most cases, additives are used to stabilize the suspension and prevent the agglomeration of the solid phase. The suspension should be sieved before using, or a filter should be installed in the

supply line of the suspension, in order to avoid that large aggregates obstruct the injector.

The liquid phase can be water or an organic solvent (typically ethanol) or a mixture [15]. Chen and Trice [16] calculated that the energy to vaporize an ethanol-based suspension is about 40% of the energy to vaporize a water-based suspension. This means that, if ethanol is used instead of water, a higher plasma enthalpy is available to melt the powder. However, in some specific applications, water may be preferable. Li et al. [17], for example, showed that a steam jet treatment during PS reduces the decomposition and loss of OH- groups of hydroxyapatite. Moreover the ethanol is expected to vaporize within the plasma, but it burns if it gets in contact with oxygen. This causes the formation of a long flame (Fig. 1.2), which results in a great heat flux to the substrate/coating. Finally, the selection of the most appropriate carrier is conditioned by the chemical reactivity with the powder to deposit.

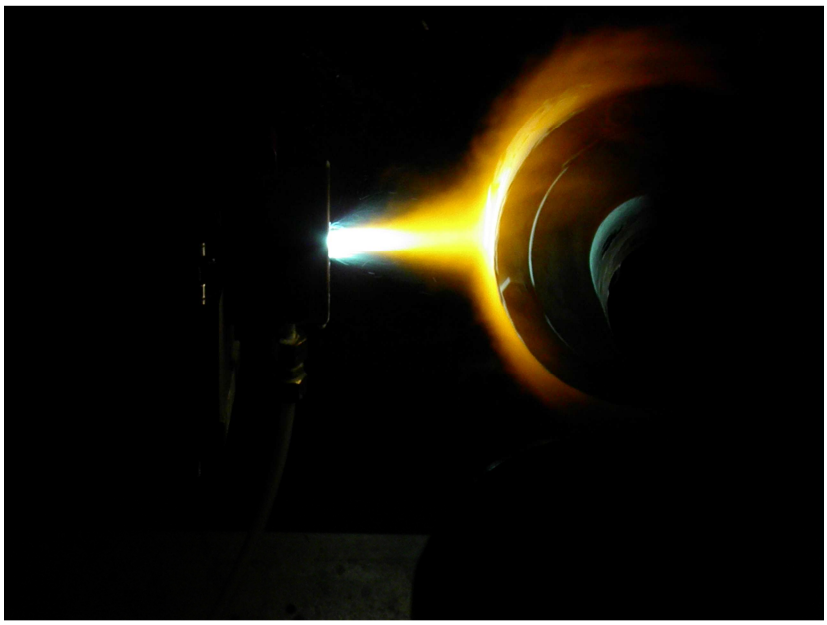

***Figure 1.2**:* Suspension plasma spray with ethanol as a suspension fluid

An important variable is the percentage of the solid phase in the suspension: high percentages of solid usually result in a high deposition rate, but an appropriate plasma power and heating ability are also required. Furthermore a higher percentage of solid deeply affects the rheological properties of the suspension, and it can lead to clogging.

The feeding apparatus is usually based on pneumatic systems or peristaltic pumps and the injection of the suspension is usually achieved through an atomizer or a nozzle. For example, Blazdell and Koruda [14] used a continuous ink jet printer to feed the suspension. Shan et al. [18] compared the solution/plasma interaction using different types of injection: liquid stream

and gas-atomized droplets. The liquid stream was simulated both as a continuous stream, with primary breakup, and as a mono-dispersed droplets jet. The Authors showed that the gas-atomizers produce smaller droplets than liquid stream injectors, while the mono-dispersed droplets jet allows injecting the solution droplets into the plasma core, which makes the droplets heated effectively. The liquid stream injection with primary breakup shows an intermediate behaviour with respect to the other two systems.

In addition, the point, the angle, and the velocity of the suspension injection into the plasma should be properly set, since these parameters affect the trajectory of the particles within the plasma.

When the liquid droplets/suspension jet reach the plasma they are dragged and accelerated. The drag force of the plasma produces a shear stress in the droplets, which may lead to atomization of the largest ones [9, 19]. This phenomenon is called aerodynamic breakup and it depends upon droplet size, surface tension and shear force. The aerodynamic breakup takes place very quickly, in milliseconds from the contact of the suspension with the plasma. At the same time, the liquid phase evaporates and then the hot gas directly affects the powders. The particles are thus heated and they begin to sinter and melt. The particles can undergo melting evaporation or sintering as in the conventional PS, but in SPS these phenomena may be more pronounced. This is due to the smaller powder size in SPS [20], which implies higher specific area and then greater surface energy. The sintering time strongly depends on temperature and particles diameter, while the agglomeration of melt fine droplets is almost immediate [21]. Consequently the melting control is important to avoid an excessive growth of the droplets.

The use of a suspension also implies some adjustments to the deposition set-up with respect to conventional PS. For example, in SPS the torch is generally closer to the substrate than in traditional PS. This fact is also due to the small size of the particles, which suffer solidification in flight and deceleration much more than micrometre-sized particles do. However a shorter spraying distance can cause overheating problems to the substrate or to the first layers of the coating. This is particularly true for SPS, since the deposition of sub-micrometre-sized particles implies a great number of torch passes to reach a specified coating thickness.

1.1.4 Coatings Microstructure

As mentioned above, thermally sprayed coatings usually have a lamellar microstructure. Also in SPS coatings the microstructure may be still considered lamellar, but with significant

differences in the degree of flattening and in the size of the lamellae [9]. SPS coatings usually show a finer microstructure, which is characterized by splats with a lower degree of flattening, resulting in a “granular” structure [22]. Sometimes the particles' flattening is so low that the final microstructure is similar to that of sintered materials. The inter-splat porosity completes the coating's characteristics.

In suspension thermal spray the heat input to the coating/substrate is important, due to the low spray distance and the high number of torch passes used. In fact, it may happen that the surface temperature exceeds 850°C during the deposition [23], and it may occur that the superficial layers of the coating change their microstructure [24]. This implies that the coating temperature should be monitored very carefully and, if required, cooling systems should be employed to avoid an excessive heating.

The microstructural and phase homogeneity of the coatings depends on the thermal history and trajectory of each particle into the plasma. The latter, in turn, is closely related to the suspension injection. In fact, as suggested by Kozerski et al. [25], the particles which are injected into the core of the plasma are completely melted and, when they impinge on the substrate, they produce dense zones formed by large lamellae. Instead, the particles that remain on the plasma plume generate sintered zone consisting of very fine grains. Accordingly, the coatings obtained via SPS often show zones with different microstructures and degrees of crystallinity.

1.2 *Biomaterials*

Biomaterials may be defined as:

"A nonviable material used in a medical device, intended to interact with biological systems."
(1st Biomaterials Consensus Conference, 1986, Chester, UK)

"A material intended to interface with biological systems to evaluate, treat, augment, or replace any tissue, organ, or function of the body."
(2nd Biomaterials Consensus Conference, 1992, Chester, UK)

The first characteristic of a biomaterial is the biocompatibility, i.e. the ability to induce an appropriate response within the human body after implantation.
Biomaterials may be metals, ceramics, polymers and composites and, according to their composition, they exhibit peculiar properties. For example metals have good mechanical properties and high toughness, instead ceramics generally offer high wear and corrosion resistance, even if they are hard and fragile.
According to their interaction with the human body, biomaterials can be "bioinert", "bioactive" and "bioresorbable".

1.2.1 Bioinert materials

The first studies on materials for medical applications were designed to find components which could be mechanically strong and chemically inert. For this reason, the first biomaterials, which were introduced in the '20s, were metal alloys, such as Stellite, stainless steel 18-8 and Vitallium [26].
Subsequently polymers such as PMMA and nylon were applied, with the same goal of using materials which reacted as less as possible with the surrounding environment.
A great advance in the field of biomaterials occurred at the end of World War II. In this period many veterans required surgery and hence the attention of the scientific community was driven on the need for new biomaterials; on the other hand, novel durable and inert materials, originally developed for the military applications, had become available [26].
Substantially, the purpose of the first implants was to replace the damaged organ without being rejected. Accordingly, even if no material is completely inert in biological environment,

the aim of the first “bioinert” materials was to avoid any toxic reaction and to minimize the formation of a non-adherent fibrous capsule at the interface with the host tissue [27]. Nowadays various kinds of bioinert materials are used, including metal alloys, ceramics such as zirconia and alumina and polymers such as ultra-high molecular weight polyethylene (UHMWPE) and polymethylmethacrylate (PMMA). These materials are chosen mainly because of their mechanical properties. For example, UHMWPE is wear resistant and possesses self-lubricating properties.

The drawback of the so-called “first generation” biomaterials is given by their tissue-implant interface. In fact, although bioinert materials do not cause adverse reactions by the host tissues, they inevitably get covered by a fibrous capsule when they are implanted in the human body. The capsule is not bonded with the implant, and therefore micro-movements may occur. For this reason bioinert materials should operate primarily in compression [28], in order to limit the relative movements between implant and host tissue which may deteriorate the functionality of the prosthesis or the original tissue properties at the interface, or both [26].

Various methods have been proposed to increase the adhesion between bioinert materials and living tissues. For example, it is possible to modify the superficial morphology of the implant: the so-called biological and morphological fixations are obtained by means of this procedure [28]. The former is achieved when the bone grows within the open porosity of the implant; the ingrowth leads to a mechanical connection of bone to the biomedical device. The latter occurs when the growing bone attaches into the superficial irregularities of the implant, and it can be enhanced by increasing the roughness or making fenestration. Among these methods, the biological fixation is able to ensure the best fixation, but it requires the use of porous materials, which may be mechanically inadequate [26]. An alternative solution is cementation, which consists in the fixation of the prosthesis with a polymeric or ceramic cementing paste [29].

1.2.2 Bioactive materials

The second generation of biomaterials was born at the end of the ’60s, when professor L. L. Hench proposed a new group of glasses able to bond with bone, the so-called “bioglasses” [30].

The study of these new materials stemmed from a specific request: a material that could survive the exposure to the human body without any adverse reactions. In fact, at that time,

the problem of rejection was still unresolved. So, professor Hench began to study new materials for medical applications on the basis of a hypothesis:

"The human body rejects metallic and synthetic polymeric materials by forming scar tissue because living tissues are not composed of such materials. Bone contains a hydrated calcium phosphate component, hydroxyapatite [HA] and therefore if a material is able to form a HA layer in vivo it may not be rejected by the body."

In 1971 the first paper about Bioglass® was published [31].

The biomaterials of second generation, commonly called "bioactive materials", have the ability to bond with the host tissue. In particular, when a bioactive glass is implanted, it induces the formation of a superficial layer of hydroxy-carbonate apatite (HCA). The HCA is very similar to the mineral component of bones and therefore the implant is not perceived as a foreign body. Accordingly, bioactive materials are not covered by a fibrous capsule, as occurs to bioinert materials, but their surface directly bonds to the new host tissues. The result is a strong adhesion between the implanted material and the living tissues, which drastically reduces the problems of rejection and relative micro-movements between the prosthesis and the host tissue. This mechanism is known as "bioactive fixation" [28]. After few months, the bond between bones and bioactive materials reaches a strength comparable to that of bone. Moreover, some specific bioactive materials are able to bond also with the collagen of soft tissues [28].

The index of bioactivity (Ib), which relates the level of bioactivity with the time necessary to obtain more than 50% of bonded interface ($t_{0.5bb}$), is a sort of fingerprint of the bioactivity [26]; i.e., it is defined:

$$Ib: = (100/t_{0.5bb}) \qquad (1)$$

Usually bioactive glasses possess the highest Ib values [32], and glasses with Ib greater than 8 are able to bond also with soft tissue [33].

The bioactivity of a material can be assessed in different ways. The most effective one certainly relies on *in vivo* tests, namely experimentation on living organisms. Unfortunately such tests involve risks to the patient and raise moral problems when they are run on animal models.

In vitro methods, which mimic specific biological phenomena in an artificial laboratory environment, are most commonly used to assess the bioactivity of new materials. However *in*

vitro tests are not able to reproduce the complexity of living organisms and hence they remain preliminary trials. In fact, *in vivo* tests are generally performed on materials that have already been extensively tested *in vitro*. A relatively easy approach to test materials *in vitro* consists in soaking them in a simulated body fluid (SBF) [34]. SBF is an acellular fluid that has the same ionic composition of human plasma. These tests are carried out by soaking the sample into a fixed volume of SBF for a specified period under controlled conditions. The purpose is to verify the ability of the biomaterial to develop HCA on its surface. The significance of SBF tests is still under debate due to their intrinsic limits, such as the inability to verify antibodies reactions [35]. Nevertheless SBF tests remain the principal mean to acquire a preliminary insight into the bioactivity of new materials.

1.2.3 Bioresorbable materials

Bioresorbable materials are gradually dissolved in the body and, at the same time, they are replaced by new living tissue that completely replace the implant material [36]. Since natural tissues can repair and replace themselves throughout life, bioresorbable materials are the optimal solution to produce high performance bone implants [26]. In fact, in this way the problems associated to the long term stability of the implant are prevented, since the prosthesis itself is gradually replaced by the living tissue.

The main problem associated with resorbable biomaterials is given by their mechanical performance over the period of time required for the substitution, when living tissues are still forming and the implanted material is already being dissolved. In fact the strength and the stability of the interface should survive during the degradation process. Moreover the resorption rate and the host tissue formation rate must match. In order to adjust the dissolution rate, several methods can be used, such as the addition of doping elements to the biomaterial or the adjustment of the shape and size of the bioresorbable device [36]. Moreover, the substances released by the biomaterial during its dissolution must be acceptable to the human metabolism. On account of this criticism, a new target is to dope biodegradable materials with substances which may induce genetic stimulation [37, 38]. In this way the natural healing of tissue can be favoured.

Some resorbable biomaterials are currently used in clinical practice. For example, polymers such as poly(lactic-acid) and poly(glycolic-acid) are employed for the sutures [26]. These materials are able to withstand for an appropriate time, and then they are metabolised to CO_2 and H_2O. Even some ceramic materials, such as tricalcium phosphate, may be resorbable if

they are used in porous devices or in particulate form [39]. However, these materials can not undergo high mechanical stresses during the resorption phase.

1.2.4 Bioceramics

Bioceramics are an important family of biomaterials. Depending on their composition and microstructure, they can be bioinert, bioactive or bioresorbable. Unfortunately all bioceramics are penalized by their inherent brittleness, which limits their use.

Figure 1.3 shows the bioactivity spectrum of some bioceramics of clinical interest.

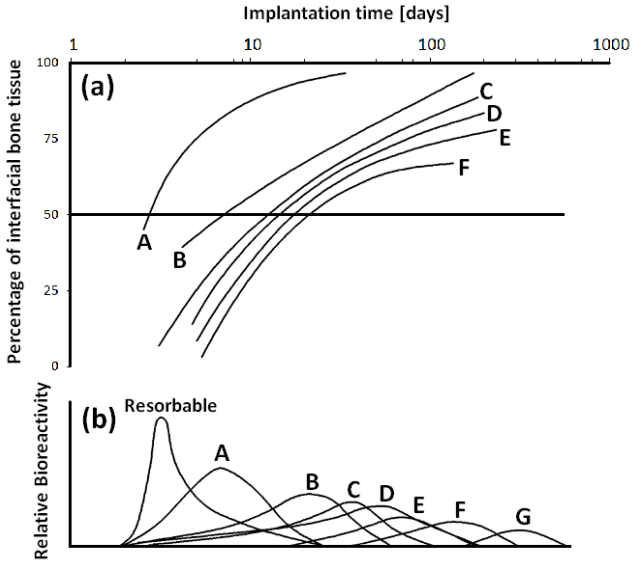

Figure 1.3: Bioactivity spectrum for various bioceramic implants:
(a) time dependence of formation of bone bonding at the implant interface, and (b) relative rate of bioreactivity
A: Bioglass® 45S5, B: KGS glass-ceramic, C: Bioglass® S53P4, D: A/W glass-ceramic,
E: dense synthetic HA, F: KGX glass-ceramic, G: Al_2O_3. Adapted from [33]

The first bioceramic employed in clinical applications was high-purity alumina [33]. Such oxide has good biocompatibility, high chemical durability, and excellent tribological properties. Therefore, it is used in total hip prostheses and dental implants. Limitations in the use of alumina are due to its poor flexural strength. Moreover, alumina may induce stress shielding of bones. This effect is due to the difference between the stiffness of bone tissue and that of alumina [40], which are respectively about 7-25 GPa (for cortical bone) and 400 GPa. This means that the mechanical load is borne almost entirely by the alumina prosthesis, and thus the bone stresses become subnormal (i.e. the remaining host bone is “shielded” by the implant). This alters the natural remodelling of the bone and therefore the stress shielding can induce the cancellous bone to atrophy or even cause the loss of the implant [33]. Accordingly,

it is necessary to consider very carefully all aspects in the design of a prosthesis [40]. Finally, another problem of alumina is that it can be degraded in the body environment. However an alumina with adequate purity and microstructure is expected to have a lifespan of 30 years under load conditions [33]. Since this is the life expectancy of a hip prosthesis, this ceramic can be successfully used for this application. In fact alumina non-cemented cups press-fitted into the acetabulum of the hip are quite common [40]. An additional way to apply the bioinert ceramics, such as alumina and zirconia, is to employ them in a porous form, which promotes the ingrowth of bone tissues.

1.2.5 Hydroxyapatite

Hydroxyapatite (HA) is probably the most important crystalline biomaterial, since its structure and chemical composition are very similar to those of the mineral component of bones. This resemblance ensures high stability and biocompatibilty in biological environment. Its stoichiometric formula is $Ca_{10}(PO_4)_6(OH)_2$, with a Ca/P ratio of 1.67.

The biological hydroxyapatite (usually a hydroxy-carbonate apatite, HCA), which is mainly present in bones and teeth, contains many impurities, because its structure is prone to ion substitutions. The most important structural defects in biological hydroxyapatite are the partial substitution of OH^- groups by carbonate groups and calcium deficiency. There are also many secondary substitutions by ionic groups such as carbonate (CO_3^{2-}) magnesium (Mg^{2+}), sodium (Na^+), potassium (K^+), fluoride (F^-), chloride (Cl^-). To conclude, other elements are present only in trace amounts, such as barium (Ba^{2+}), strontium (Sr^{2+}), and lead (Pb^{2+}).

A comparison between a synthetic hydroxyapatite and a natural one is reported in Table 1.1.

	Ca/P	**Ca**	**P**	**Na**	**K**	**Mg**	**CO_3^{2-}**
Biological HA	1.65	24.5	11.5	0.7	0.03	0.55	5.8
Synthetic HA	1.67	39.6	18.5	traces	traces	traces	-

Table 1.1: Comparison between biological and synthetic HA, wt.%. Adapted from [48].

1.2.5.a Bioactivity of HA

The bioactivity of HA has been supported by *in vitro* and *in vivo* tests, and clinical trials.

The biological reactivity of HA is closely related to its composition and degree of crystallinity. In fact, while a stoichiometric and highly crystalline HA is almost stable in a biological environment, a poorly crystalline and/or chemically substituted one can undergo a fast degradation. Other factors such as the Ca/P ratio, the presence of secondary phases and

the microstructure (porosity, size of the grains) affect the reactivity of HA. Also the composition and the pH of the solution may influence the stability of hydroxyapatite. Other calcium phosphates are often associated to HA. They may appear as secondary phases or degradation products of HA, and the most common ones are: oxyhydroxyapatite (OHA) and oxyapatite (OA), α-tricalcium phosphate and β-tricalcium (α-TCP and β-TCP, respectively), dicalcium phosphate (DCP) and amorphous calcium phosphate (ACP). The calcium phosphates suitable for biomedical applications are listed in Table 1.2.

Name	Symbol	Chemical Formula	Ca/P ratio	Crystalline Phase
Tetracalcium phosphate	TTCP	$Ca_4(PO_4)_2O$	2	
Hydroxyapatite	HA	$Ca_{10}(PO_4)_6(OH)_2$	1.67	Hydroxyapatite
Oxyhydroxyapatite	OHA	$Ca_{10}(PO_4)_6(OH)_{2-2x}O_x$	1.67	
Oxyapatite	OA	$Ca_{10}(PO_4)_6O$	1.67	
α-Tricalcium Phosphate	α-TCP	$Ca_3(PO_4)_2$	1.5	
β-Tricalcium Phosphate	β-TCP	$Ca_3(PO_4)_2$	1.5	Whitlockite
Octacalcium Phosphate	OCP	$Ca_8H_2(PO_4)_6.5H_2O$	1.33	
Dicalcium Phosphate Dihydrate	DCPD	$CaHPO.2H_2O$	1	Brushite
Dicalcium Phosphate	DCP	$CaHPO_4$	1	Monetite

Table 1.2: Calcium phosphates of biomedical interest. Adapted from [26] and [52].

In particular, only two calcium phosphates are stable at room temperature when they are in contact with an aqueous solution, i.e. DCP and HA. If the pH of the solution is lower than 4.2, DCP is the stable phase; otherwise, if the pH greater than 4.2, HA becomes stable [37]. Since the pH of the human body is indicatively 7.4, HA is the most stable calcium phosphate under these conditions.

The chemical reactions that occur *in vitro* on the surface of hydroxyapatite have been studied by Kim et al. [41] via immersion in SBF. The dissolution process starts from structural defects such as dislocations and grain boundaries [42]; then calcium and phosphorus are released. The HA surface has a negative charge, and thus it interacts specifically with the positive calcium ions in the fluid [41]. Accordingly a Ca-rich ACP layer forms on the surface. Due to the accumulation of calcium ions, the surface assumes a positive charge, which interacts with the negative phosphate ions in the solution. Consequently, a layer of ACP with excess of phosphate ions, i.e. a Ca-poor ACP, is formed on the surface. This layer acts as a precursor for the formation and crystallization of biological HA [41]. Since the water solubility of HA is the

lowest among those of calcium phosphates, the Ca-poor ACP, in SBF, could be stabilized by a dissolution and re-crystallization into HA. Therefore the HA crystals continue to grow by absorbing calcium and phosphorous ions from the SBF, which is indeed a fluid supersaturated with respect to HA [34]. In this process, secondary ions, such as magnesium, carbonate and sodium, may be incorporated into the HA structure.

This set of reactions occurs in absence of cells and proteins. In a biological environment, the stability of HA is also affected by the cellular activity occurring in the human body. In fact, Nagano et al. [43] reported that osteoclasts may play a key role in the dissolution of HA, and consequently in the formation of HCA [43]. On the other hand, the surface charge of HA induces the adsorption of proteins [41], and proteins are considered to reduce the HA formation rate [41].

A schematic overview of the reactions occurring between a HA coating and bone is reported by Sun et al [44]. The first two steps are consistent with those observed in *in vitro* tests:

1) partial dissolution of the HA coating that causes a rise of the calcium and phosphate ion concentration in the local environment around the implant
2) precipitation of HA crystals on the coating surface and ionic exchange between HA crystals and surrounding tissues
3) formation of a carbonated calcium phosphate layer incorporating a collageneous matrix; bone growth toward the implant
4) bone remodelling: osteoclasts resorb the bone tissue and reduce the local pH to approximately 4.8, which leads to a fast resorption of both the biological HCA and the synthetic HA coating
5) Further ingrowth and remodelling of bone at the bone-coating interface and, to conclude, biological fixation as a result of the bidirectional growth of a bonding layer

1.2.5.b Thermal properties of HA

HA is usually processed by sintering, in order to obtain bulk components, or by plasma spraying, to produce coatings. Both methods imply heat treatments which are likely to degrade the original HA [45]. This is particularly true for the plasma spraying process, since the temperature of the plasma may exceed 15000 K [3]. Such a high temperature is known to degrade HA. The main processes which occur during the heat treatment of HA are dehydroxylation and decomposition [46]:

$Ca_{10}(PO_4)_6(OH)_2 \rightarrow Ca_{10}(PO_4)_6(OH)_{2-2x}O_x \square_x + xH_2O$ (step 1)
(hydroxyapatite) → (oxyhydroxyapatite)

$Ca_{10}(PO_4)_6(OH)_{2-2x}O_x \square_x \rightarrow Ca_{10}(PO_4)_6O_x \square_x + (1-x)H_2O$ (step 2)
(oxyhydroxyapatite) → (oxyapatite)

$Ca_{10}(PO_4)_6O_x \square_x \rightarrow 2Ca_3(PO_4)_2 + Ca_4(PO_4)_2O$ (step 3)
(oxyapatite) → (tricalcium phosphate) + (tetracalcium phosphate)

$Ca_3(PO_4)_2 \rightarrow 3CaO + P_2O_5$ (step 4a)
(tricalcium phosphate) → (calcium oxide) + (phosphorus pentoxide)

$Ca_4(PO_4)_2O \rightarrow 4CaO + P_2O_5$ (step 4b)
(tetracalcium phosphate) → (calcium oxide) + (phosphorus pentoxide)

Where □ refers to lattice vacancies in the OH positions along the crystallographic c-axis in the structure of hydroxyapatite.

Since HA powders are hygroscopic, a low-temperature thermal treatment removes the absorbed water by evaporation, but it does not cause any change in the HA structure. However water is also present inside the HA lattice structure. Dehydroxylation occurs when HA loses (OH^-) groups ad high temperature. This process takes place in two steps with the formation of OHA and then OA (step 1 and 2). If the temperature does not exceed a critical point, these new phases can be retransformed into HA in presence of water [47]. Otherwise, if the critical temperature is surpassed, the HA crystal structure changes and suffers a complete and irreversible dehydroxylation [49]. If the temperature increases further, HA starts to decompose. The decomposition of HA leads to the formation of other calcium phosphates (step 3) such as TCP and TTCP. These phases in turn can decompose into calcium oxide and phosphorus pentoxide (step 4a and 4b). Approximate values for the dehydration and decomposition temperatures can be considered [49]:

<800 °C	slow dehydroxylation
800-1350 °C	fast dehydroxylation
1350 °C	critical point: decomposition and irreversible dehydroxylation

However, the temperatures of HA modification are strongly influenced by various factors, such as heating rate, initial state of the HA, and environment.

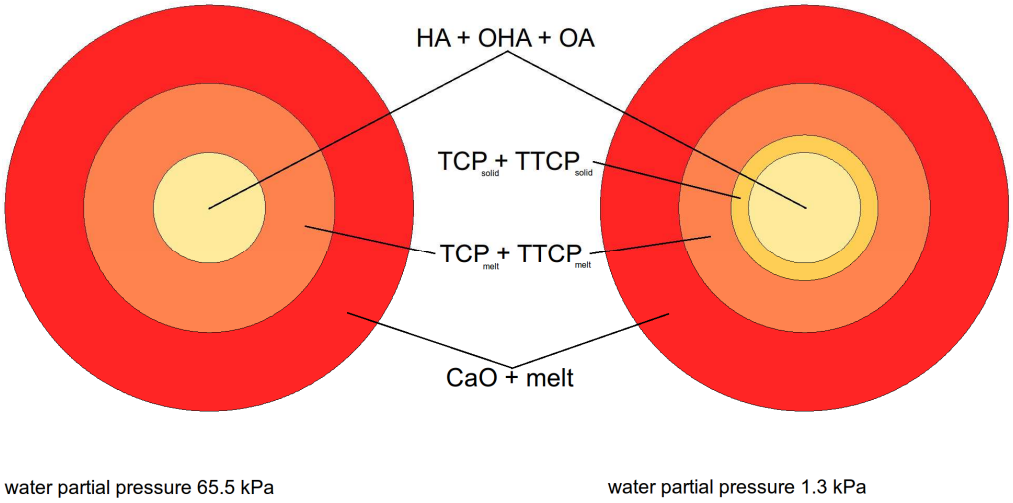

***Figure 1.4**:* Hydroxyapatite particles during thermal spray. Effect of the environment. Adapted from [44]

For example, a high degree of crystallinity of the starting HA usually reduces the tendency to decompose. Furthermore, the "real" composition of HA has a remarkable importance. Raynaud et al. [50] observed that the degree of HA decomposition is strongly related to the Ca/P ratio. The Authors produced several HAs with a Ca/P ratio ranging from 1.5 up to 1.67. They treated such HAs at 1000°C for 15 hours. The Authors reported that a smaller value of the Ca/P ratio usually corresponded to a greater degree of decomposition. In fact, more than 90% of the HA with a Ca/P ratio of 1.51 decomposed to TCP after the heat treatment. On the contrary the stoichiometric HA (Ca/P ratio of 1.67) showed a much higher stability. The Authors also produced Ca-rich HAs, which however were found to be a biphasic mixture. The HA present in this composite was not degraded by heat treatment. Thus the use of stoichiometric or Ca-rich HA is recommended to avoid decomposition. The thermal stability of HA can also be increased by means of appropriate chemical substitutions. Chen and Miao [51] reported that replacing the OH^- group with F^- can increase the thermal stability of HA. In fact, when more than 60% of the OH groups are replaced, decomposition of the HA matrix is effectively restrained.

Also the environment in which the heating process takes place is very important to prevent the decomposition of HA, especially the partial pressure of water. Gross et al. [52] reported that, with a partial water vapour pressure of 500 mm Hg, HA is stable up to about 20°C below its melting temperature. Instead, if the partial pressure of water is 900 mm Hg or higher, HA can be melted without decomposition. Therefore, processing HA in an atmosphere containing water vapour could reduce both dehydroxylation and decomposition.

1.2.5.c Decomposition phases of HA

It is very important to exert a close control on the thermal reactions of HA, since TCP, ACP and TTCP have a higher degree of bioactivity than HA [26], but they are also less stable in a biological environment. In fact, the order of the dissolution rates of the phases present in a partially decomposed HA is as follows [46]:

CaO >>TCP> ACP > TTCP >> OHA/OA >> HA (in SBF)

This implies that the presence of decomposition phases may reduce the *in vivo* mechanical reliability of HA-based components. In fact, as shown in Figure 1.4 for the plasma spray process, the decomposition of HA starts from the exterior of the particles. Therefore, since phases such as TCP and TTCP are less stable than HA, preferential dissolution at the grain boundaries may occur. Most of all, the presence of CaO should be avoided since it is cytotoxic due to its high alkalinity.

1.2.5.d Doped-HA

The scientific research is now mainly addressed to identify appropriate dopants in order to control the properties and the thermal behaviour of HA. Fluoride is a well known dopant of HA, since the mineral part of teeth is composed of F-substituted HA; on the other hand many other elements can be used in order to provide particular properties to HA. For example Cerium seems to confer an antibacterial effect [53], while strontium and silicon are supposed to stimulate osteogenesis in some genes [54, 55]. In particular, numerous studies report that silicon has a positive effect on the gene expression and on the stimulation of new bone tissue production [56, 57]. Moreover the substitution of HA with silicon ions may also provide additional benefits such as the inhibition of grain growth [58]. Si-substituted HAs were also tested as a coating materials. Xiao et al. [59] and Gomes et al. [60] produced Si-substituted HA coatings via VPS and PS respectively. Both studies confirmed the better cellular response of modified HA with respect to pure HA.

1.2.6 Bioactive glasses

As previously mentioned, bioactive glasses are a family of special glasses, which have the ability to bond to bone. The first and best known bioactive glass, Bioglass® 45S5 (wt.%: 24.5 Na_2O, 24.5 CaO, 6 P_2O_5, 45 SiO_2,), was discovered at the end of the ’60s by professor L.L.

Hench [30, 31]. This finding led to a revolution in the world of prosthetic materials, since previous implants were unable to chemically bond to living tissues.

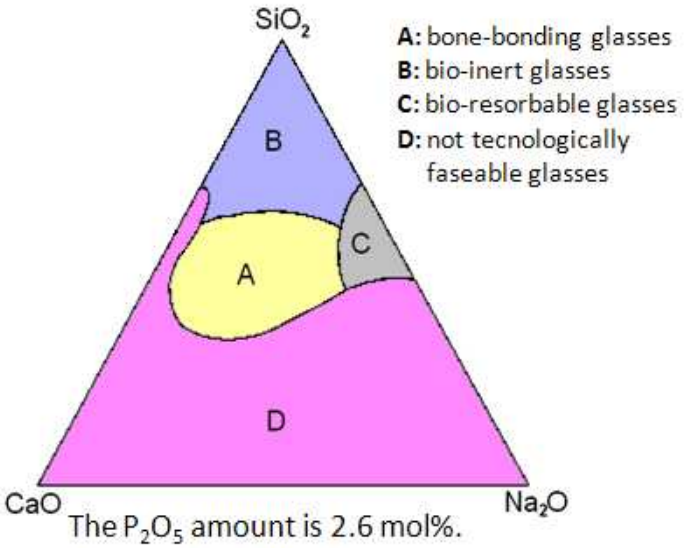

***Figure 1.5**:* System of Bioglass® 45S5, effect of composition on bioactivity. Adapted from [33].

As supposed by Hench, the bone bonding ability of bioactive glasses comes from their ability to form a surface layer of HCA [30]. The mechanisms of HCA layer formation, and the resulting bond with living tissues, have been extensively studied. In particular, a model in 12 steps has been proposed by Hench to describe the interfacial reactions. In that model, the first 5 steps consist of ionic reactions between the glass and an acellular, protein-free, physiological solution, while the subsequent steps also involve cells and proteins [28]:

0)	bioactive glass
1 & 2)	formation of SiOH bonds on the glass surface
3)	polycondensation of SiOH + SiOH → Si-O-Si
4)	adsorption of amorphous Ca, PO4, CO3
5)	crystallization of hydroxyl carbonate apatite (HCA)
6)	adsorption of biological moieties in HCA layer
7)	action of macrophages
8)	attachment of stem cells
9)	differentiation of stem cells
10)	generation of matrix
11)	crystallization of matrix
12)	proliferation and growth of bone

The first two steps can be explained by an ionic exchange that occurs between the bioactive glass and the surrounding environment. In fact, the alkaline ions of the glass are exchanged with H^+ ions from the body fluids. This leads to a partial dissolution of the glass network, and SiOH bonds form at the interface. Then the SiOH bonds condense to a hydrated silica gel. Thus, the ions coming from the environment are adsorbed on the surface of the silica gel, and HCA starts to form.

The early stages occur in few hours, while the processes that require the cells mediation may take some days [33].

The composition of bioactive glasses is relatively similar to those of traditional glasses, indeed it is based on mixtures of oxides, usually from the system Na_2O - K_2O - CaO - MgO - P_2O_5 - SiO_2. Compared to commercial soda lime glasses, bioactive glasses contain more alkaline oxides and a lower silica percentage. Moreover, as a general trend the composition of bioactive glasses does not include oxides which may increase the chemical durability of the glass such as aluminium, titanium, and zirconium oxides [33]. These compositional differences with respect to traditional glasses make bioactive glasses more reactive. In fact, high-durability glasses, which are slowly leached when immersed in aqueous media, are not bioactive since they are not able to form a HCA layer. In particular, glasses with a silica content lower than 55 wt.% usually show high bioactivity, while glasses containing more than 60 wt.% of silica induce the formation of fibrous tissue. Glasses with an intermediate composition (silica wt.% between 55 and 60) generally exhibit a low bioactivity [28]. Therefore the reactivity of bioactive glasses can be governed through their composition.

One more interaction between bioactive glasses and cells has been discovered recently. In fact, some studies suggest that the Si ions released by bioactive glasses in body environment stimulate osteoblast turnover. In particular these ions are thought to promote the growth and osteogenic differentiation of primary osteoblasts [61].

Furthermore, it is known that Si and Ca ions released by bioactive glasses are able to promote the upregulation and activation of some families of genes in osteoprogenitor cells [38].

1.2.6.a Sol-gel bioactive glasses

Although the composition of bioactive glasses greatly influences their bioactivity, this is not the only factor to consider. For example, bioactivity can be observed even on pure silica samples, if they have a proper structure [62]. This can be achieved producing glasses via sol-gel instead of a traditional melt-quenching method. The different behaviour of sol-gel glasses

is due to their structure, which is the result of a condensation of SiOH bonds. That process resembles the spontaneous mechanism occurring in the human body, and thus sol-gel glasses assume an appropriate structure to promote the HCA precipitation in biological environment.

1.2.6.b Crystallization of bioactive glasses

As in the case of HA, bioactive glasses are also often processed by sintering or thermal spraying. In bioactive glasses, decompositions do not occur, but generally they crystallize [63]. The effect of crystallization on bioactivity of bioactive glasses is still a matter of debate, although it is generally recognized that a wide crystallization lead to a reduction of the bioactivity [64, 65]. For this reason, in the last years special glass compositions have been developed in order to reduce the crystallization, and thus to preserve the bioactivity of the glass after processing [66-69]. It is worth noting that the kind of crystal phases, which forms in a bioactive glass, depends on glass composition and on thermal treatment, and each crystalline phase has a different effect on bioactivity. For example Xin et. al [70] reported that the *in vitro* bioactivity of sintered Bioglass® 45S5 was not deteriorate by the formation of wollastonite fine crystals on glass surface.

The crystallizations of bioactive glasses are not always a drawback due to the production process, but they may be specifically induced to achieve special structures. In fact, since it is possible to promote specific crystallizations by introducing appropriate oxides in the glass composition, an important sub-category of bioactive glasses has been developed: the bioactive glass-ceramic. An important composition is that of the apatite-wollastonite (AW) glass-ceramic. The AW, which was discovered by Kokubo in the middle of the ‘80s, [71] has a composite microstructure in which crystals of oxyfluorapatite ($Ca_{10}(PO_4)_6(O;F)_2$, 38 wt-%) and wollastonite ($CaO.SiO_2$, 34 wt-%) are dispersed in a glassy matrix (SiO_2 - CaO - MgO). Due to the glass-ceramic structure, the AW has improved mechanical properties with respect to bioactive glasses. Furthermore, developing specific crystalline phases, glass-ceramic with special features can be produced. For example, special bioactive magnetic glass-ceramics have been designed for hyperthermia treatment of cancer [72].

1.3 *Bioactive Coatings*

Bioactive ceramics have been employed in many clinical applications during the last decades, for non-load-bearing applications, such as periodontology [37].

The use of bioactive ceramics in structural components is strictly limited by their intrinsic brittleness, which can lead to sudden and unpredictable fractures. Furthermore, these materials generally have low strength. Although some bioactive materials have been designed to have good mechanical properties, such as the AW glass-ceramic [73], their use is limited to components under compressive loads.

In order to overcome such limitations, bioceramics can be successfully used as coatings on a strong bioinert metal implant to improve its adhesion to bone tissue.

For example, this approach is commonly applied in total joint hip replacement. A hip implant must primarily meet mechanical requirements, since it is severely stressed. The elements composing a total joint hip replacement are the acetabular cup, and the femur part [40], which is composed by the stem and the head of the femur. Since the acetabular cup and the femoral head are mainly stressed in compression, and they are subjected to intense wear, these parts can be made of ceramic such as alumina and zirconia (the cup also in UHMWPE). The stem, instead, is subjected to compression and flexion. Accordingly, this component must be realized with a tough material as stainless steel, titanium and its alloys or Cr-Co alloy [40]. Nowadays it is an established practice to increase the adhesion of the stem through the use of bioactive coatings. The increased adhesion has been demonstrated to be positive in terms of life expectancy of the prosthesis and rehabilitation of the articulation [74].

Bioactive ceramic coatings have been successfully used on dental screws as well. In this case a screw, usually made of titanium or its alloys, is fixed into the jaw to lock a dental prosthesis. The introduction of a bioceramic coating greatly improves the screw stability and hence its life expectancy [75].

HA coatings deposited by plasma spraying are extremely diffused in medical practice. This kind of coatings has been used on metallic implants in dentistry and orthopaedics since the middle of the ’80s [44]. Accordingly, numerous studies have investigated the behaviour of these coatings.

1.3.1 Properties of bioactive coatings

The microstructure of coatings strongly depends on the production technique and on the

feedstock materials. Generally speaking, a good coating should have a compact structure, small grain size with high cohesion, and no defects such as cracks or large pores [9]. A defect-free microstructure usually results in good mechanical properties and resistance. If functional coatings are considered, such as bioactive ones, these parameters may not be the most important ones. In fact, although a good adhesion and cohesion are essential properties for all kinds of coatings [76], other properties can play an important role. As far as the bioactivity is concerned, porosity is a crucial parameter, since it influences the interactions at the implant-host tissue interface, especially the reaction rate. In fact, the open porosity controls the specific area in contact with body fluids [77, 78]. Moreover a porous coating allows a deeper penetration of cells inside the biomaterial, and thus higher levels of cell attachment can be reached [79]. Porosity can also be a way to tune the stiffness of a material, as it happens for natural bones [80]. In this way, it is possible to reduce the stiffness of biomedical materials, to match that of natural bone tissue, thus limiting the so-called “stress shielding” effect [40]. On the other hand, an excessive porosity can lead to poor cohesion and low bonding strength, which may cause some parts of the coating to peel off during the dissolution process. It is worth noting that debris and fragments from bioactive materials are usually innocuous from a chemical point of view [81]. In commercial HA coatings, the porosity may vary from 1% up to 50% [44].

Also the surface roughness of a bioactive coating affects the dissolution rate and bone growth. In fact, the surface exposed to the physiological medium increases with increasing roughness. Moreover the beneficial effect of morphological and biological fixation becomes relevant. A marked roughness is also positive for the biological activity, since the surface asperities promote both the absorption of organic metabolites and the cell attachment [82].

Another key parameter is the coating thickness. The thickness, indeed, affects both the resorption and the mechanical properties of bioactive coatings. Most of the commercial coatings for orthopaedic use are produced in the thickness range 50-75 μm [44]. Lynn and DuQuesnay [83] tested the mechanical fatigue resistance of plasma sprayed HA coatings with a thickness ranging from 0 to 150 μm. The Authors observed that, if the coating thickness is lower than 100 μm, it does not affect the fatigue life of the substrate. Instead when a thicker coating (150 μm) is applied, the fatigue life of the substrate is reduced. During the test, the coatings did not peel off if their thickness was in the 25-50 μm range. On the contrary, 75-150 μm thick coatings delaminated but, in this case, the substrate’s failure occurred before the coatings’ one. In fact, the metal of the substrate cracked before the coatings delamination.

Yang et al. [84] analysed the effect of the coating thickness in intramedullary implantations in canine femora. The coatings were plasma sprayed and two different thicknesses were tested: 50 and 200 μm. The study demonstrated that the 50 μm thick implants performed better than the 200 μm ones. In fact, the thinner deposits showed a greater adhesion to the substrate, and also a higher shear strength at the coating-cancellous bone interface. Consequently, as regards the HA coatings, the optimal thickness should not exceed 100 μm. However, for highly bioactive coatings, Borrajo et al [85] recommend thickness values greater than 30 μm. In fact very thin coatings may be completely dissolved before the formation of the HCA layer occurs.

1.3.2 Hydroxyapatite coatings

1.3.2.a Clinical performances

HA coatings have been widely studied, and their clinical performance has been determined also in the long term.

The first clinical trials of HA coatings date back to 1985 when Furlong and Osborn [86] applied a coating on femoral stems. Besides the femoral stem, which still remains the major application for HA coatings, other common destinations are knee implants, screws for fixing bone fractures, and dental prostheses.

Some applications, such as bone screws, are not permanent, since they must be removed. In that case, the purpose of the HA coating is to accelerate as much as possible the fixation of the prosthesis. Since these implants must be removed after few months, the force required for their extraction may be indicative of the bone bonding ability of the HA coating. For example, Sandén et al. [87] studied the effects of HA coatings on the pedicle screws. Three groups of patients were arranged: the first one received uncoated stainless-steel screws, the second one screws which were partly coated with HA, and the third one screws which were fully coated. The torque required to remove the completely coated screws was approximately 20 times greater than that necessary to extract the uncoated screws. The partially coated screws required an extraction torque about 15 times higher than that of uncoated screws. These results indicate that, in the medium term, the HA coatings greatly increased the bone-implant adhesion.

It is commonly recognized that HA coatings favour the prosthesis adhesion and also the long term stability. Rajaratnam et al. [88] performed a long-term study on femoral components in total hip replacement. The Authors reported that, after 21 years, only 2.6% of the HA-coated prostheses failed. These results are better than those obtained with uncoated or cemented

prostheses. Similar conclusions were achieved by Melton et al. [89], who worked on the total knee replacement. The Authors reported that osteolysis was observed only in the 4.5% of analysed implants. Furthermore, more than 96% of the implants survived up to 18 years without aseptic loosening. These data indicate that HA-coated total knee prostheses have a survival rate comparable or even superior to that of cemented ones. Even in dental implants, some advantages have been observed thanks to the use of HA-coated screws [90]. Nevertheless, some studies claim that HA-coated prostheses have a frequency of success similar to that of uncoated implants. For example Simunek et al. [91] reported that in root-form dental implants the failure rate of HA-coated implants is analogous to that observed for uncoated ones. Moreover, the same Authors observed a high marginal bone loss, which may be negative for the implant. Therefore the effectiveness of HA coatings greatly depends on the prosthesis type and destination [44].

Year	Installation	Net power	Phase composition	Porosity [%]	Adhesion [Mpa]
2000	Metco, USA	37.7	high ACP, CaO (XRD)	-	13 for pure HA, 17.3 HA + 60%Ti
2001	Plasma Technik M1100C, Switzerland	40.2	-	3.5-4	2.7-9.2
2003	SG-100 Praxair, USA	12	Strong CaO peak, high ACP	18.9	18.5
2003	Metco 3MB, USA	27.5-42	Strong CaO peak at 42 kW	12 - 7	-
2004	Plasma Technik M1000, F4 gun	28	65% cryst. HA35% ACP	-	-
2005	Sulzer Metco, F4 gun, (VPS)	45.2	n.a. except by XRD: low: cryst. HA; high: ACP, TCP, TTCP, CaO	-	4.5-6
2007	Metco 3MB	35	HA, TTCP, TCP, ACP, CaO	-	18.1-24.1
2008	Metco 3MB	28-36.4	70-55% HA 10.7-13.9% TCP, 4.1-6.9% TTCP, 4.7-10.9% CaO, 10.7-13.2% ACP (low to high power)	10.7-9.1 (low at high power)	-

***Table 1.3**:* Overview of used plasma installations, power ranges and characteristics of the deposited HA coatings. Adapted from [92].

1.3.2.b Innovative thermal spray techniques

Although the production and the clinical use of HA coatings are well established, the study of new coatings is still in progress. The research is addressed to define innovative post-spray treatments, composite coatings, and deposition techniques.

For example Vilotijević et al. [92] used an innovative PJ-100 plasma installation. The plasma jet generated by means of this equipment has improved characteristics with respect to the one generated by a conventional torch. In particular, the plasma reaches a laminar flow condition, with a speed which is 5-10 times higher than that usually observed for conventional installations. The resultant HA coatings showed a low porosity (0.4-1.1%) and a high amount of fully molten particles. Moreover coatings with a degree of crystallinity higher than 80-90% could be obtained, with an adhesion strength greater than 60 MPa. Unfortunately no *in vitro* or *in vivo* tests were performed to assess the bioactivity of the coatings. This is a key point, since the low porosity and the high degree of crystallinity conferred good mechanical properties to the coatings (see Table 1.3), but they are also expected to hinder the reaction kinetics, which induces great stability and weak bioactivity.

Yugeswaran et al. [93] used a gas tunnel type plasma torch, namely a high-power plasma jet, to produce HA and Yttria Stabilized Zirconia (YSZ)-HA composite coatings. The torch has a double anode and a special design which drives the gases to form a vortex and to move in a tunnel-like shape. The plasma jet is affected by the gas movement, and the efficiency of the deposition process is higher than that of traditional plasma spray. The addition of YSZ significantly increased the coating hardness and corrosion resistance, while the porosity and sliding wear rate were reduced. Both the composite coatings and the HA ones were able to promote the development of HCA *in vitro*, after 10 days of immersion in SBF. The coatings were not cytotoxic.

Low power torches may represent an alternative approach. Demnati and co-workers [94] designed a portable low-energy plasma device to spray HA coatings. The aim was to coat small-sized prostheses with complex geometries using a relatively simple and small equipment, without the need for high technical requirements (power supply, water cooling rate, exhaust...). By means of this new system, high-crystallinity coatings were produced.

Another new technique suitable for the production of HA coatings is the SPS. One of the first example of bioactive coatings produced by means of SPS was proposed by Tomaszek et al. [10]. The Authors demonstrated the flexibility of this method by producing different types of TiO_2-HA composite coatings. In fact, they analysed both pure HA coatings with a TiO_2 bond

coat, and TiO_2-HA graded coatings. The addition of TiO_2 was expected to increase the coating adhesion.

Further investigations allowed to determine the optimal parameters for the deposition of HA via SPS [95, 96]. The coatings were also analysed by means of *in vitro* tests, in order to assess their bioactivity [25]. As expected, the HA behaviour was influenced by the deposition parameters. From a microstructural point of view, highly crystalline HA coatings, with a degree of crystallinity exceeding 90%, could be produced. Quite interestingly, the deposits showed a peculiar microstructure including dense zones with well molten big lamellae and sintered zones with very fine sub-micrometric grains [25]. The coexistence of these different morphologies suggests that the particles followed multiple trajectories inside the plasma, which were characterised by different heating conditions. Two different methods of suspension injection were also tested: continuous stream jet and pneumatic atomization; the former was preferred [95, 96].

1.3.2.c Post-spray treatments

Another way to improve the properties of HA coatings is to perform post deposition thermal treatments; the greatest part of these treatments are designed to increase the crystallinity and reduce the porosity of the coatings. Among post-spray processes, furnace heat treatments, and laser treatments are the most important. They are able to increase the degree of crystallinity and to convert the decomposition phases into HA.

Lu et al. [97] investigated the effects of time and temperature: temperatures were in the 500-800 °C range, while the times were in the 2-6 hours range. The Authors observed that temperature had a stronger efficacy with respect to time.

Yang [98] analysed the adhesion of plasma-sprayed hydroxyapatite coatings after a heat treatment in vacuum conditions. Treatments in the 500-600°C range were effective to release the compressive residual stresses in HA coatings and hence to increase the adhesion to the substrate. Nevertheless the adhesion strength dropped if the coatings were processed at temperatures exceeding 600°C.

An alternative solution is given by laser treatments, which are superficial and therefore they do not involve the substrate nor cause adverse interface reactions between coating and substrate. On the other hand, laser treatments require a careful setting of the processing parameters to reach an adequate depth [99], and, most of all, to avoid a further decomposition of HA [100].

A different type of post spray treatment is the water vapour treatment. Cao et al. [101] performed a post spray water vapour treatment keeping the samples at 125 °C in water vapour for 6 hours. The process promoted the transformation of the amorphous and secondary phases into crystalline HA, thus reducing the amount of TTCP, TCP and CaO.

The water vapour positively affects HA in post-spray treatments, but also during the deposition process. In fact a steam treatment during spraying may reduce HA decomposition and loss of OH^- groups [17]. It is worth noting that post spray treatments generally increase the mechanical properties and the stability of HA coatings, but they also imply a reduction of bioactivity [101-103]. This is caused by the increase in the degree of crystallinity and the reduction of the porosity.

1.3.2.d HA-based composite coatings

As previously discussed in the case of TiO_2-HA samples, a different approach relies on the production of composite coatings, in which the powders of two or more materials are processed simultaneously. HA-based composite coatings are generally designed to increase the mechanical properties and the adhesion with respect to pure-HA ones. For example, HA-Ti alloy composite coatings [104-106] have been proposed to reduce the difference between the coefficients of thermal expansion (CTE) of the coating and the substrate. Moreover the addition of a metal can increase the toughness of HA coatings.

Also ceramic powders, such as ZrO_2 [93, 107], can be sprayed with HA to produce coatings with high mechanical properties. The ZrO_2 addition, in fact, confers greater hardness and wear resistance to the coating. Secondary phases are generally added to a HA coating in order to increase its mechanical properties. Sometimes composite systems are produced to enhance the HA bioactivity. In fact, since bioactive glasses have the greatest bioactivity, they can be used to boost the HA reactivity. Carvalho et al. [108] for example, produced bioactive glass-HA composite coatings which exhibited greater bioactivity than HA ones.

Also multi-layered coatings, which include various strata of different composition, are special multi-phase systems and, in this respect, they may be assimilated to “composite materials”. The simplest example is given by the introduction of an appropriate bond-coat, which is an additional layer applied between the coating (more precisely, the “top coat”) and the substrate. The addition of a bond layer may offer several advantages, and primarily it improves the adhesion of the coating to the substrate. Bond coats are generally composed of TiO_2 [10, 109] if the substrate is a Ti alloy, but they may also be produced with ZrO_2 or other materials [110].

A further evolution of this approach is the production of graded coatings, whose composition gradually changes as a function of depth [10, 103, 111, 112]. In this way, the additional interface between the bond coat and the topcoat is eliminated, and the variation of properties within the coating is more gradual. Generally speaking, this leads to improved properties with respect to standard bi-layered systems [10].

Of course, the introduction of a bond coat or the production of a graded coating are expected to preserve the system bioactivity, since the external surface is still made of a bioactive material. Instead, if a composite coating combines HA with a bioinert second phase, the overall bioactivity may be dramatically reduced. Moreover the introduction of bioinert particles within a coating which is intended to be biointegrated can be dangerous. In fact, although the debris resulting from HA coatings do not injure the host tissue, bioinert particles could have negative effects. These debris, indeed, are not reabsorbed, so they can reside within the human body for long time [113] and the risk that they could drift to a junction is therefore high.

1.3.3 Thermal sprayed bioactive glass coatings

Only few articles in the literature report the clinical use of bioactive glass coatings. For example, Alonso-Barrio et al. [114] discussed the use of bioactive glass coatings applied to stems in hip replacements. The study was carried out over a period of 8 years, and the survival rate of the prostheses was greater than 91%.

However, the greatest part of the literature refers to preliminary research studies on the production and characterization of bioactive glass coatings. Both *in vitro* and *in vivo* tests have been carried out, but the results are not enough to define the clinical performance of bioactive glass coatings in a definitive way.

The first studies on bioactive coatings produced by thermal spraying date back to the middle of the ’90s [115]. These investigations showed that thermal spraying does not induce a significant crystallization on bioactive glasses, and that their bioactivity is not adversely affected by the process.

1.3.4.a Adhesion of bioactive glass coatings

One of the major problems, which still limit the use of bioactive glass coatings, is their poor adhesion to the substrate [37]. Several methods have been proposed to solve this problem. For example, the substrate can be pre-treated by sand-blasting [116-118]. Through this process,

the roughness of the substrate is increased. Consequently the contact area between coating and substrate is increased and the irregularities on the surface may favour a mechanical fixing of the coating.

As previously mentioned, a method to increase the coating adhesion is to reduce the interfacial stresses due to the CTE mismatch. Verné et al. [119] produced a titanium-bioactive glass composite coating on a Ti-6Al-4V substrate. In this way the residual stresses due the CTE mismatch were reduced. Moreover the addition of titanium to the coating did not affect the bioactivity of the bioactive glass.

Another method to improve the coating adhesion is to introduce a bond coat. For example, Lee et al. [117] proposed to deposit a titanium bond coat upon a Ti-6Al-4V substrate. As already seen for the sandblasting procedure, the purpose of the interlayer was to increase the roughness of the substrate so as to promote a strong mechanical bonding of the top coat. Instead Goller [116] introduced a 20 μm thick ceramic bond coat. The interlayer was made of Amdry 6250 (60% Al_2O_3, 40% TiO_2), and it increased the coating bonding strength of about three times. The Author focused on a ceramic bond coat, instead of a metal one, because its coefficient of thermal expansion (CTE) is more similar to that of the bioactive glass. In this way, the residual stresses can be significantly reduced. Moreover the Amdry interlayer may act as a barrier between the biological environment and the metallic substrate. Accordingly the diffusion of metal ions from the substrate, as well as the corrosion of the substrate, can be significantly reduced.

1.3.4.b Innovative thermal spray techniques

Several studies have been focused on the production of bioactive glass coatings by means of innovative technologies .

An interesting evolution of the standard PS technique is the reactive deposition [118, 120, 121]. In this method, the synthesis of the glass is contextual to the deposition. Therefore the preliminary step to produce the glass (for example, by standard melting techniques or sol-gel method) is bypassed. In order to minimise the unavoidable gradients in the glass composition, Helsen et al. [118] produced an aqueous suspension of the raw materials required to produce the glass. Then the suspension was mixed in an attritor and spray dried. The obtained powder was then pressed and sintered, and finally the sintered material was milled to obtain the feedstock powder for the PS process.

The powder production required several steps, but this method avoided the preliminary glass

melting and grinding procedures, which are highly energy- and time-consuming.

The coatings obtained via reactive deposition were bioactive. Moreover, a special adhesion test was designed to reproduce the real condition of use, and the coatings showed a good adhesion to the substrate even after *in vitro* trials [120, 121].

Another non-conventional thermal spray technique used to produce bioactive glass coatings is the high velocity suspension flame spray (HVSFS) [24, 122-124].

HVSFS is an evolution of HVOF, in which the torch is modified to enable the direct injection of liquid suspensions instead of dry powders. Consequently the technique allows the use of sub-micrometric and nanometric powders. Bolelli et al. [124] used HVSFS to coat Ti plates with the AW glass-ceramic. The so obtained AW coatings showed a dense structure with a good interlamellar cohesion and limited porosity. The activity in SBF of the coatings was remarkable, inducing the formation of a silica rich layer and HCA crystals. However, the HCA did not create a continuous superficial layer, but it formed various spots dispersed throughout the coating thickness. Bolelli et al. [24] produced also Bioglass® 45S5 coatings via HVSFS. The resulting coatings showed a microstructural gradient, with a small and dispersed porosity in the deeper layer and larger and spherical pores in the superficial layer. This effect is probably due to a viscous flow sintering of the superficial layer. The surface was supposed to reach temperatures high enough to activate the sintering process thanks to the deeper layer which acts as a thermal barrier during the spray process. The coatings showed a high biocompatibility, as demonstrated by *in vitro* tests carried out with osteoblast-like cell. The same research group also studied the production of coatings by HVSFS using high reactivity bioactive glass, both with [122] and without [123] a TiO2 bond coat. The coatings proved to be extremely reactive *in vitro*. Furthermore, their entire thickness reacted with SBF and hence, after soaking, only some residual bioactive glass particles were present in the coatings. Most of the glass was transformed into silica gel and HCA. The TiO_2 bond coat improved the adhesion of the coatings to the substrate without altering their microstructure.

Xiao et al. [125] used a liquid precursor plasma spraying process to produce Bioglass® 45S5 coatings. The process consists in the injection of liquid precursors inside the plasma. The chemical reagents react during the deposition giving rise to the glass. The precursors were the same organic compounds used in the production of glass by the sol-gel method. The coatings consisted of two phases: an amorphous phase and a secondary crystalline phase of calcium-sodium-silicate. As often observed in coatings produced by PS using a liquid feedstock, the surface exhibited areas with two different morphologies, namely pancake-like splats and

nanoscale spherical particles. The coatings were tested in SBF: HCA was observed already after 4 hours of soaking. The HCA layer continued to grow as soaking time increased.

Year	Tech.	Substr.	Coating Composition	Thickness [µm]	Adhesion Strength [MPa]	
1995	PS	Ti6Al4V	Biovetro®	80	21-32 [N]*	
1995	PS	Ti6Al4V	glass [wt.%: 50 SiO_2, 25 CaO, 15 Na_2O, 10 P_2O_5]			
			HA, composite, glass [wt.%: 50 SiO_2, 25 CaO, 15 Na_2O, 10 P_2O_5]			
1996	PS	Ti6Al4V	Ti bond coat + Bioglass® 45S5	130+50		
1997	React. PS	Ti	glass [wt.%: 52 SiO_2, 30.5 CaO, 9.8 Na_2O, 6.2 P_2O_5, 1.5 CaF_2]	150	>35**	
1998	VPS	Ti6Al4V	AP40/TAP/RKKP	150	21-22 (1.5)**	
			AP40/TAP/RKKP, composite, Ti			
1998	PS	Ti alloy	Biovetro®	80		
1999	PS	Ti6Al4V	HA, composite, Bioglass® 45S5	160		
1999	React. PS	Ti6Al4V	glass [wt.%: 52 SiO_2, 30.5 CaO, 9.8 Na_2O, 6.2 P_2O_5, 1.5 CaF_2]	50	40.1 (4.8)**	
					69.4 (9.4)^	
2000	React. PS	Ti6Al4V	glass [wt.%: 52 SiO_2, 30.5 CaO, 9.8 Na_2O, 6.2 P_2O_5, 1.5 CaF_2]	50	48.6 (7.9)**	43.6 (1.1) post *in vitro***
					84.2	75.5 post *in vitro*
2000	PS	Ti6Al4V	HA, composite, glass [wt.%: 50 SiO_2, 25 CaO, 15 Na_2O, 10 P_2O_5]	100-130	52-56#	<20 after 30 days *in vitro*#
			HA	120	53.6#	
2001	PS	Ti6Al4V	glass [wt.%: 50 SiO_2, 20 Na_2O, 16 CaO, 6 P_2O_5, 2 Al_2O_3, 1 MgO]	50-100		
2004	PS	Ti	Amdry 6250 bond coat + Bioglass® 45S5	20+80	27.18 (2.24)#	8.56 (0.57) no b-coat #
2009	HVSFS	Ti gr2	AW-glass	100		
2010	HVSFS	Ti gr2	BioK	50-60		

Table 1.4: Properties of bioactive glass coatings produced via thermal spray. Adapted from [126]. Values in the bracket indicate standard deviation. *Scratch critical load. **Shear test. ^ Tensile test (derived from shear test). #According to ASTM C-633

1.3.4.c Composite coatings

In order to combine the high bioactivity of bioactive glasses with the specific characteristics of different materials, composite coatings can be produced. For example, as mentioned above,

the reduction of the CTE mismatch between substrate and coating can be achieved by means of composite systems, but other types of functionality can be developed in this way. For example, bioactive glasses have the highest bioactivity index among biomaterials, while plasma sprayed HA coatings usually show better stability than bioactive glass ones [114, 127]. Then, the production of bioactive glass-HA composite coatings can be a successful approach to improve the performance of bioactive coatings and also to control their bioactivity rate. In fact, the higher the HA volume fraction, the higher is the long term stability. Then, it is possible to obtain coatings with the desired resorption rate by modifying their microstructure and composition [108, 128, 129]. Moreover, the HA may increase the mechanical properties of the coating; in particular the adhesion with the substrate.

Chapter 2:

Experimental Procedures

2.1 Comparison of different bioactive glasses by means of *in situ* Raman spectroscopy during *in vitro* tests.

(Published: D. Bellucci, G. Bolelli, V. Cannillo, A. Cattini, and A. Sola. In situ Raman spectroscopy investigation of bioactive glass reactivity: Simulated body fluid solution vs TRIS-buffered solution. Materials Characterization. (2011) pp. 1021-1028.)

2.2 Suspension plasma sprayed bioactive glass coatings.

(Published: A. Cattini, L. Łatka, D. Bellucci, G. Bolelli, A. Sola, L. Lusvarghi, L. Pawłowski, and V. Cannillo. Suspension plasma sprayed bioactive glass coatings: Effects of processing on microstructure, mechanical properties and in-vitro behaviour. Surface and Coatings Technology. 2012 . DOI:10.1016/j.surfcoat.2012.10.076 Article in press)

2.3 Production and *in vitro* characterization of hydroxyapatite coatings with and without a bioactive glass topcoat.

2.4 Suspension Plasma Sprayed hydroxyapatite/bioactive glass composite coatings. Comparison of different microstructures.

2.5 Production and characterization of a graded hydroxyapatite/bioactive glass coating.

2.1 *Comparison of different bioactive glasses by means of in situ Raman spectroscopy during in vitro tests.*

Introduction

In this study, *in situ* Raman micro-spectroscopy was applied to investigate the *in vitro* reactivity of various bioactive glasses [130]. Three experimental bioactive glasses belonging to the $Na_2O\backslash K_2O$ - CaO - P_2O_5 - SiO_2 system were analysed, moreover the standard 45S5 Bioglass® was considered as a term of comparison. The compositions of the three new glasses were inspired by the 45S5 Bioglass®. In particular, a novel glass composition, named BioK, was obtained by substituting the sodium oxide with potassium oxide in the 45S5 Bioglass® formulation; in this case, the potassium oxide was expected to reduce the tendency of the parent glass to crystallize during possible processing and/or sintering treatments [66]. The composition of the other glasses, named BG_Na and BG_Ca, were formulated in order to contain respectively as much Na_2O and as much CaO as possible, still remaining within the region A (Fig. 2.1) of the Na_2O-CaO-SiO_2 ternary diagram. In fact, compositions belonging to the region A are able to form strong bonds with living tissues, hence the region is known as the "bioactive bonding boundary" [131].

In the present study, in order to simulate the *in vivo* environment, a simulated body fluid (SBF) was used, according to the protocol developed by Kokubo et al. [34]. Moreover the same experiment was carried out immersing the glasses in a simple TRIS-buffered solution [132], taken as a reference. In this way, two fundamental items were addressed, i.e. the effect of the glass composition and the nature of the soaking fluid on the overall reactivity.

Raman spectroscopy was chosen as the technique of analysis since it is virtually insensitive to water or aqueous solutions, therefore it can be performed directly *in situ* during *in vitro* tests. In this way, it is possible to go deep inside into the reaction mechanisms, since glass modifications can be followed directly in solution, thus avoiding any air-induced contamination or ageing.

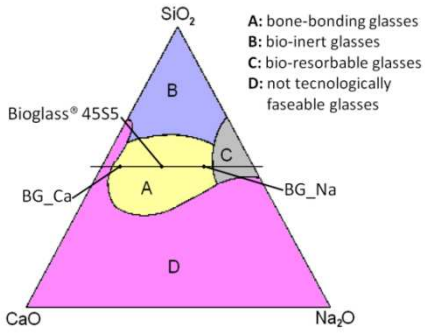

Figure 2.1: Na_2O-CaO-SiO_2 ternary diagram showing the compositions of the glasses under examination. The P_2O_5 amount is fixed at 2.6 mol%.

2.1.1 Materials and methods

2.1.1.a Bioactive glasses

The glass compositions are reported in Table 2.1. The experimental glasses (BG_Na, BG_Ca and BioK) were produced from commercially available raw powders (SiO_2, Na_2CO_3, $CaCO_3$, $Na_3PO_4 \cdot 12H_2O$, $Ca_3(PO_4)_2$, $K_3PO_4.H_2O$ and K_2CO_3 by Carlo Erba Reagenti, Italy), which were properly weighted (Table 2.2), mixed in a laboratory shaker for 2 h and melted in a platinum crucible. The following thermal cycle was performed: heating from room temperature to 1100°C at 10°C/min; holding at 1100°C for 1 h; heating from 1100°C to 1450°C at 10 °C/min; holding at 1450°C for 30 min. The melt was cast into a graphite mould at room temperature and annealed at 550°C for 2 h.

	Na_2O	K_2O	CaO	P_2O_5	SiO_2
Bioglass® 45S5 [30]	24.4	-	26.9	2.6	46.1
BG_Na	33	-	15.6	2.6	48.7
BG_Ca	4.6	-	45.6	2.6	47.2
BioK	-	24.4	26.9	2.6	46.1

Table 2.1: Composition (molar %) of the analysed bioactive glasses.

Samples were cut and ground to the desired size (10 × 10 × 5mm) using SiC papers. Polishing was performed on a short nap cloth using diamond pastes (3 and 0.5 μm) and an alcohol-based lubricant. Samples were then cleaned in an ultrasonic bath for 15 min in acetone and left to dry.

	SiO_2	$Ca_3(PO_4)_2$	$CaCO_3$	$Na_3PO_4.12H_2O$	Na_2CO_3	$K_3PO_4.H_2O$	K_2CO_3
BG_Na	32.1	-	17.1	21.6	29.2	-	-
BG_Ca	35.8	10.2	47.8	-	6.2	-	-
BioK	30.9	-	30.1	-	-	13.4	25.6

Table 2.2: Raw materials (expressed in g per 100 g batch) used to produce the analysed glasses.

2.1.1.b Soaking Fluids

A Simulated Body Fluid solution (SBF) was prepared according to the standard protocol proposed by Kokubo et al. [34]. A Tris-buffered solution (hereafter TRIS) was prepared by dissolving 6.1 g/l of tris(hydroxymethyl)aminomethane (Sigma-Aldrich, USA) in deionized water and buffering the pH of the solution at 8 using a 1 M HCl solution. For both solutions, the sample surface-to-fluid volume ratio was 20 ml/cm^2, as suggested by Kokubo et al. [34]. During the immersion tests, both fluids were refreshed every day [133].

2.1.1.c Experimental Set-up

Different glass samples were prepared for different solutions and times of immersion. Every glass sample was immersed in a beaker containing the soaking fluid - SBF or TRIS - which was continuously stirred and thermostated at 37 °C. Every sample was completely covered by the soaking fluid and the beaker was sealed to avoid any evaporation. At fixed time periods, i.e. 1.5, 6, 24, 48, and 96 h, in order to perform the Raman measurements, the corresponding sample was taken out from the beaker with its original soaking solution (SBF or TRIS) and transferred into a plastic capsule. Great attention was paid to keep every sample completely covered by the solution at any time, in order to avoid any contact with the atmosphere. Therefore, all the Raman spectra were acquired directly on immersed samples. In this way, no contaminations occurred and the samples did not undergo the drying and cracking phenomena which are frequently observed in the literature for conventionally analysed samples [134]. To conclude, after 96 h of immersion, the samples immersed in SBF were extracted, air-dried and transferred into closed capsules. The Raman spectra were acquired again one month later.

2.1.1.d Raman Instrument Details

Raman spectra were recorded by using a Jobin-Yvon Raman Microscope spectrometer. A laser emitting at 632.8 nm was employed, which had an output power of 20 mW at the sample. Photons scattered by the sample were dispersed by a 1800 lines/mm grating monochromator, and simultaneously collected on a CCD camera; the collection optic was set at 10×ULWD objective. The spectra collection set-up of ten acquisitions, each of them taking 40 s, was adopted. A preliminary test was performed in order to check the transparency of both soaking fluids to the laser beam employed in the Raman apparatus. Moreover Raman spectra were acquired on a commercial hydroxyapatite powder (CAPTAL® Hydroxyapatite, Plasma Biotal Ltd, UK) in order to have a direct term of comparison for the interpretation of the patterns collected on the bioactive glasses.

All spectra were normalized by re-scaling each pattern such that the difference between the maximum intensity and the minimum one was 100 (arbitrary unit).

2.1.1.e Microstructural Characterization

The effect of ageing on the samples microstructure (surfaces and polished cross-sections) was investigated by means of a scanning electron microscope, SEM (ESEM Quanta 200, FEI Co., Eindhoven, The Netherland). Moreover, a local chemical analysis was performed by X-ray energy dispersion spectroscopy, EDS (Inca, Oxford Instruments, UK). The SEM was operated in low-vacuum mode with a water pressure of 0.5 Torr.

2.1.2 Results and discussion

Figs. 2.2 and 2.3 show a series of *in situ* Raman spectra obtained on the considered bioactive glasses, put in contact with the SBF and TRIS solutions, respectively. The 200-1200 cm^{-1} spectral range was considered because the main peaks of both silicate glasses and HCA fall within this interval [135, 136]. For comparison purposes, the graphs of the as-produced glasses were reported as well. It is interesting to observe that the spectra of the original glasses (directly compared in Fig. 2.4a) present some similarities. In particular:

• A broad peak is present at about 635 cm^{-1}, which can be ascribed to the Si-O-Si groups. This peak is usually observed for glasses belonging to the Na_2O-CaO-SiO_2 system [137] and moves toward higher wave numbers for glass compositions with a low SiO_2 content [138]. Further peaks from 800 to 1150 cm^{-1} are associated to the Si-O-Si bond in silica tetrahedra with a different number of non-bridging oxygens (NBO). In particular, the 860 cm^{-1}, 920 cm^{-1} and 975 cm^{-1} peaks can be ascribed to monomers SiO_4 (4 NBO), dimers Si_2O_7 (3 NBO), rings and chains Si_2O_6 (2 NBO), respectively. Finally, the peak at about 1030 cm^{-1} can be assigned to vibrations involving two-dimensional structures Si_2O_5 (1 NBO) [137].

• Besides the silica features, in the spectra an intense band is present at 950 cm^{-1}. It can be assigned to the vibration (symmetrical stretching) of the PO_4 group [135]. This is the most intense peak, and it partially hides the aforementioned peak at 920 cm^{-1}; the peaks at 975 and 1030 cm^{-1} appear as shoulders on the right hand side of this peak.

• The BG_Na spectrum (Fig. 2.2b) resembles the 45S5 Bioglass® one (Fig. 2.2a). Nevertheless the peaks occurring in the 950-1100 cm^{-1} range are broader and stronger, especially the “shoulder” at about 1050 cm^{-1}. This is probably due to the higher Na_2O content

in the BG_Na composition, since this is a very strong modifier, which is likely to augment the Si-O-NBO vibrations and the stretching vibrations [138].

• The spectrum of the BG_Ca sample is similar to the previous ones, however the peak at 975 cm^{-1} is less visible, and there is an unidentified peak, at about 1002 cm^{-1}, which is probably related Si-O-Si stretching.

• Despite the aforementioned differences, the 45S5 Bioglass®, BG_Na and BG_Ca spectra look mutually similar since these glasses belong to the same Na_2O-CaO-P_2O_5-SiO_2 system. This analogy does not hold anymore when the BioK glass is considered, since its spectrum is sensibly different due to the presence of the K_2O instead of the Na_2O in the glass composition.

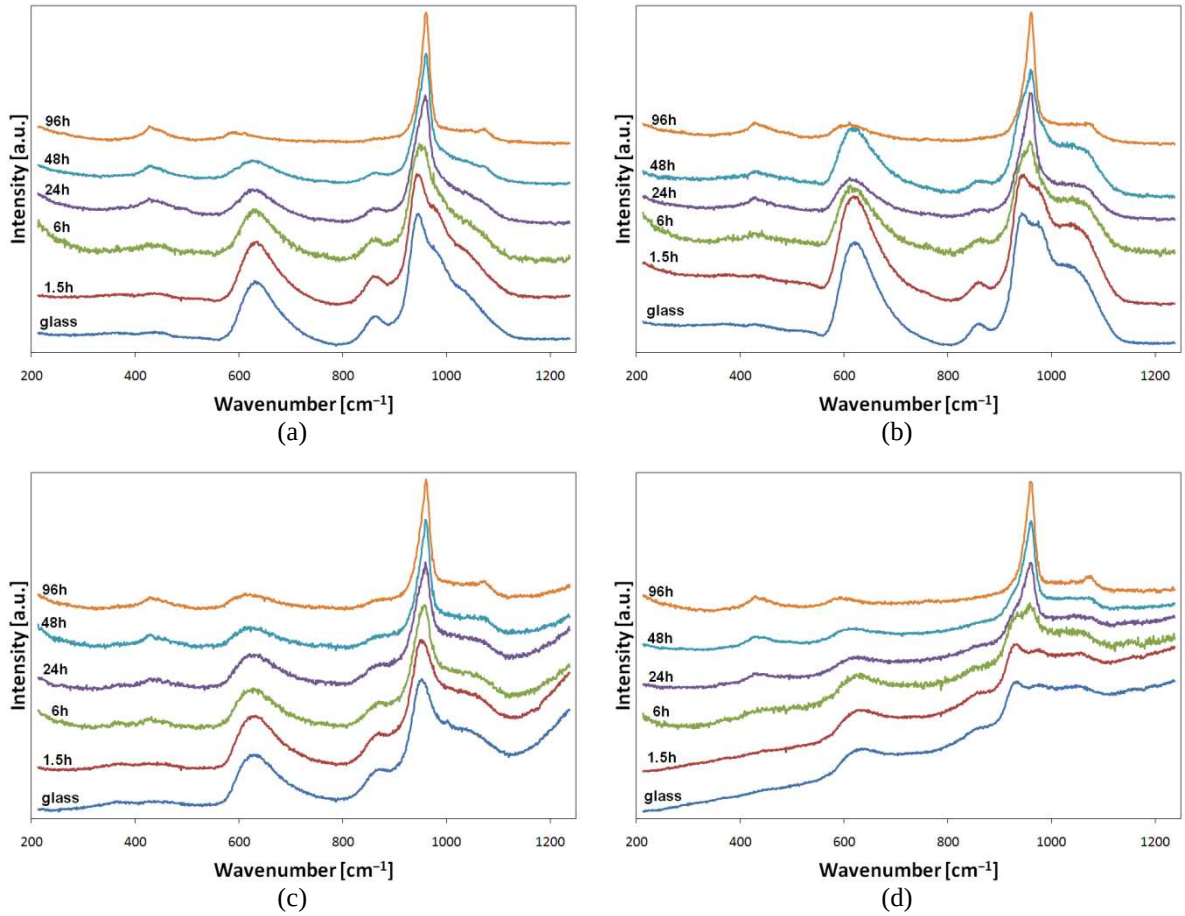

Figure 2.2: Raman spectra acquired on bioactive glasses immersed in SBF for different times: (a) 45S5 Bioglass®, (b) BG_Na, (c) BG_Ca, (d) BioK

When the bioactive glasses react in TRIS or SBF solution, their spectra evolve gradually, as reported in Figs. 2.2-2.4. In particular, as shown in Fig. 2.4b, the spectra of the samples immersed 96 h in SBF become very similar to that of commercial hydroxyapatite, which is also included in Fig. 2.4b as a term of comparison. It is interesting to observe that, independently of the glass composition, the main changes in the Raman spectra after immersion in SBF occur in the band at 800-1150 cm^{-1}. In fact, the peaks associated with the

Si-O-Si stretching vibrations become less intense, the peak associated with the PO_4 groups shifts to higher wave numbers (at about 960 cm^{-1}) while its relative intensity greatly increases. Moreover a peak at about 1070 cm^{-1} appears. This peak, which is associated to a carbonate group [139], is particularly pronounced for the reacted glasses compared to the hydroxyapatite spectrum (Fig. 2.4), since the *in vitro* grown hydroxyapatite is carbonated (HCA).

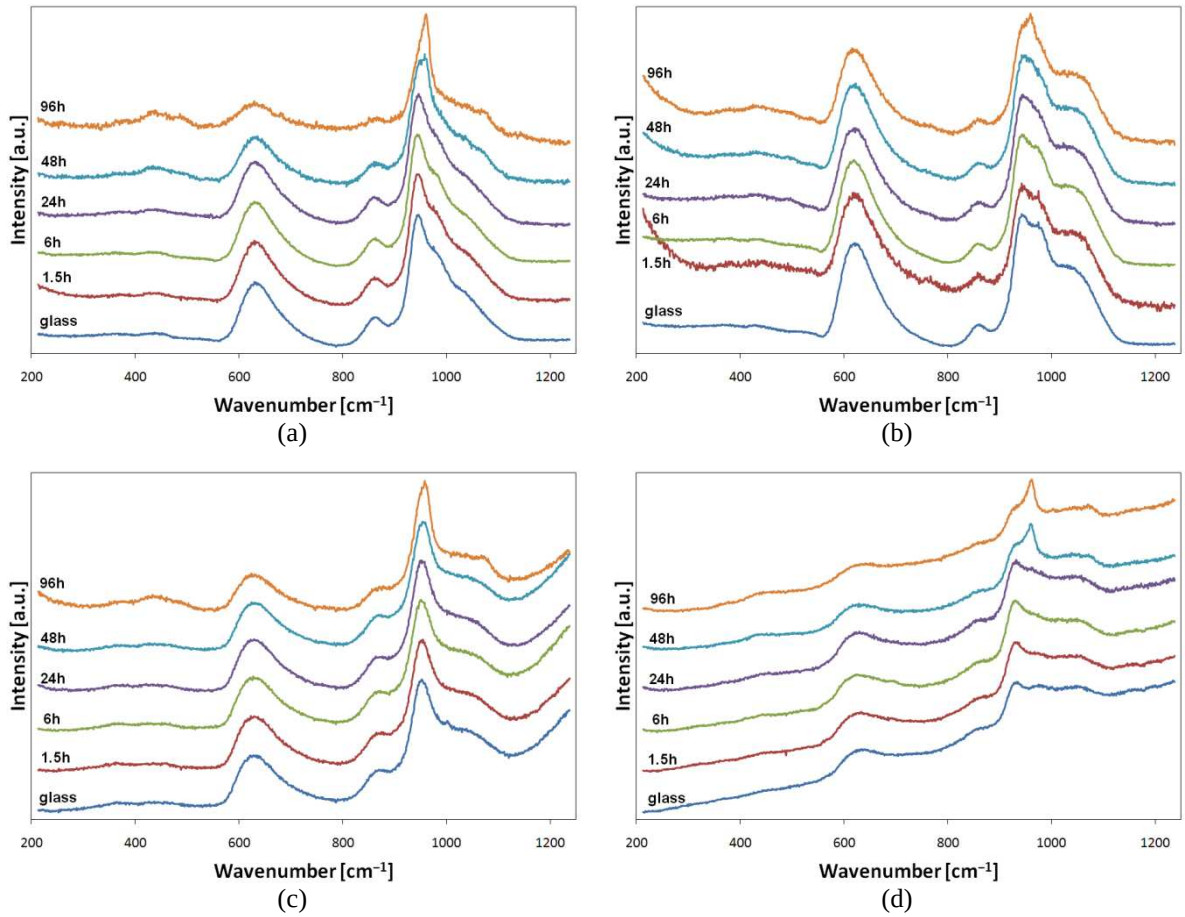

Figure 2.3: Raman spectra acquired on bioactive glasses immersed in TRIS for different times: (a) 45S5 Bioglass®, (b) BG_Na, (c) BG_Ca, (d) BioK

As already mentioned, all the samples show a similar evolution after immersion in SBF (Figs. 2.2 and 2.4b) however the direct comparison between the corresponding spectra proves that 45S5 Bioglass® and BioK are the glasses that promote a faster formation of HCA. In fact, already after 24 h, the main peaks of PO_4 shift to 960 cm^{-1}; then, after 6 h of immersion, a peak at 430 cm^{-1} appears. The peak at 860 cm^{-1}, which is associated to the SiO_4 monomers, disappears in all the spectra (except that of BG_Ca) after 96 h. When the spectra of the glasses soaked in TRIS (Fig. 2.3) are compared with those of the samples immersed in SBF (Fig. 2.2), it is possible to observe that the former fluid promotes a slower evolution than the latter. In particular, the spectra obtained after only 6 h in SBF (Fig. 2.2) are similar to those

acquired after 96 h in TRIS (Figs. 2.3 and 2.4c). The different reaction rate is mainly due to the composition of the immersion media. In fact, SBF is a solution supersaturated with respect to apatite [16], instead TRIS is basically a tris(hydroxymethyl)aminomethane solution in water and hence the ions necessary to form HCA entirely derive from the ion leaching phenomena and subsequent dissolution of the glass network. For this reason, the development of a HCA surface layer is easier in SBF than in TRIS, especially if the glass composition is relatively poor in calcium. This fact is confirmed by the spectra acquired on BG_Na (Fig. 2.3b), which is the glass with the lowest content of calcium among the presented samples. Indeed, the formation of HCA on the BG_Na samples immersed in TRIS is very slow and the typical peak of hydroxyapatite at 960 cm^{-1} is not very intense and defined even after 96 h (Fig. 2.4c). To conclude, it is worth noting that the peak at 1070 cm^{-1}, which is associated to the carbonate group, is slightly stronger in the spectra of the samples in TRIS than in those of the glasses in SBF. Since TRIS does not contain any carbonate ions, the shoulder at 1070 cm^{-1} could be due to carbonate species dissolved by TRIS from atmospheric CO_2.

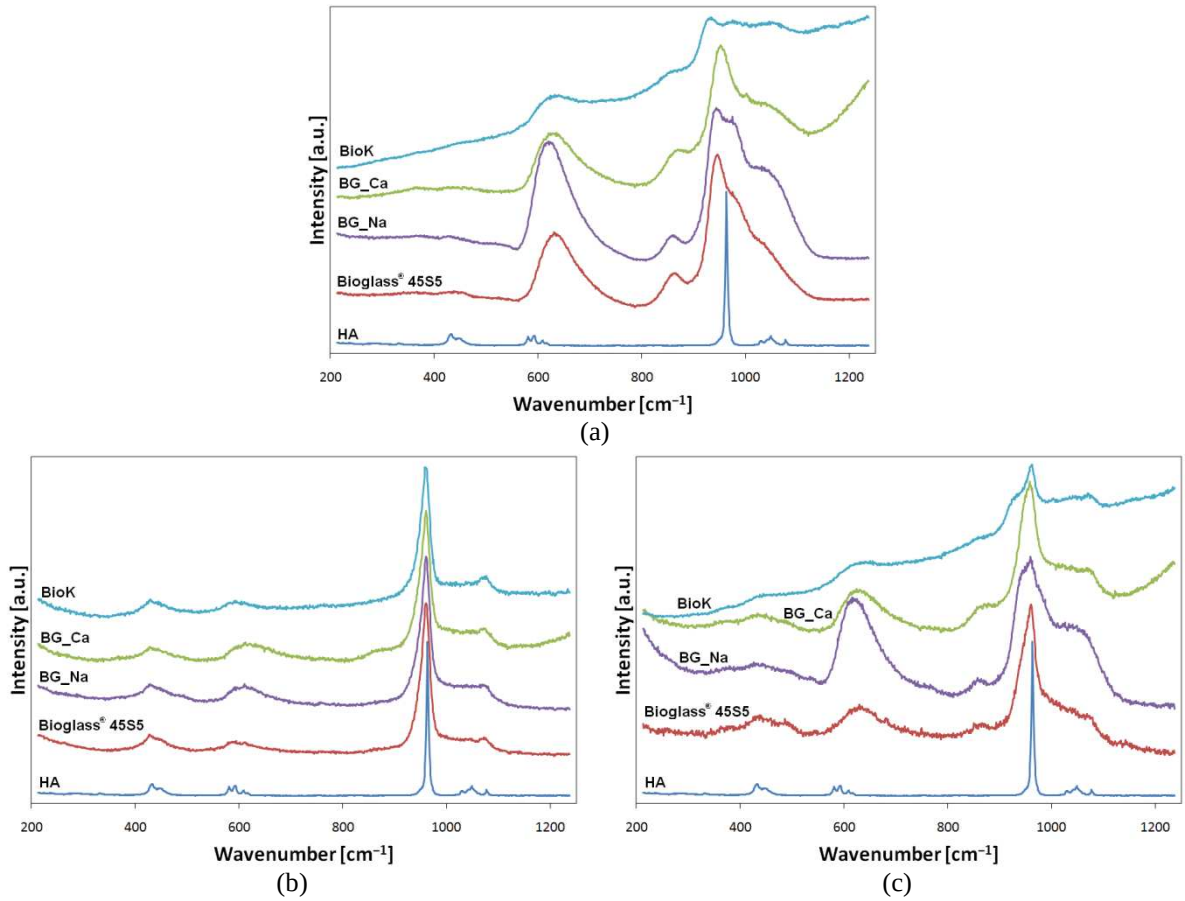

Figure 2.4: Raman spectra acquired on bioactive glasses, before and after soaking, compared with the spectrum of commercial HA: (a) As produced glasses, (b) glasses after 96 h in SBF, (c) glasses after 96 h in TRIS

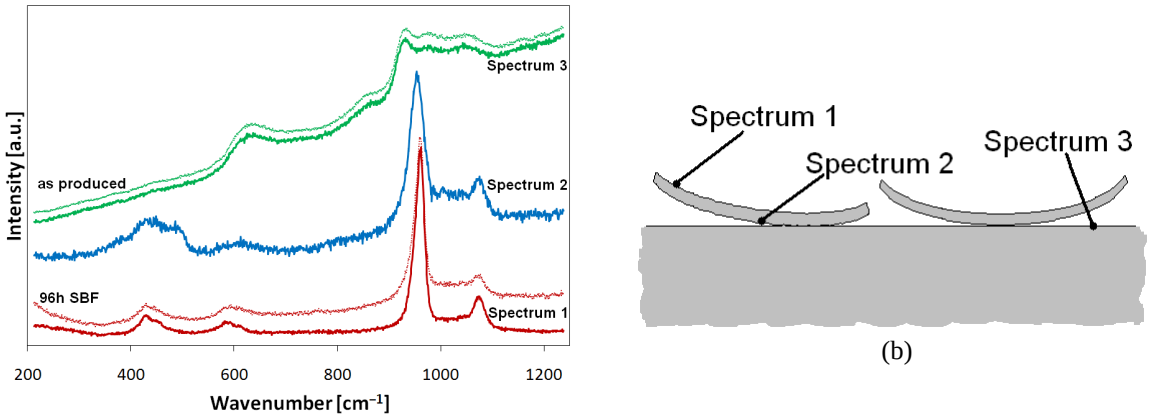

Figure 2.5: Effect of ageing on the BioK sample soaked in SBF:
(a) Raman spectra acquired on the locations indicated in (b), i.e. on the external surface of the flakes (Spectrum 1 — red bold line), the internal surface of the flakes (Spectrum 2 — blue bold line) and the underlying glass bulk (Spectrum 3 — green bold line). In (a) the spectra of the sample after 96 h in SBF (red faint line) and the as-produced glass (green faint line) are reported as well as terms of comparison.

Since the growth of HCA is more appreciable on the glasses immersed in SBF, these samples were further investigated. Once extracted from SBF, the glasses were kept in air (in a clean and safe place) for one month and characterized again (Fig. 2.5a). After the ageing in air, the surface of the samples appears completely changed, thus confirming the deep effect of air on the immersed glasses. In particular, the surface layer is macroscopically cracked and partly detached, as schematized in Fig. 2.5b. This phenomenon is very striking in all the investigated samples except for BG_Ca, whose surface layer looks adherent and crack-free. Raman spectra were acquired on the outer surface of the "flakes", on the inner surface of the flakes adhering to the underlying glass, and on the glass substrate itself (Fig. 2.5). Spectra acquired on the outer surface (Spectrum 1, Fig. 2.5) are virtually identical to those acquired before the extraction, except for the peak at 1070 cm^{-1} which, in this case, is more intense. This fact may be due to a further carbonation of the HCA layer occurred during the ageing. The spectra acquired on the internal surface of the flakes (Spectrum 2, Fig. 2.5) are similar to those of the HCA precipitated on bioactive glasses. However, these spectra show a broad band in the 300-550 cm^{-1} range, which can be associated to siliceous bulk vibrational modes, typical for silica gel [132], thus confirming the model originally proposed by Hench to explain the HCA precipitation on bioactive glasses [32]. Finally, the spectra of the glass substrate (Spectrum 3, Fig. 2.5) are very similar to those of the unreacted glasses. The effect of ageing on the microstructure at a local level was further investigated by means of a scanning electron microscope. Micrographs of the aged BG_Na and BG_Ca surfaces are reported in Fig. 2.6. The BG_Na and BG_Ca samples look rather similar. A silica gel layer covers the surface of both glasses. It is possible to observe white spherical micro-agglomerates, with the typical

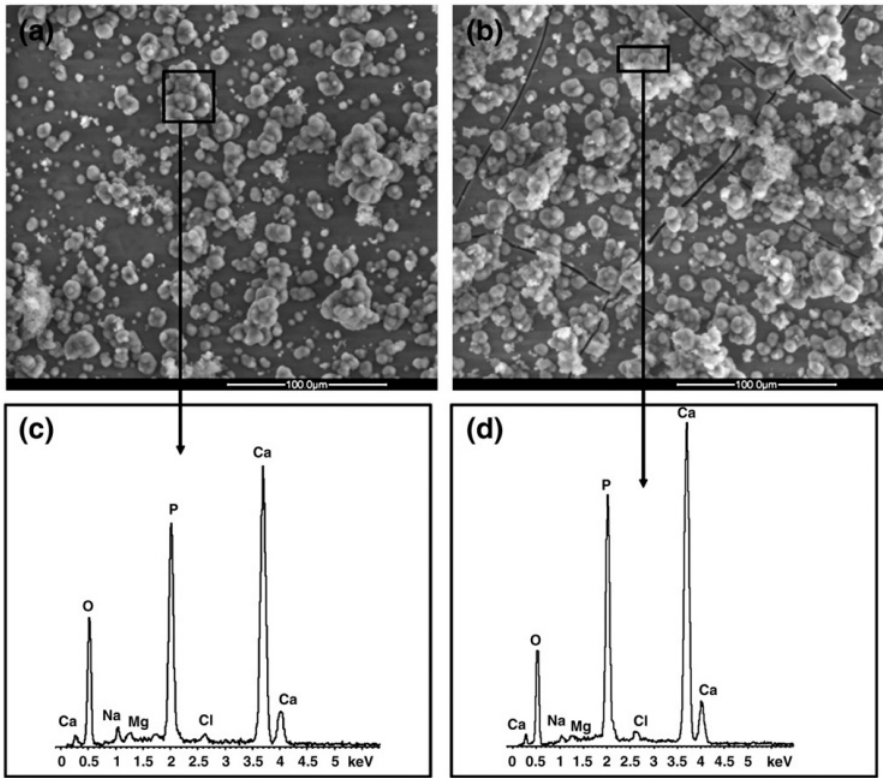

Figure 2.6: Micrographs of the BG_Na (a) and BG_Ca (b) surfaces after one month-ageing in air. (c, d): results of the EDS analysis carried out on the whole areas reported in (a) and (b).

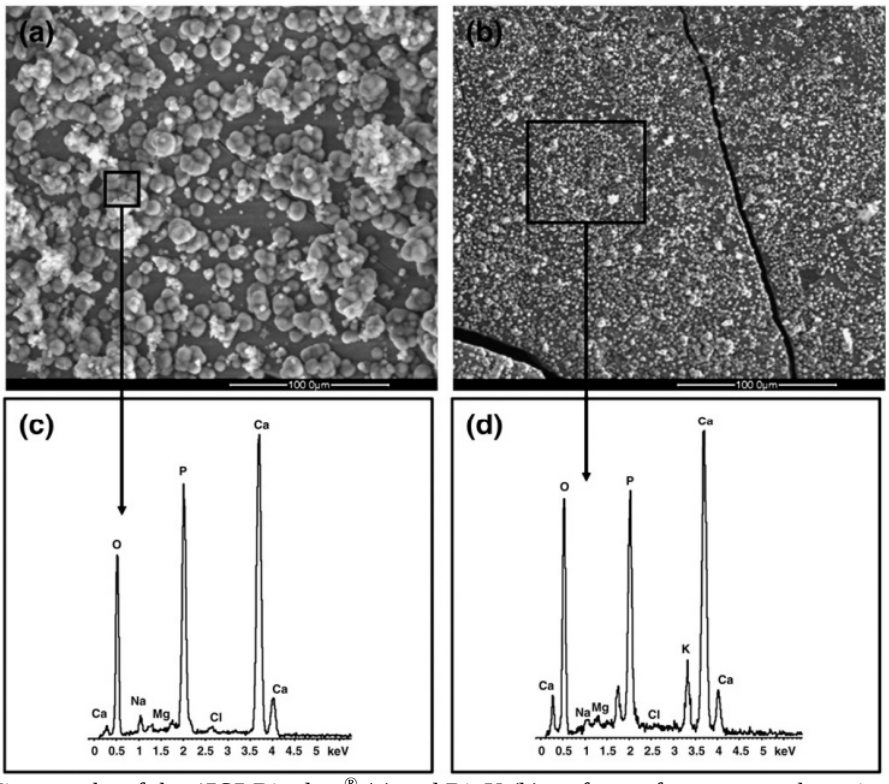

Figure 2.7: Micrographs of the 45S5 Bioglass® (a) and BioK (b) surfaces after one month-ageing in air. (c, d): results of the EDS analysis carried out on the whole areas reported in (a) and (b).

morphology of the HA precipitated in SBF. An EDS analysis was also performed to assess the composition of these precipitates (Fig. 2.6c-d)). Apart from local fluctuations, the Ca/P ratio in the globular features approaches 1.4, which is similar to that of stoichiometric HA (~1.67 [140]). Micrographs of the aged 45S5 Bioglass® and BioK surfaces are reported in Fig. 2.7. While the 45S5 Bioglass® surface is rather similar to the BG_Na and BG_Ca ones, the HA deposits on the BioK sample are relatively smaller. Moreover fine cracks can be seen on the entire BioK surface. Nevertheless the EDS analysis performed on the BioK sample (in the reported area of Fig. 2.7b) confirmed the presence of Ca and P in a proportion similar to that in HA. The detection of Si (Fig. 2.7d) is due to a silica gel layer underneath the HA precipitates, while the presence of K can be referred to an incomplete ion leaching from the glass. Therefore, from this point of view, the development of smaller HA deposits and the survival of K ions in the glass suggest that the bioactivity reactions are at is in an earlier stage in BioK glass than in the 45S5 Bioglass®. The cross-sections (Fig. 2.8) of the aged BioK and 45S5 Bioglass® samples look rather similar, and the main difference concerns the morphology of the HA precipitates.

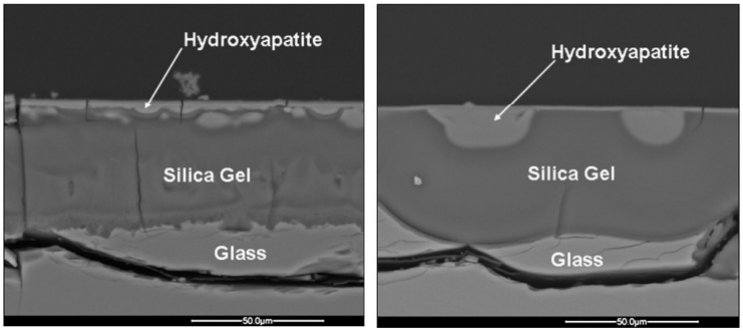

(a) (b)

Figure 2.8: Micrographs of the 45S5 Bioglass® (a) and BioK (b) cross-sections after one month-ageing in air.

2.1.3 Conclusions

In this work, the *in vitro* reactivity of different bioactive glasses, belonging to the $Na_2O\backslash K_2O$-CaO-P_2O_5-SiO_2 system, was analysed by means of *in situ* Raman spectroscopy. Moreover, the reactivity was evaluated in two different media (SBF/TRIS). The comparison between soaking fluids, i.e. SBF and TRIS, leads to suppose that the TRIS may be a good substitute for SBF when a slow reaction rate is required. The main problem dealing with the use of TRIS is that in this case the development of HCA does not depend only on the ability of the glass to promote its nucleation and growth, but it also depends on the amount of Ca and P that the glass releases into the environment.

All the glasses analysed in this study were able to form HCA on their surface, and the characteristic Raman peaks appear after only 6 h of immersion in SBF. Direct comparison between the four considered glasses showed that 45S5 Bioglass® and BioK are able to promote a fast formation of HCA. In any case, all the glasses, after only 96 h of immersion in SBF, had a layer of HCA that can be seen to the naked eye.

2.2 *Suspension plasma sprayed bioactive glass coatings*

Introduction

In this study bioactive glass coatings were deposited via suspension plasma spraying [141]. The BG_Ca glass [69, 130], having composition (in wt.%): 4.7 Na_2O, 42.3 CaO, 6.1 P_2O_5, 46.9 SiO_2, was chosen due to its low tendency to crystallize even at high temperature [69], and its pronounced bioactivity. Fine powders of the glass were produced and dispersed in ethanol to form a suspension used as a feedstock. The various deposition parameters were tested to define the influence of deposition process conditions on final properties of coatings. Various sets of spray parameters were applied in order to define the influence of the deposition process on the final coating properties. Moreover, the coatings were submitted to *in vitro* tests, to assess their bioactivity.

2.2.1 Materials and methods

2.2.1.a Bioactive glass suspension

The BG_Ca glass (4.7 Na_2O, 42.3 CaO, 6.1 P_2O_5, 46.9 SiO_2 in oxide wt. %) was produced by means of a standard melt-quenching method as described in Chapter 2.1.1.a. The molten glass was splashed into room-temperature water and the obtained frit was dried overnight at the temperature of 110°C. Then, the frit was milled in an agate jar and sieved through a 63 µm sieve. The powders were further attrition milled in ethanol (95 vol. %) using 0.8 mm zirconia balls with Beycostat C213 as a dispersant (2 wt% of the dry powder). Ethanol was chosen as milling and suspension medium since bioactive glasses reacts chemically with water [142]. The final powders had a monomodal distribution with a mean particle size of 4.9 µm (Fig. 2.9), as determined with a Partica LA-950V2 (Horiba) granulometer. The feedstock suspension was formulated by dispersing 20 wt. % of solid phase in 80 wt. % of ethanol.

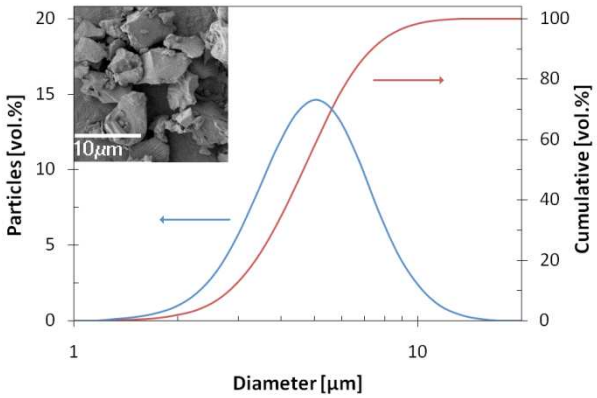

Figure 2.9: Particle size distribution of feedstock powder.

2.2.1.b Coatings deposition

In this study, a SG-100 torch (Praxair, S.T., Indianapolis, IN, USA), with an internal radial continuous-stream injector, was used. The injector was located inside the torch, 16 mm from its exit. During each spray run, the suspension was continuously stirred in order to avoid any precipitation or aggregation phenomena.

In order to assess the feasibility of the new SPS technique, preliminary coatings were sprayed onto 316L stainless steel discs (diameter: 25 mm, thickness: 8 mm) and the deposition parameters were changed over a very wide range, as specified in Table 2.3, column 2.

Spray parameters	**Screening of parameters**	**Final depositions**
	Plasma spray	
Substrate:	316L stainless steel	Ti6Al4V
Electric power [kW]:	10 to 40	see Table 2.4
Working gases composition:	Ar and H_2	
Argon flow rate [slpm]:	45	
Hydrogen flow rate [slpm]:	2.5 to 7.5	7.5
Spray distance [mm]:	40 to 80	See Table 2.4
Torch scans for one session:	2 to 6	4
Sessions for one experiment:	1 to 5	5
Torch scan speed [mm/s]:	375 to 800	750
Scan-step [mm]:	6 to 11	10
Cooling between sessions [°C]:	down to 70	
	Suspension injection	
Diameter of injector [µm]:	300 and 500	300
Suspension flow rate [g/min]:	from 20 to 60	30
Static pressure in suspension container [MPa]:	0.16-0.17	0.16-0.17

Table 2.3: Optimization of spray parameters.

Then, in order to refine the optimal parameters, five additional depositions were performed on Ti6Al4V titanium alloy discs (diameter: 25 mm, thickness: 8 mm as before) according to the sets detailed in Table 2.3, column 3, and in Table 2.4. For clarity reasons, the coatings on Ti6Al4V were denoted as BGCa1-BGCa5 (Table 2.4).

Experimental run	Power [kW]	Spray distance [mm]	Max temperature, mean [°C]
BGCa1	36	50	344 ± 34
BGCa2	40	50	569 ± 36
BGCa3	38	60	473 ± 29
BGCa4	36	70	278 ± 32
BGCa5	40	70	461 ± 47

Table 2.4: Spray parameters.

Since preliminary tests on mirror-like polished substrates showed that the coating adhesion was poor, the surface roughness was increased by sandblasting with 250 µm corundum powder at a pressure of 5 bar to reach the roughness of R_a=3.4 µm. After sandblasting, the substrates were ultrasonically washed with ethanol and acetone.

During the final depositions on Ti6Al4V substrates, the coatings' surface temperature was monitored using a pyrometer IN 5 Plus (Impac). The mean value of the maximum temperature reached during the deposition is reported in Table 2.4.

2.2.1.c Mechanical Characterization

Scratch tests were performed on the as-sprayed coatings with the Open Platform Micro-Combi set-up (CSM Instruments, Switzerland) equipped with a conical Rockwell-type diamond indenter with a spherical tip of 200 µm radius. The applied load was increased linearly from 20 mN to 30 N, with a loading rate of 10 N/min and a scratch length of 3 mm. The acoustic emission was analysed in order to define the critical loads, whose value was also verified by ESEM-based optical analysis. For each sample, five scratch tests were carried out to obtain representative values.

Depth-sensing nano-indentation tests were performed on the coatings' cross-section. The samples were preliminary mounted in resin, cut and polished following a standard metallographic procedure. The maximum applied load was 50 mN, with a loading rate of 40 mN/min and a holding time of 15 seconds. The elastic modulus was calculated according to the Oliver and Pharr method [143]. At least 15 indentations were performed for each sample. The mechanical characterization was focused on the samples BGCa1-BGCa5.

2.2.1.d *In vitro* tests

In vitro tests were carried out on the BGCa1-BGCa5 samples by immersing them in a simulated body fluid (SBF) according to the standard protocol defined by Kokubo et al. [34]. The SBF volume-to-coating surface ratio was fixed to 20 ml/cm^2. The SBF was refreshed

every 2 days in order to simulate the dynamic soaking conditions. The samples were extracted from the SBF, washed with bi-distilled water, dried at room temperature and characterised (morphology and chemical composition) after time periods of 1, 3, 7, and 14 days.

2.2.1.e Microstructural Analysis

The surface and polished cross section of the coatings were observed with an environmental scanning electron microscope, ESEM (ESEM Quanta 200-FEI Company, Eindhoven, The Netherlands), operated in low-vacuum mode (pressure: 0.5 Torr) and equipped with a X-EDS microanalysis system (Inca, Oxford Instruments, U.K.). For selected samples, BGCa1-BGCa5, the ESEM evaluation was repeated after SBF tests. The coatings were also analysed by means of X-ray Diffraction (XRD) before and after soaking in SBF, with a X'pert PRO diffractometer (PANalytical, Almelo, The Netherlands) employing a Cu-Kαradiation. Data were collected in the 2θ range of 10°-65° with a step of 0.017° and a time interval of 71.12 s (X'Celerator detector).

The surface of as-sprayed samples and SBF-soaked ones was investigated by micro-Raman Spectroscopy (Jobin-Yvon Raman Microscope Spectrometer, HORIBA Jobin Yvon S.A.S.,Villeneuve d'Ascq, France). He-Ne laser emitting at 632.8 nm was employed, with an output power of 20 mW without any filter and a 100x objective.

2.2.2 Results and discussion

2.2.2.a Screening of spray parameters

A feasibility study was performed spraying more than 40 different coatings, as detailed in Table 2.3, column 2. The morphological and compositional evaluation of such exploratory samples via ESEM, XRD and micro-Raman spectroscopy revealed that the coatings' properties were governed mainly by following operational parameters:

- spray distance;
- electric power input to plasma;
- hydrogen content in working gas mixture.

A few initial spraying experiments were unsuccessful, since it was not even possible to melt the glass powder completely (Fig. 2.10). To overcome this problem, the electric power input was increased up to 40 kW and the hydrogen flow rate was augmented up to 7.5 slpm.

In this way, the glass particles reached the melting point, as confirmed by the ESEM observation. Indeed, due to the increase in the electric power input and the hydrogen flow

rate, it is reasonable that the "Ability-of-Heating" factor (AHF) of the plasma [2], i.e. its capacity to heat and melt the particles, increases up to exceed the Difficulty-of-Melting factor (DMF) of the powder (which depends on the heat content per unit mass of the particles, on the diameter of the largest particle in the distribution and on the density of the particle) [2]. In fact, the particle may be melted in plasma jet only if the parameter DMF which characterizes it is lower than the parameter AHF characterizing plasma jet [2].

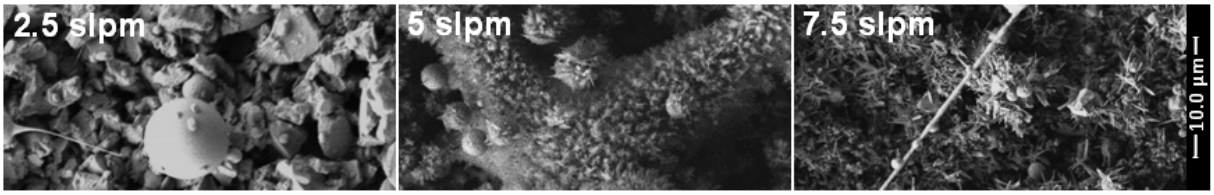

Figure 2.10: Preliminary coatings produced with different hydrogen flow rates (2.5/5.0/7.5 slpm). The other spray parameters were set as follows: Ar flow rate 45 slpm; electric power input 25 kW; spray distance 60 mm; linear substrate speed 500 mm/s; scan-step 6 mm; static suspension pressure 0.05 MPa; suspension feed rate 50 g/min.

The spray distance was another important parameter. In fact, the coatings contained the particles which re-solidified in-flight for spray distances greater than 70 mm. On the contrary, the coatings surface showed large drops of glass for spray distances smaller than 50 mm what proved that the convective heat flux from plasma jet melted the material.

The outcome of this initial parameters' screening for the depositions of BGCa1-BGCa5 samples was the following: (i) hydrogen flow rate was set to 7.5 slpm; (ii) electric power input was increased from 36 to 40 kW; and, (iii) spray distance was fixed to be in the 50-70 mm range. Also, the injector, having an inner diameter (ID) of 300 µm, was preferred to the larger one of 500 µm. It appeared that the smaller ID of injector allowed a good penetration of the suspension into the plasma jet. The other parameters (scan speed, time of deposition, etc) were selected in order to avoid an excessive heating of the substrate.

2.2.2.b Microstructure of as-sprayed final coatings

The final coatings were continuous and homogeneous, regardless of the specific deposition parameters; in particular, the samples showed a very rough surface that included both large flattened splats and partially crystallized zones, as reported in Fig. 2.11a. A similar microstructure has been reported in the literature for hydroxyapatite coatings produced by SPS [25]. It is likely that such *two-zone* microstructure derives from the different thermo-mechanical behaviour of small and large particles in the feedstock powder, since they possess different heat capacities and follow dissimilar trajectories in the plasma jet [20]. Previous

investigations on SPS coatings have shown that, when the suspension is injected into the plasma flow, the liquid solvent evaporates and the remaining particles can agglomerate and are expected to melt or to remain solid, according to their specific trajectory in plasma jet. When they impinge on the substrate (or on the previously deposited particles), the well-molten particles usually result in dense and flat zones, whereas the fine particles, which are likely to re-solidify in flight, create agglomerated zones with fine and partially sintered grains [20].

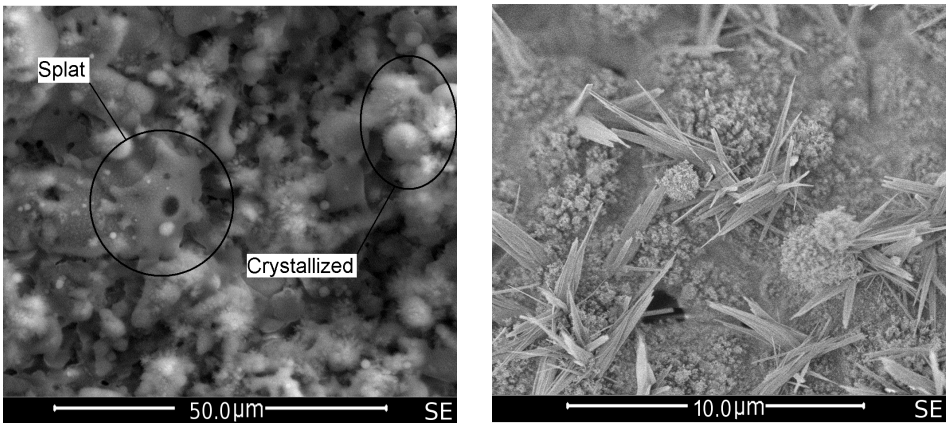

(a) (b)

Figure 2.11: SEM micrographs (secondary electrons): the area representative of the surface morphology of the coatings (BGCa3 run) with molten splats and crystallized zones outlined (a); high magnification of a crystallized area (b) (note that the acicular morphology typical of $CaSiO_3$ can be observed as suggested in [144])

In the present investigation, such agglomerated areas underwent a partial crystallization, as suggested by the development of micrometric acicular structures; an example is given in Fig. 2.11b. Similar needle-like crystals have already been described in the literature and they have been associated with the growth of wollastonite, $CaSiO_3$ [144].

The development of a rough morphology may be advantageous for bioactive coatings, since the surface asperities promote both the absorption of organic metabolites and the cell attachment [82].

The ESEM inspection of the cross sections revealed that all the samples possessed a lamellar microstructure, which is typical of thermal sprayed coatings (Fig. 2.12). It is worth noting that the coating-substrate interfaces were continuous and almost crack-free. Moreover the microstructural features, such as the characteristic splat dimension, were relatively fine, as a result of the small particle size of the glass powders used for the SPS deposition. The coatings' thickness varied between 31 (± 7) µm for BGCa4 and 40 (± 6) µm for BGCa1 and hence perfectly fitted the requirements for biomedical applications. In fact it is usually reported that a coating thickness of approximately 50 µm may provide a good balance between fatigue resistance and resorption times [145].

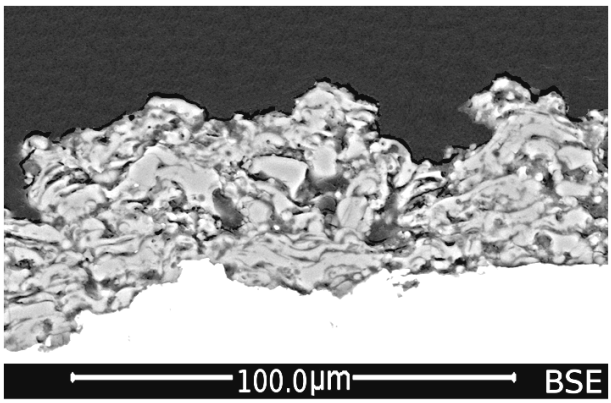

Figure 2.12: SEM micrographs (back scattered electrons) representative of the cross-section microstructure of the final coatings (BGCa1 run).

Thanks to its relatively high crystallization temperature [69], the BG_Ca glass experienced a very limited devitrification during the deposition process. Indeed the broad band in the 20°-35° 2θ range of the XRD patterns (Fig. 2.13) confirmed that the coatings were mainly composed of glassy phase. The partial crystallization of the glass caused the formation of silicate-based secondary phases such as $CaSiO_3$ and Ca_2SiO_4, as proved by the weak peaks occasionally visible in the XRD patterns. The presence of $CaSiO_3$ detected by the diffraction is consistent with the SEM observation of typical needle-like crystals, as mentioned before (Fig. 2.11b).

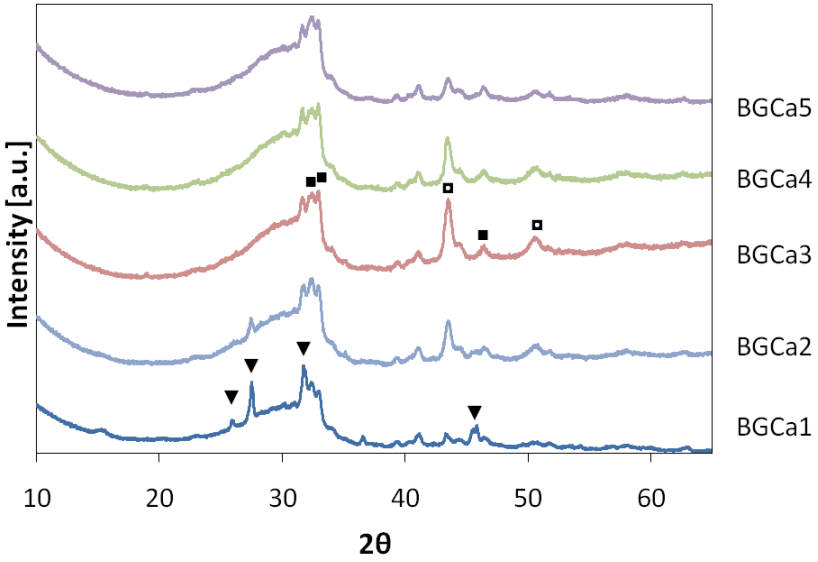

Figure 2.13: XRD patterns of the as-sprayed samples. Symbols: ▼ $CaSiO_3$, ■ Ca_2SiO_4, ◘ substrate

Qualitative evaluations of the XRD patterns also suggest that the BGCa1 and BGCa2 samples possess larger amounts of crystalline phases than the BGCa3 – BGCa5. This may be due to the high heat flux delivered from the plasma jet to the deposited material, since these samples were produced using the shortest spray distance (Table 2.4). This heat flux may have either

slowed down the cooling of flattened splats, promoting crystallisation during splat formation, or caused re-crystallisation of previously deposited glass splats during subsequent torch scans. It is worth noting that the development of $CaSiO_3$, which is characteristic of this CaO-rich glass formulation [69], is expected to preserve the bone-bonding ability of the coatings, since this material is also highly bioactive [146].

To conclude, the XRD patterns presented well-defined peaks which can be attributed to the metal substrate, due to the relatively low thickness of the coatings and the limited X-ray absorbance capacity of the glass.

2.2.2.c Mechanical properties of as-sprayed samples

The Vickers hardness and the elastic modulus of the coatings were determined via depth-sensing nano-indentation.

Run	Thickness [µm]	Hardness, $HV_{0.05N}$	Elastic modulus [GPa]	Critical load [N]
BGCa1	40 ± 6	98 ± 17	23.1 ± 4.2	21.1 ± 4.4
BGCa2	33 ± 7	66 ± 10	20.8 ± 3.4	19.3 ± 2.7
BGCa3	36 ± 9	60 ± 13	21.0 ± 3.4	18.9 ± 0.6
BGCa4	31 ± 7	34 ± 6	15.6 ± 5.6	18.2 ± 5.4
BGCa5	39 ± 8	85 ± 22	18.2 ± 4.3	17.9 ± 1.9

Table 2.5: and mechanical properties of coatings (mean value ± standard deviation).

From the results reported in Table 2.5, it is possible to observe that the BGCa4 sample exhibited the lowest values of both Vickers hardness and elastic modulus. This is not surprising, since such coating was processed under less favourable spraying conditions (Table 2.4) with respect to the other final samples, being the electric power relatively low (36 kW) and, at the same time, the spray distance relatively long (70 mm). As a result, the maximum coating temperature remained as low as 280°C (see Table 2.4). This suggests that a significant fraction of the sprayed material impinged at low temperature and that there was little chance for sintering of the previously-deposited material. It should be noted that this is also the thinnest coating on Ti6Al4V substrates (Table 2.5). The BGCa1 coating has the best mechanical performance, suggesting that the corresponding set of deposition parameters represents a good balance between the melting capacity of plasma jet (AHF) and the in-flight residence time of the particles. The mechanical properties of the BGCa1-BGCa5 samples are slightly worse than those reported in the literature for other bioactive glass coatings. For example, in a recent contribution by Altomare et al. dedicated to Bioglass® 45S5 coatings

obtained by the high-velocity suspension flame spray (HVSFS) technique [24], the hardness was reported to reach values as high as 290-500 HV and the elastic modulus 40-57 GPa, according to the specific deposition parameters. Nevertheless a direct comparison is not straightforward, since SPS and HVSFS are inherently different techniques, although they both employ powder suspensions. In particular, the HVSFS method usually confers a higher velocity to the sprayed particles, which is likely to promote the flattening process of the splats. This is evident in the coatings investigated by Altomare et al. [24], which possess a very compact microstructure with few spherical pores. In the present contribution, instead, the coatings produced by SPS retain a greater inter-splat porosity, which directly affects the mechanical properties. However it is worth noting that a richer porosity, which results in a large reactive surface, may be advantageous, since it can aid the coating bioactivity [77]. The analogy has some limits because of the different grain size and composition of the feedstock powders used, since the Bioglass® 45S5 particles sprayed by Altomare and her colleagues were finer (1 - 2 μm average size) than the present ones.

Even if the elastic properties of the BGCa1-BGCa5 coatings are lower than those declared in the literature for Bioglass® 45S5 coatings obtained via HVSFS, they resemble those of the cortical bone, whose elastic modulus is in the 7-30 GPa range [147]. This could be beneficial to limit the so-called stress shielding effect, which may cause a dangerous reduction in bone density after implantation.

The critical loads were defined by combining the analysis of the acoustic emission and the ESEM inspection of the scratch lines, as shown in Fig. 2.14. The results were similar for all the final coatings and they were comparable to those generally found in the literature for bioactive glass coatings, namely 16-32 N [126].

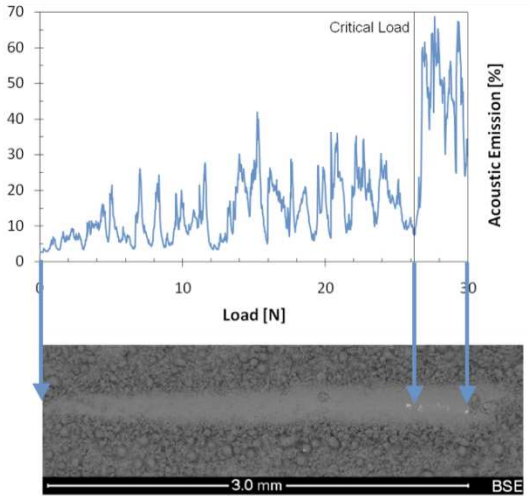

Figure 2.14: Definition of the critical loads for the BGCa1 sample by combining the acoustic emission analysis and the ESEM inspection (backscattered electrons)

2.2.2.d *In vitro* tests

As shown in Fig. 2.15, the ESEM investigation of the samples after soaking in SBF indicates the progressive development of the “cauliflower-like” agglomerates which are characteristic for *in-vitro* grown HCA [148].

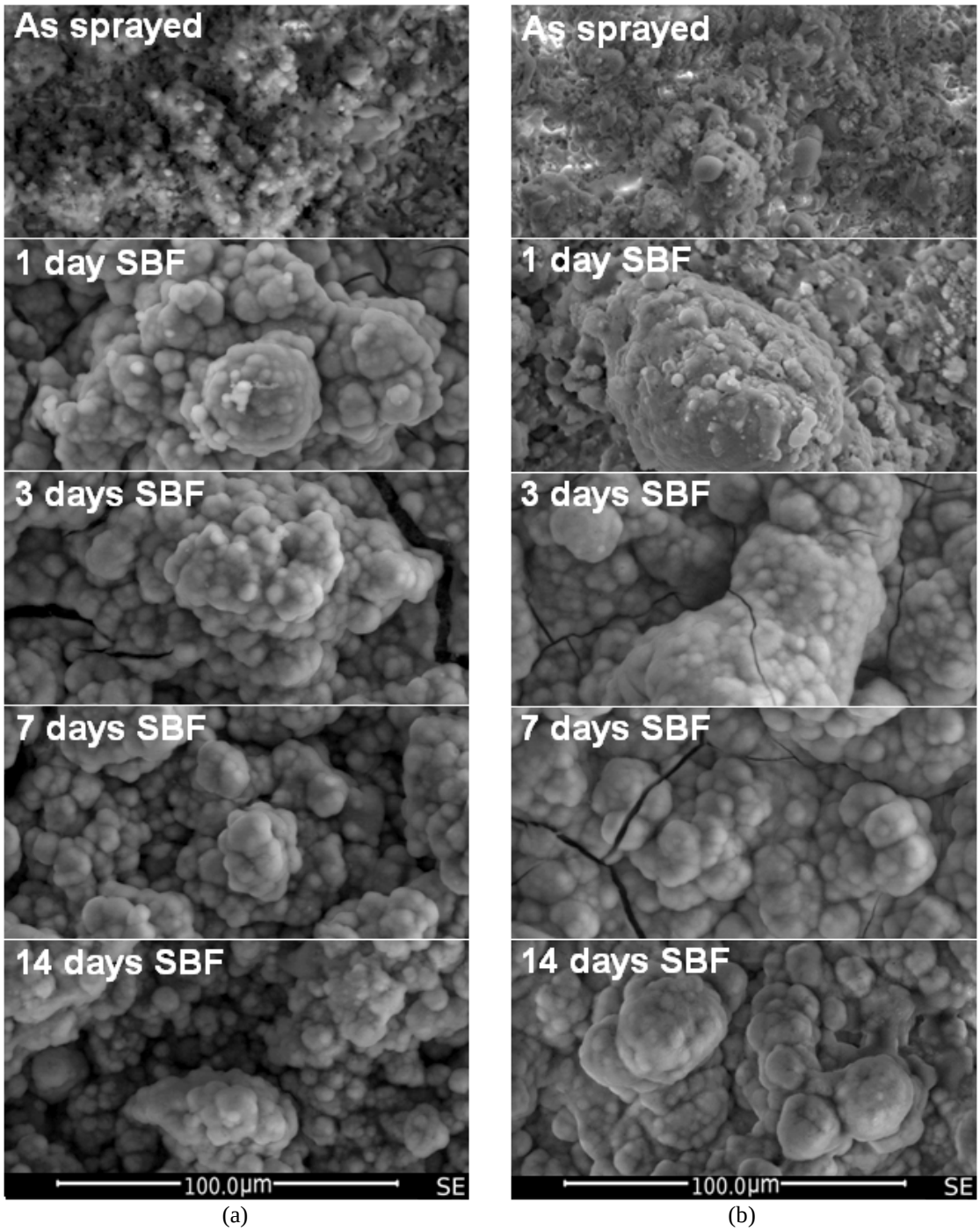

(a) (b)

Figure 2.15: Surface evolution of the samples immersed in SBF for increasing times:
(a): BGCa3 run belonging to the first group (1G) and (b): BGCa1 run belonging to the second group (2G)

According to the growth rate of such dome-like features, the coatings on Ti6Al4V substrates can be classified in two groups: the samples BGCa3, BGCa4 and BGCa5, belonging to the

first group (1G), showed well-defined formations already after one day of immersion in SBF (Fig. 2.15a); the other two coatings, belonging to the second group (2G), reached well-defined spherical structures after 3 days in SBF (Fig. 2.15b). It is likely that such difference in the coatings' reaction rate results from their microstructure; specifically, the coatings possess a different porosity, which leads to dissimilar reacting and exchanging surfaces which, in turn, are responsible for different behaviours in SBF. In fact the BGCa1 and BGCa2 coatings (belonging to 2G) were processed with a lower spray distance than those belonging to 1G, therefore they were more affected by the heat flux from the plasma jet. As a consequence, the 2G coatings were mainly formed by the dense zones described previously and they were less porous than the 1G samples. This fact delayed the reaction between the 2G coatings and the SBF. Moreover, the 2G coatings (BGCa1 and BGCa2) contained a larger amount of crystalline phases (as seen in Fig. 2.13), which may have reduced the rate of dissolution of the coatings since crystalline phases are typically less reactive than glassy ones.

The difference between the two groups can be appreciated also by the inspection of the cross sections. In fact, already after one day in SBF, the cross-section of a 1G sample typically shows a multi-layered structure, which is exemplified in Fig. 2.16. The X-EDS chemical analysis, supported by the available literature [149], makes it possible to identify the strata according to the following scheme:

- superficial layer, which is rich in calcium and phosphorus (zone 1 in Fig. 2.16): hydroxy-carbonated-apatite;
- intermediate layer, which is mainly composed of silicon oxide (zone 2 in Fig. 2.16): silica gel;
- deep layer, which still preserves the composition of the starting feedstock (zone 3 in Fig. 2.16): residual glass splats.

The clear distinction between such layers was delayed up to the third day of immersion in SBF for the 2G samples. However, the stratification progressively disappeared with increasing soaking times and, after 14 days in SBF, all the surface deposits were entirely composed of calcium phosphate with a few residual traces of silicon. This result suggests that the original glass coatings were gradually resorbed and then completely replaced by the re-precipitated hydroxyapatite (HA). It is worth noting that, according to the ESEM and X-EDS observations, the reaction kinetics between the coatings and the SBF is (qualitatively) analogous to that commonly reported in literature for silicate-based bioactive glasses in bulk form, since a gradual growth of HA may be observed, mediated by the transient development of a silica gel layer [126, 130].

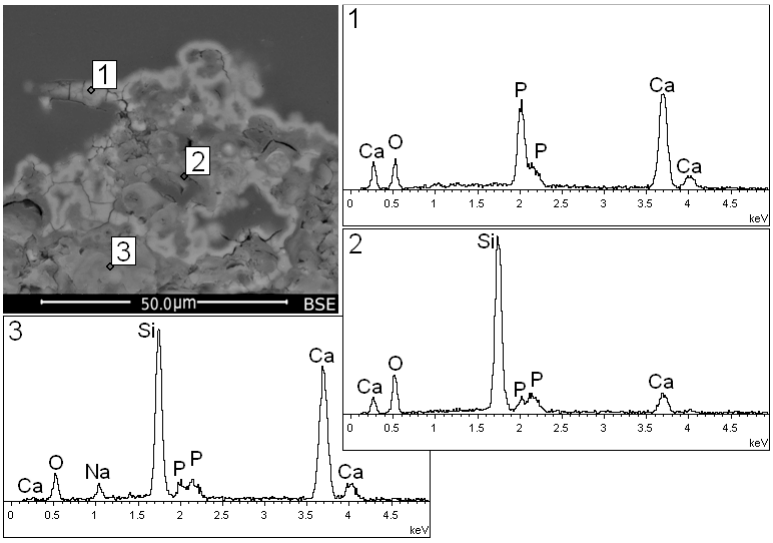

Figure 2.16: ESEM micrograph (backscattered electrons) and EDS microanalysis of the cross section of a sample belonging to the first group (BGCa4) after 1 day of soaking in SBF.

The diffraction patterns of the samples immersed in SBF (Fig. 2.17) are consistent with the ESEM data. The identification of the HA was based on a wide peak at about 2θ = 32°, which corresponds to the main peak of hydroxyapatite, and a secondary peak at about 2θ= 26°. The XRD spectra of 1G samples showed such peaks already after one day of immersion, whereas the spectra of the 2G samples exhibited them after three days of immersion. In both cases, the broad shape of the XRD peaks indicates that the hydroxyapatite had a microcrystalline and defective structure, as often stated for HA precipitated in SBF [150].

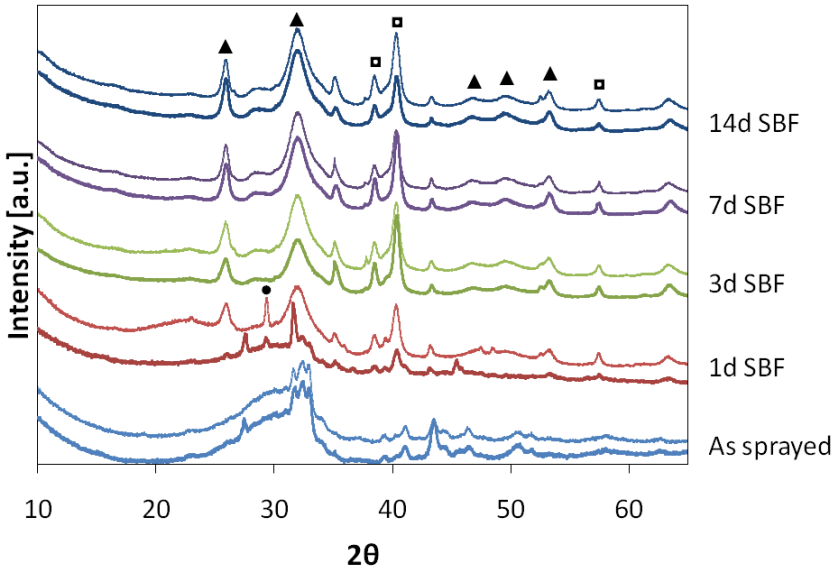

Figure 2.17: XRD patterns of the samples immersed in SBF for increasing times: thin lines correspond to the sample BGCa5, representative of the first group (1G), bold lines correspond to the sample BGCa2, representative of the second group (2G). ▲ hydroxyapatite, ◘ Ti6Al4V, ● $CaCO_3$.

Besides, in the XRD patterns of samples 2G, the peaks of the crystalline phases (most notably, those belonging to $CaSiO_3$) became more clearly recognisable after 1 day of soaking, which suggests that the reactivity of crystalline phases with the SBF solution is slower than that of the glassy phase. This corroborates to the previous comments on the role of crystallinity in determining the behaviour of the 1G and 2G samples. For increasingly long soaking times, the $CaSiO_3$ peaks progressively got weaker and eventually disappeared. This indicates that crystalline phases also react with SBF, consistently with the mentioned reports on the bioactivity of $CaSiO_3$, although at a slightly lower rate than the glassy phase. Therefore the BG_Ca glass represents an interesting solution, since it basically remains amorphous, and hence bioactive, after the deposition and even the secondary crystalline phases resulting from the SPS process are still bioactive.

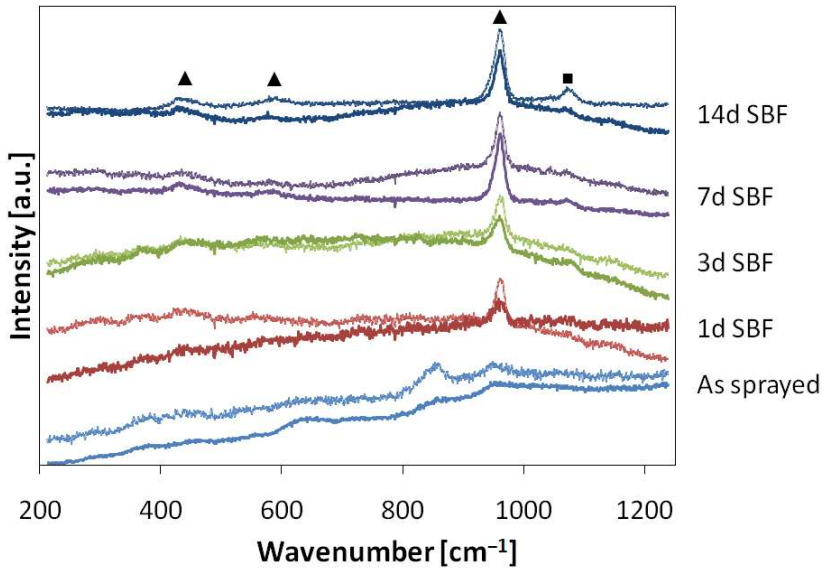

Figure 2.18: Raman spectra of the samples immersed in SBF for increasing times: thin lines correspond to the sample BGCa5, representative of the first group (1G), bold lines correspond to sample BGCa1, representative of the second group (2G). The Raman peaks correspond to the vibrations of: ▲ hydroxyapatite, ■ carbonate group.

The Raman spectra, shown in Fig. 2.18, followed the same evolution for all samples. In fact, independently of the spraying parameters, a peak at about 970 cm^{-1} appeared already after one day in SBF; then, with increasing immersion times, such peak shifted towards 960 cm^{-1}. Two secondary peaks were detectable after 3 days of soaking. To conclude, an additional peak appeared at 1070 cm^{-1} for longer times. All these peaks are consistent with the typical pattern of HA grown in SBF. More precisely, the Raman spectra evolution was similar to that previously observed for bulk glasses [69, 130]. In fact, the peak at 970 cm^{-1}, which is associated to the phosphate groups, quickly moved to 960 cm^{-1}, which is the main peak of hydroxyapatite. Similarly, also the secondary multiple peaks were due to hydroxyapatite,

while the peak at 1070 cm^{-1} was caused by the carbonate group, thus suggesting that the growing hydroxyapatite was carbonated, as often stated in the literature concerning SBF tests on bioactive glasses [130].

It is interesting to note that the XRD and SEM analyses allowed dividing the samples into 2 groups based on their reaction rate (Figs 2.15 and 2.17). Inversely, the Raman spectra evolution was the same for all samples (Fig. 2.18). This indicates that, regardless of the differences in the reaction rates revealed by the ESEM and XRD studies, all the samples were immediately covered by a very thin layer of hydroxyapatite when immersed in SBF. Therefore the micro- Raman spectroscopy, which is highly sensitive to the surface of the samples, was not able to detect the differences between the coatings.

2.2.3 Conclusions

In this study, the suspension plasma spray technique was employed to obtain coatings starting from a suspension of micron-sized bioactive glass powders. A preliminary screening of processing parameters revealed that the microstructure was mainly governed by the hydrogen flow rate, the spray distance and the electric power input to plasma. Glass coatings suitable for biomedical applications were achieved working with a hydrogen flow rate of 7.5 slpm, a spray distance of 50 to 70 mm and a power of 36 to 40 kW. The use of a bioactive glass, characterized by a reduced tendency to crystallise, helped to obtain amorphous coatings, with a very limited development of crystalline phases. Both the thickness and the mechanical properties of the coatings are adequate for biomedical applications in orthopaedic implants.

The SBF tests proved that all the coatings were able to develop a surface layer of hydroxy-carbonated-apatite when immersed in a simulated body fluid, following interaction mechanisms previously observed also for bulk bioactive glasses. Nevertheless the overall reaction kinetics, especially in the first days of immersion, were influenced by the coatings' porosity and degree of crystallinity, which were primarily controlled by the spray distance.

2.3 *Production and in vitro characterization of hydroxyapatite coatings with and without a bioactive glass topcoat*

Introduction

The aim of this work was to test whether a bioactive glass topcoat could be able to increase the bioactivity of hydroxyapatite (HA).

With that purpose HA coatings were plasma sprayed on steel substrates starting from commercial powders (samples "PS-HA"). The HA coatings were subsequently coated with a thin layer of bioactive glass produced by suspension plasma spray (SPS), thus obtaining the multi-layered "PS-HA/SPS-BGCa" samples.

The so-called BG_Ca (wt.%: 4.7 Na_2O, 42.3 CaO, 6.1 P_2O_5, and 46.9 SiO_2) was selected as the bioactive glass since it has a high bioactivity and a relatively low tendency to crystallize at high temperature [69]. In order to assess the effectiveness of the bioactive glass topcoat, the samples with and without the BG_Ca layer were tested *in vitro*, soaking them in SBF.

2.3.1 Materials and methods

2.3.1.a Feedstock materials

Hydroxyapatite powder:

The powder was pure hydroxyapatite (HA) commercialized by Tomita (Japan). The powder is spray dried, with a mean diameter of d_{50}=120 µm and porosity of about 12% [151].

Bioactive glass suspension:

The bioactive glass (BG_Ca) was produced by the conventional melt-quenching method. Appropriate raw materials were mixed, and then molten in a platinum crucible at 1450°C. The molten glass was poured into water. The obtained frit was dried overnight at 110°C and then it was dry milled in an agate jar and sieved at 63 µm. The powder was further milled by an attrition system using 0.8 mm zirconia balls and adding the dispersant Beycostat C213 (2 wt% of the dry powder). Since bioactive glass powders have the tendency to react with water, ethanol was selected as the suspension liquid. The obtained BG_Ca powder had a monomodal distribution with a mean diameter of d_{50}=4.7 µm, (determined with a granulometer Partica LA-950V2, Horiba). The feedstock suspension was formulated by dispersing 20 wt% of solid phase in 80 wt% of ethanol.

2.3.1.b Coatings deposition

Plasma-spray runs were performed using a SG-100 torch (Praxair, S.T., Indianapolis, IN, USA). Substrates were 316L stainless steel discs (25 mm in diameter, thickness of 8 mm) which were roughened via sandblasting. The resulting roughness of substrates was R_a=4.3 µm (determined by means of Tester T500, Hommel). After sandblasting, the substrates were ultrasonically washed with ethanol and acetone.

During the PS deposition, the HA powder was supplied by means of a laboratory feeding apparatus consisting in an Ar-pressurized chamber and a vibrating system.

As regards the BG_Ca topcoat, a pneumatic system was used to feed the suspension; to avoid agglomeration and sedimentation, the suspension was continuously mixed by means of a magnetic stirrer. Both feedstock materials were supplied into the plasma by internal injection. The injection orifice was radial inside the anode at 16 mm from torch's exit. The used spray parameters are listed in the Table 2.6.

		PS-HA coating	SPS-BG topcoat
	Power [kW]:	21	40
Gases	**Ar [slpm]:**	48	45
	H_2 [slpm]:	2	7.5
	Distance [mm]:	100	70
	Torch speed [mm/s]:	500	750
	Scan step [mm]:	10	10
	Feedstock flowrate [g/min]:	10	30
	Injector diameter [mm]:	1	0.3
	Carrier gas [slpm]:	Ar, 3	-
	Static pressure [MPa]:	-	0.17
	N° of torch passages:	36	2 x 4 sessions

Table 2.6: Spray parameters

Many preliminary deposition tests were carried using tentative parameters taken from the literature [141, 152]. Then, on the basis of the preliminary trials, the final spray parameters were defined, with the aim of optimizing the compactness and the thickness of the HA layer (and also to guaranteeing a high repeatability) and of favouring the bioactivity of the glass topcoat, which must therefore remain amorphous and properly porous.

During the deposition sessions, the temperature of the coatings' surface was measured using an optical IN 5 Plus pyrometer (Impac).

2.3.1.c *In vitro* tests

In order to investigate the effect of the glass topcoat on the reactivity in physiological fluids, the samples were soaked in SBF according to the standard procedure proposed by Kokubo [34]. The SBF was refreshed every 2 days to mimic the dynamic condition of the human body. The samples were removed from the SBF after time periods of 1, 3, 7, and 14 days. The samples were carefully washed with distilled water, and after that they were dried at room temperature.

2.3.1.d Characterization

The samples were analysed before and after soaking in SBF through different techniques.

The surface of the coatings was investigated by means of X-Ray Diffraction, XRD, with a X'pert PRO diffractometer (PANalytical, Almelo, The Netherlands) equipped with X'Celerator detector. Diffraction patterns were collected in the 10°-70° 2θ range (step size: 0.017°, step time: 71.12 s).

An accurate microstructural analysis was carried out on the coatings' surfaces and polished cross sections by means of an environmental scanning electron microscope, ESEM (ESEM Quanta 200-FEI Company, Eindhoven, The Netherlands) equipped with a X-EDS microanalysis system (Inca, Oxford Instruments, U.K.). The microscope was operated both in high-vacuum and low-vacuum mode (pressure: 0.45 Torr).

The coatings' surface was analysed by micro-Raman Spectroscopy (Jobin-Yvon Raman Microscope Spectrometer, HORIBA Jobin Yvon S.A.S., Villeneuve d'Ascq, France). The laser source emits 20 mW at 632.8 nm; 100x objective and no filters were employed.

2.3.2 Results and discussion

During the deposition of the HA layer, the surface temperature did not exceed 250°C and, at the end of the process, the temperature was about 200°C.

Instead, during the deposition of the BG_Ca topcoat, the temperature was slightly higher, with an average value of about 250°C and local peaks of 330°C. However such values are relatively low with respect to those usually achieved in SPS deposition with ethanol [141]. In fact, the parameters were purposely defined to avoid an excessive heat flux to the coating in order to prevent the glass devetrification. This also limited the sintering process and therefore it conferred a porous microstructure to the glass topcoat, which is expected to enhance its bioactivity [141]. To reduce the heat flux to the sample, the spraying distance was set at a

high value (70 mm), and the coatings were sprayed in 4 different sessions, with two torch passes for each session. Moreover, in order to control the surface temperature, the samples were left to cool down below 70°C before each session.

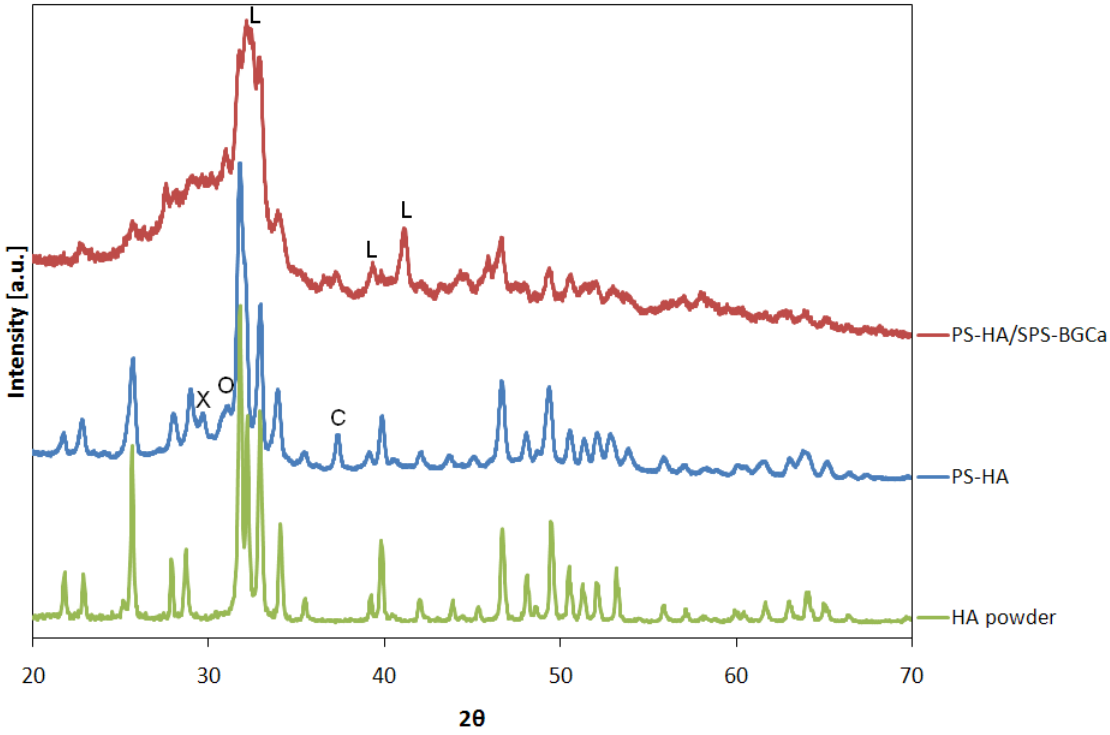

Figure 2.19: X-ray diffraction patterns of the coatings and of the HA feedstock powder
L: larnite (Ca_2SiO_4), X: TTCP, O: TCP, C: CaO

The X-ray diffraction pattern of the PS-HA sample (Fig. 2.19) confirmed that the HA basically preserved its nature after the deposition. In fact, the spectrum was basically identical to the X-ray diffraction pattern of the HA feedstock powder. However secondary phases could be detected, which resulted from a partial decomposition of the HA. In particular, the peaks in the 29°-31° 2θ range are associated to tetra-calcium phosphate, TTCP, and to tri-calcium phosphate, TCP. Instead the peak at 2θ = 37.5° corresponds to CaO. Since the amount of decomposition phases of HA may be related to the relative intensity of their peaks [153], the low intensity of these peaks suggests that secondary phases were present in low amounts.

In the PS-HA/SPS-BGCa diffraction spectrum, a broad band between 25° and 35° (2θ) is present, as often observed for silicate glasses. In addition, some new weak peaks appear, and they may be associated to Ca_2SiO_4. Moreover well-defined peaks can be attributed to the HA layer underneath the glass topcoat. The partial transparency of the topcoat to the X-rays results from the intrinsic properties of silicate glasses and from the structure of the topcoat itself, which was highly porous and relatively thin, as proved by the ESEM inspection described below.

The microstructure of the PS-HA samples was compact, with low porosity (Fig. 2.20a). Some dark areas could be observed in the cross section. Since the EDS analysis (Fig. 2.21) confirmed they were composed of HA, with atomic proportions analogous to those of the surrounding light-grey material, it is plausible that such dark areas were the cross sections of unmelted HA particles incorporated into the coating. The surface of the PS-HA coatings (Fig. 2.20b) displayed both large splats, with diameters of some tens of microns, and areas with a finer, granular microstructure.

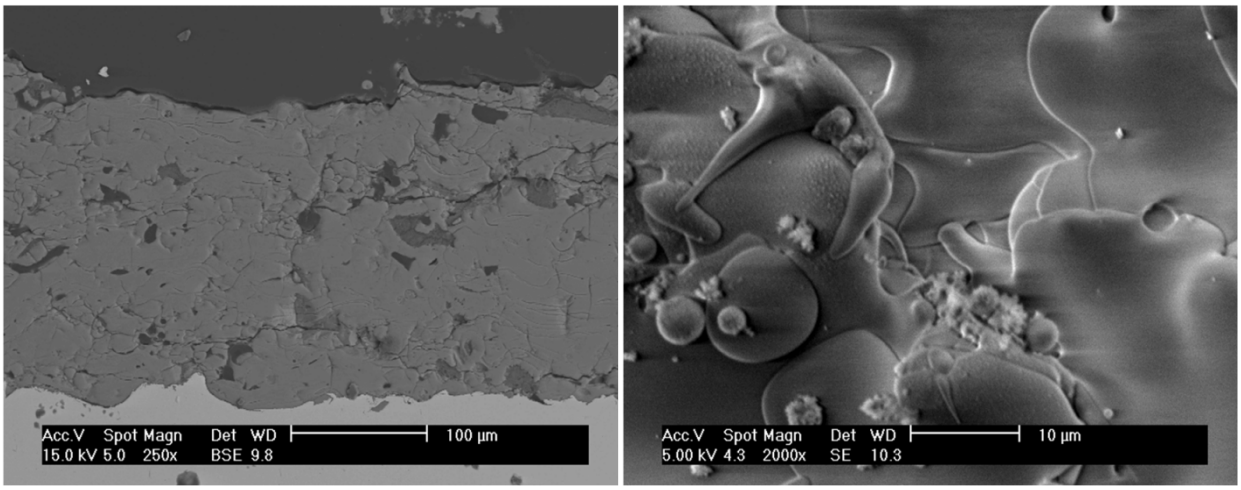

(a) (b)

Figure 2.20: PS-HA coatings: (a) cross section (b) surface

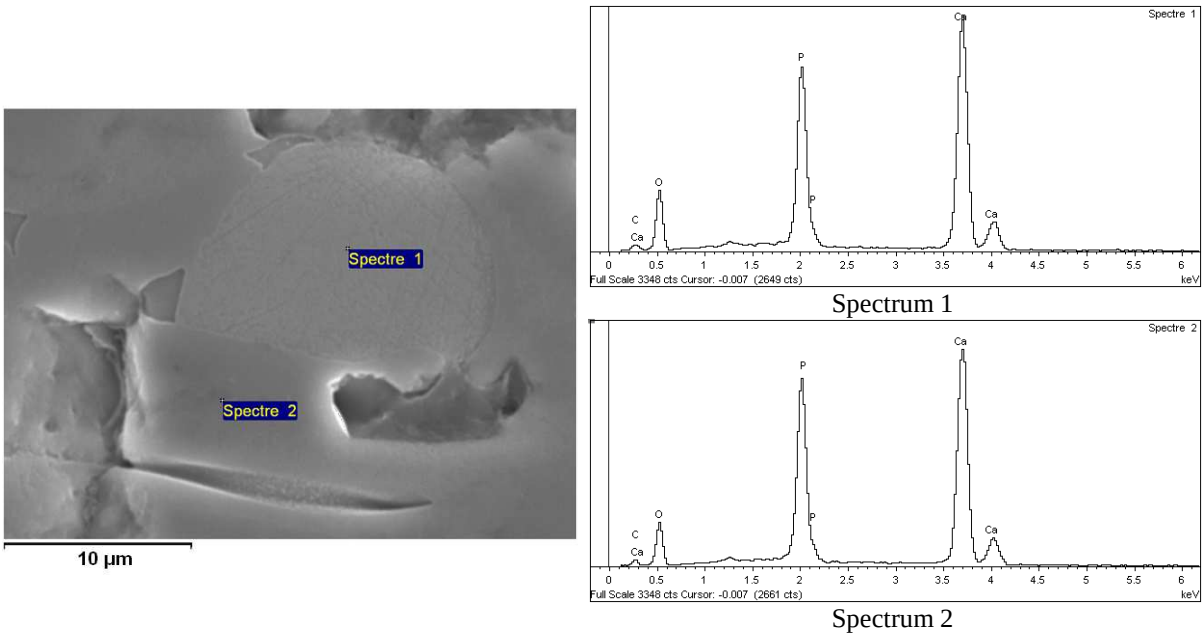

Figure 2.21: Detail of the PS-HA cross section and corresponding EDS microanalyses.

The inspection of the cross section of the PS-HA/SPS-BGCa samples confirmed that the glass topcoat was relatively thin, with an indicative thickness of about 20 μm (Fig. 2.22a). Most of all, the top layer was characterised by a very fine microstructure and by a rich porosity, quite superior to that previously detected in the HA coating of the PS-HA samples. As regards the surface morphology, the glass topcoat was extremely rough, as shown in Figure 2.22b. A high roughness may be extremely advantageous, since it increases the specific surface area available for chemical reactions and it favours the cell attachment *in vivo* [82].

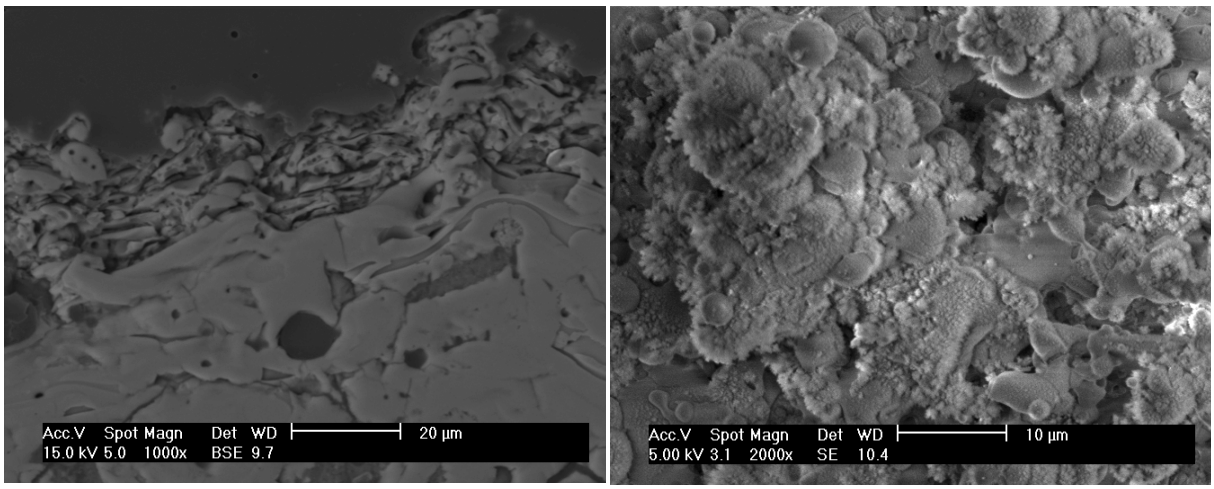

(a) (b)

Figure 2.22: PS-HA/SPS-BGCa coatings:
(a) cross section (b) surface

Furthermore very fine acicular structures could be observed on the surface of the PS-HA/SPS-BGCa coatings. They probably are the crystals of the Ca_2SiO_4 phase identified by the XRD.
After the immersion in SBF, the surface of both types of coatings was covered by the dome-like structures which are typical of HCA deposits grown *in vitro* [148]. However, a comparison between the two types of samples (Fig. 2.23) suggests that the PS-HA/SPS-BGCa system reacted more rapidly than the PS-HA one. Indeed, the fine crystalline structures originally present on the PS-HA/SPS-BGCa sample completely disappeared, and the surface quickly assumed a more globular morphology.
The diffraction spectra of the PS-HA sample did not show sensible variations (Fig. 2.24) as a result of the immersion in SBF. Starting from the first day of immersion, the peaks associated with the secondary phases (TCP, TTCP and CaO) gradually disappeared. More in detail, the peak associated to CaO vanished already after one day of immersion, whereas the peaks of TTCP and TCP completely ceased to be visible after seven days. Instead the peaks of HA did not vary with increasing immersion time.

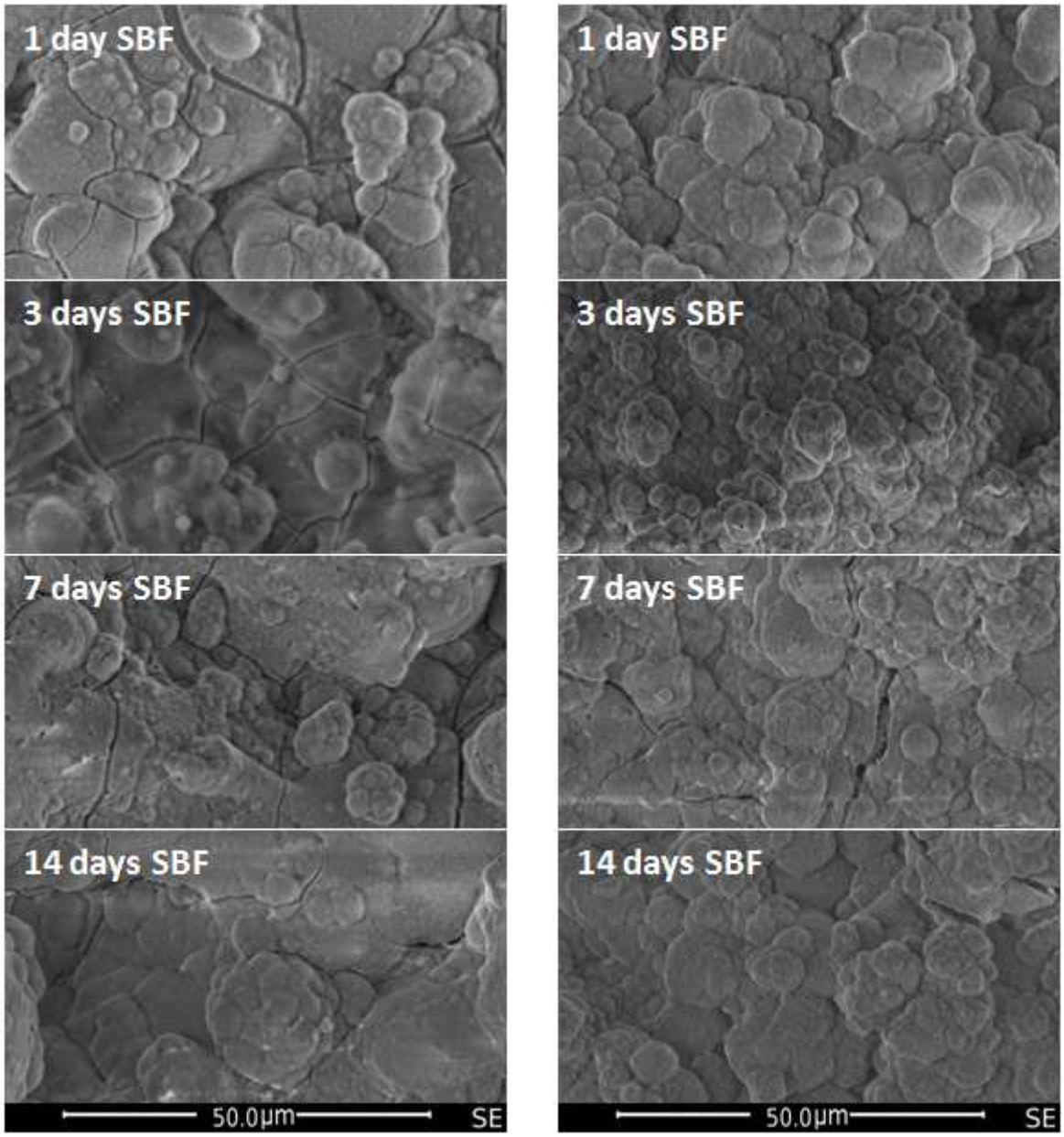

(a) (b)

Figure 2.23: Coatings' surfaces after *in vitro* test:
(a) PS-HA; (b) PS-HA/SPS-BGCa.

The diffraction patterns of the PS-HS/SPS-BGBa samples (Fig. 2.25) showed visible changes as a result of the immersion in SBF. Starting from the first day of immersion, the diffraction spectrum showed the main peaks of HA, although very broad. The width of the peaks was related to the poor crystallinity of HCA, an effect that is often observed for *in vitro* grown HCA. At the same time, the peaks due to the Ca_2SiO_4 disappeared, supporting the hypothesis that the crystallizations were mainly constituted by superficial fine crystals, readily dissolved by the SBF. The peak at $2\theta = 29.4°$, which can be observed occasionally in the XRD spectra

of the soaked samples, is due to $CaCO_3$, a mineral that may co-precipitate *in vitro* with HCA [141].

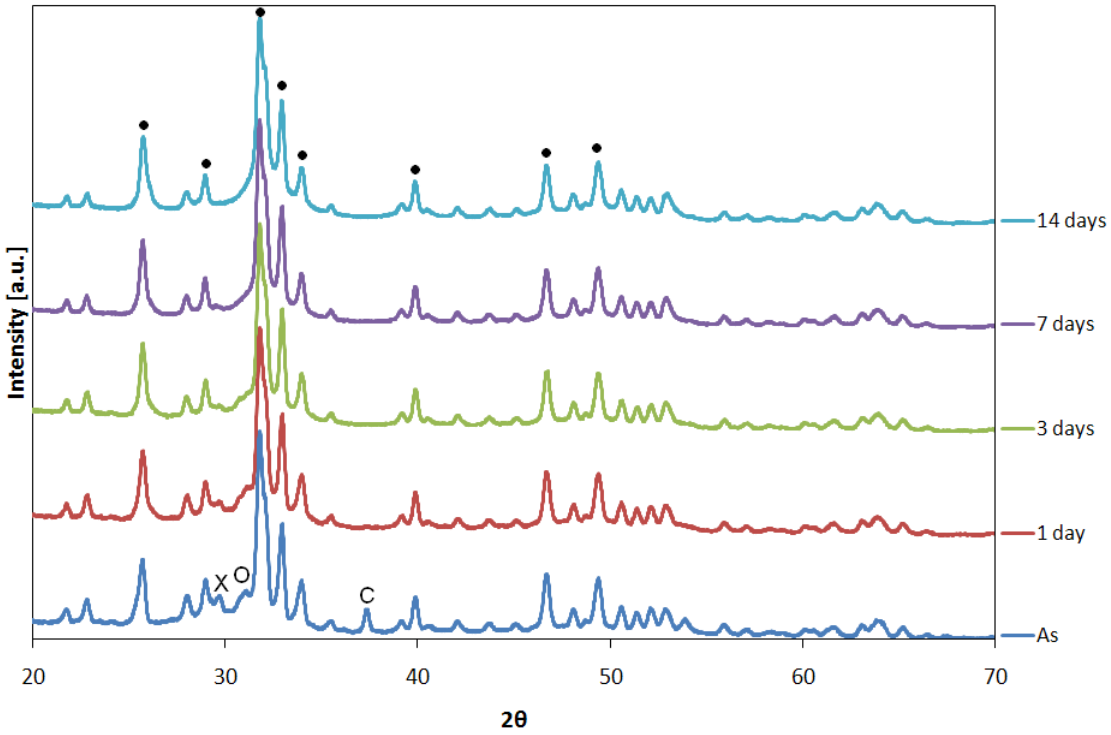

Figure 2.24: XRD, PS-HA coatings, evolution of the spectra after *in vitro* tests (As: as-sprayed – to be considered as a term of comparison).
X: TTCP, O: TCP, C: CaO, ●: HA

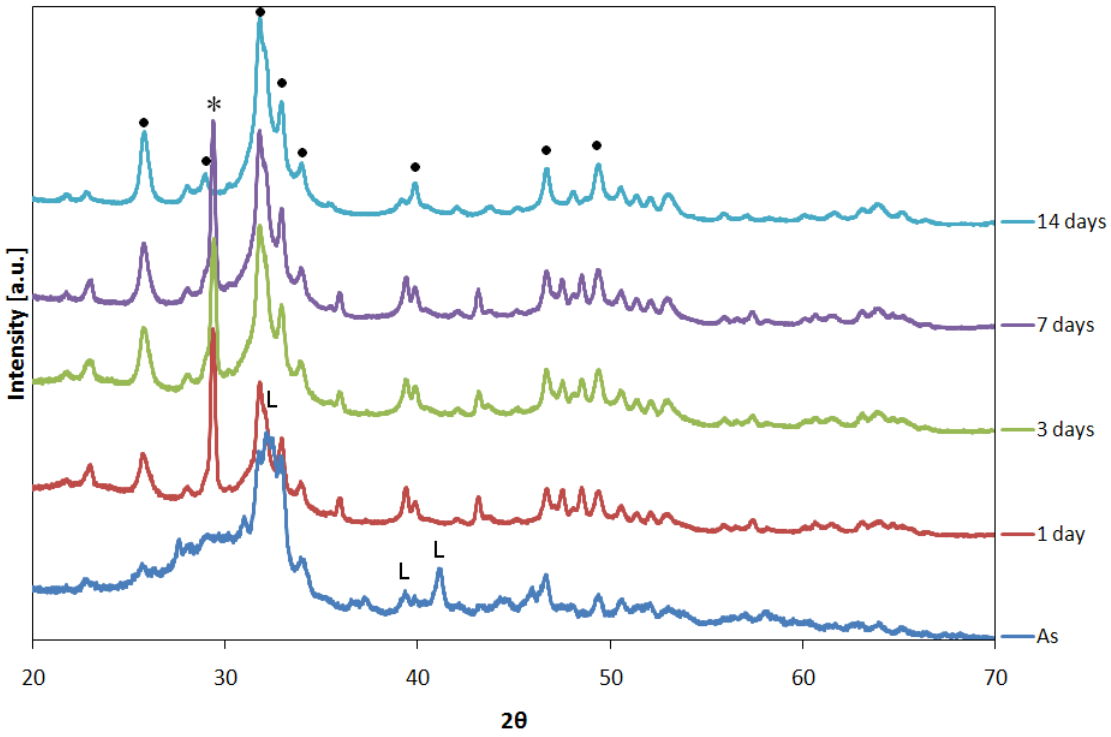

Figure 2.25: XRD, PS-HA/SPS-BGCa coatings, evolution of the spectra after *in vitro* tests (As: as-sprayed – to be considered as a term of comparison).
L: larnite (Ca_2SiO_4), *: calcite ($CaCO_3$), ●: HA

Further information on the reactions occurring in SBF could be obtained by means of Raman micro-spectroscopy. Figure 2.26 compares the spectra of the PS-HA samples soaked in SBF to that of the as-sprayed coating. In particular, if the pattern of the as-sprayed HA is considered, the peak associated to the symmetrical stretching of the PO_4 group, at about 960 cm^{-1}, can be separated in two different contributions, namely a broad and weak peak, and a sharp and intense one. The latter can be associated to HA, while the former is probably due to the decomposition phases: ACP, TTCP and TCP [154]. After immersion in SBF, the Raman peaks associated to HA became broader and less defined, but they didn't shift to different wavenumbers. The gradual change in the peak shape was probably due to the precipitation of poorly crystallized HCA on the original surface.

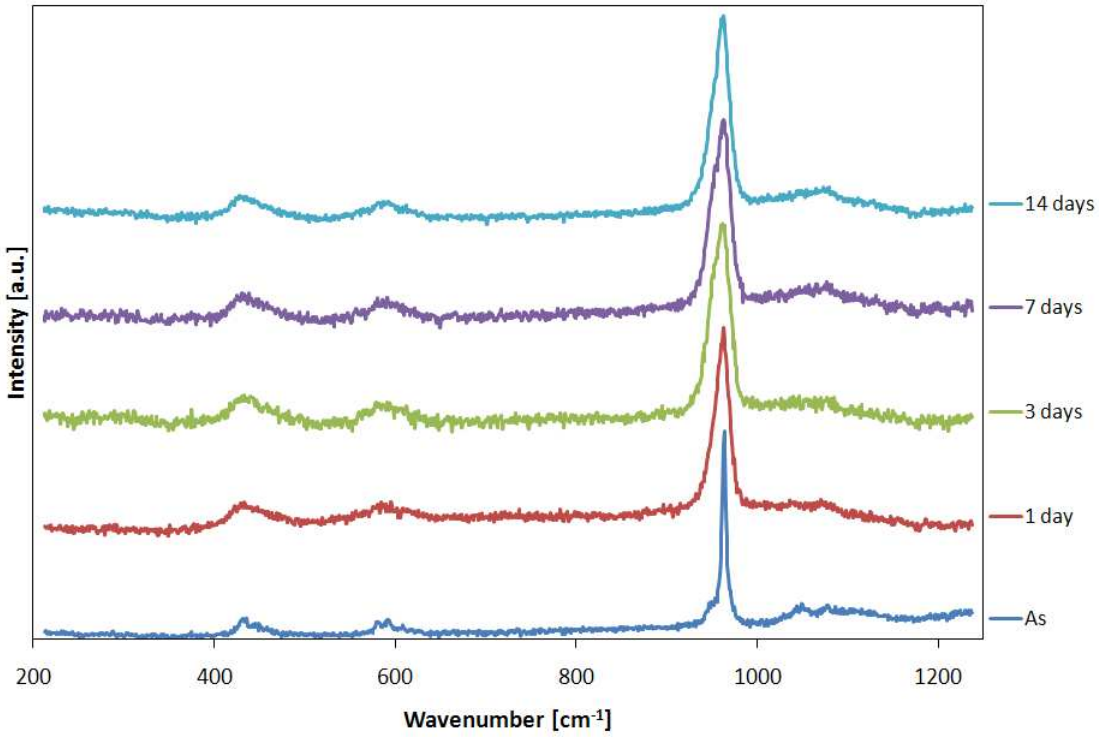

Figure 2.26: Raman spectra, PS-HA coatings, evolution of the spectra after *in vitro* tests

The Raman spectra acquired on the surface of the PS-HA/SPS-BG coatings showed a marked change after the immersion in SBF (Fig. 2.27). In the spectrum of the as sprayed coating, three bands related to BG_Ca glass were observed: two bands at about 635 cm^{-1} and from 800 to 1150 cm^{-1}, which are associated to the Si-O-Si bonds in silica, and a third band at 950 cm^{-1}, which is due to the symmetrical stretching of the PO_4 group [130]. From a qualitative point of view, the evolution of the spectra in SBF was similar to that observed for the XRD patterns: starting from the first day in SBF, the peaks of the glass are progressively replaced by those of HA. The latter, in turn, became sharper with increasing immersion time. Moreover, after

immersion in SBF, a peak at approximately 1070 cm^{-1} appeared, which is associated to the carbonate group of HCA [130]. In the spectra of the PS-HA sample the peak was less pronounced, confirming that the bioactive glass top layer increased the reactivity of the system.

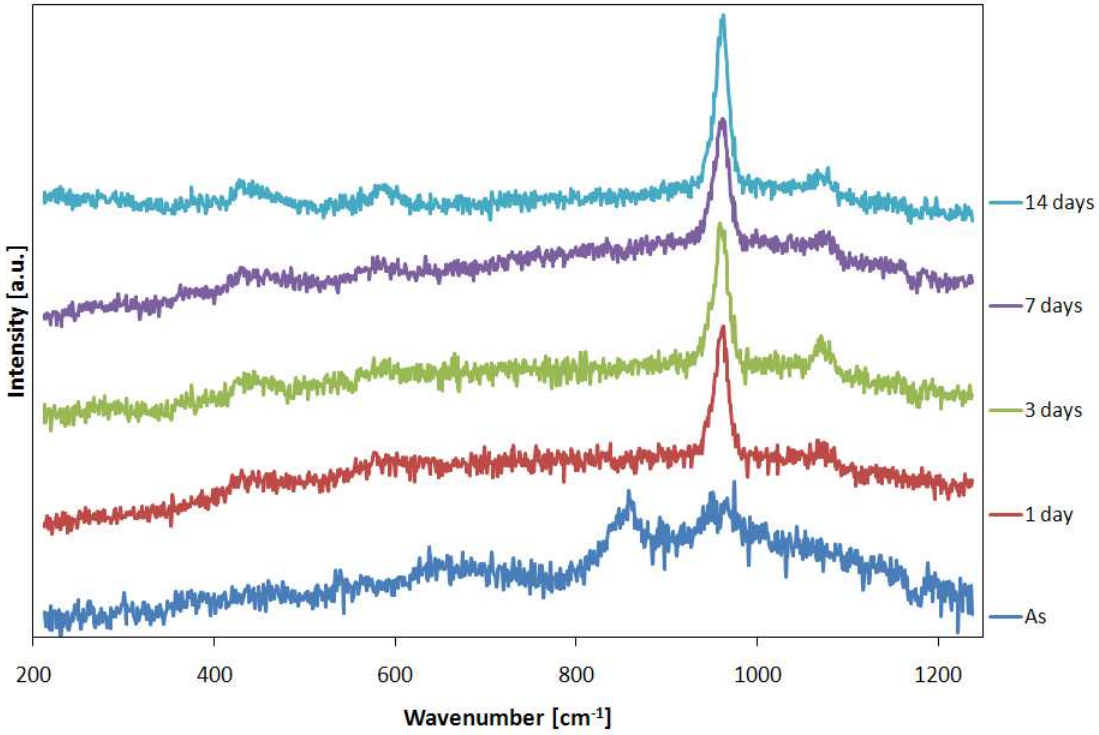

Figure 2.27: Raman spectra, PS-HA/SPS-BGCa coatings, evolution of the spectra after *in vitro* tests

Figures 2.28-2.31 propose some representative SEM images of the samples soaked in SBF. After one day of *in vitro* test, a few micron-thick reaction layer grew on PS-HA coatings; as shown by EDS analysis (Fig. 2.28), the layer had a Ca/P ratio of 1.49, a value similar to that of calcium-deficient ACP, as already mentioned in Chapter 1.2.5.

Instead, if the PS-HA/SPS-BGCa system is considered (Fig. 2.29), the topcoat entirely reacted after one day in SBF, and just silicon and oxygen were detected by EDS analysis, thus suggesting the development of a silica gel surface layer. The very high reactivity of the topcoat was due to the concomitant effect of the intrinsic bioactivity of the BG_Ca glass [69] and of the porous microstructure of the layer. In fact the rich porosity of the topcoat favoured the penetration of SBF in depth and greatly increased the specific surface area available for the chemical reactions. It is interesting to observe that, after one day in SBF, the silica gel layer, in turn, was already covered by a very thin deposit of calcium phosphate.

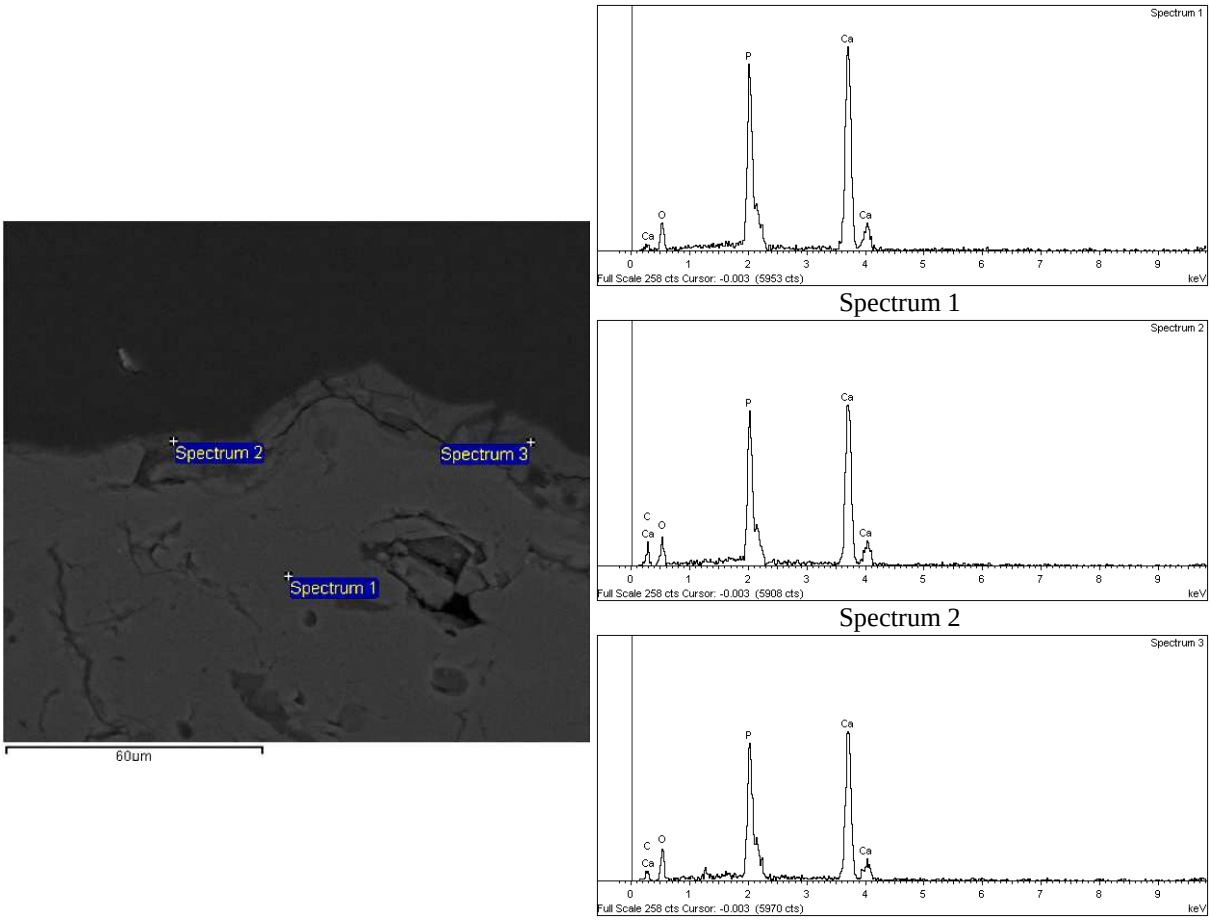

Figure 2.28: Cross section and EDS microanalysis of the PS-HA coating after 1 day in SBF
Spectrum 1: Ca/P 1.62, Spectrum 2 and 3: Ca/P 1.49

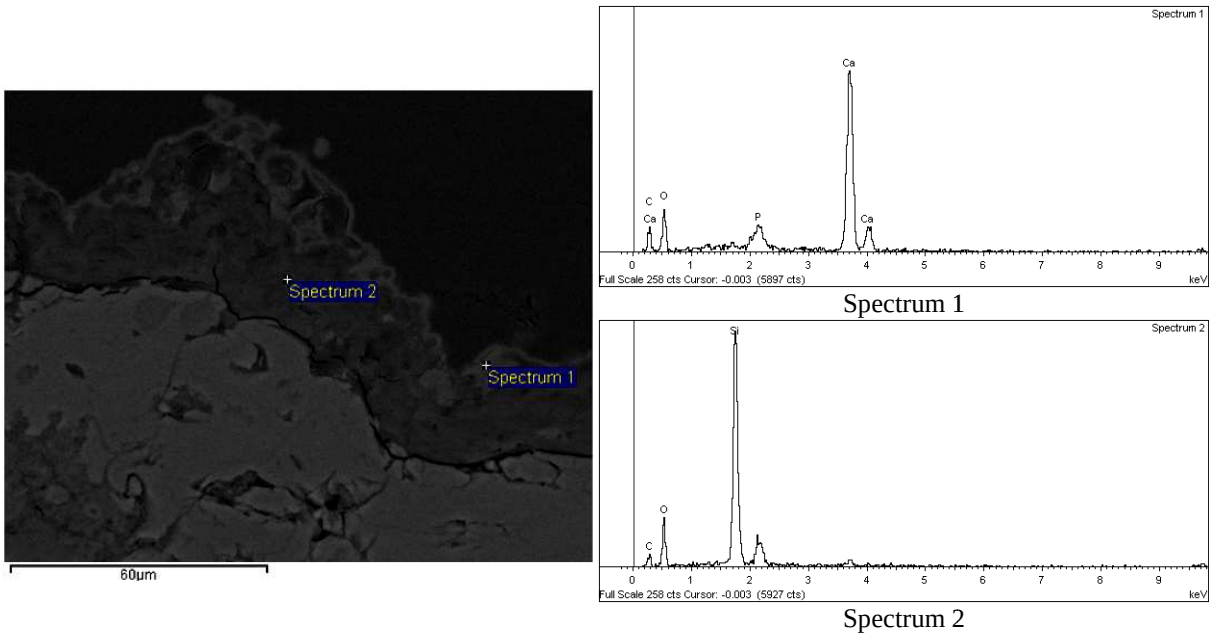

Figure 2.29: Cross section and EDS microanalysis of the PS-HA/SPS-BGCa coating after 1 day in SBF

The growth of the calcium phosphate layer continued for increasing immersion time and, after one week in SBF, the topcoat was completely converted to HCA (Fig. 2.30), with a Ca/P ratio close to that of stoichiometric HA (Fig. 2.30, Spectrum 1). Furthermore, the grown HCA was well integrated in the coating, since the interface was not easily detectable.

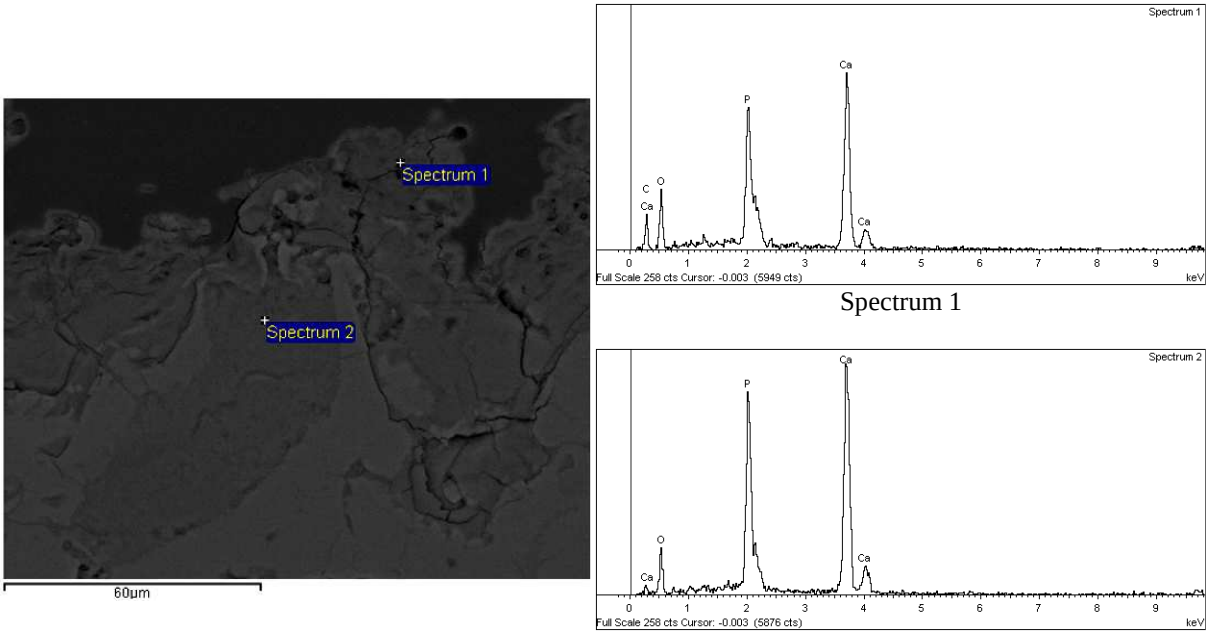

Spectrum 1

Spectrum 2

Figure 2.30: Cross section and EDS microanalysis of tha PS-HA/SPS-BGCa coating after 7 day in SBF
Spectrum 1: Ca/P 1.68, Spectrum 2: Ca/P 1.51

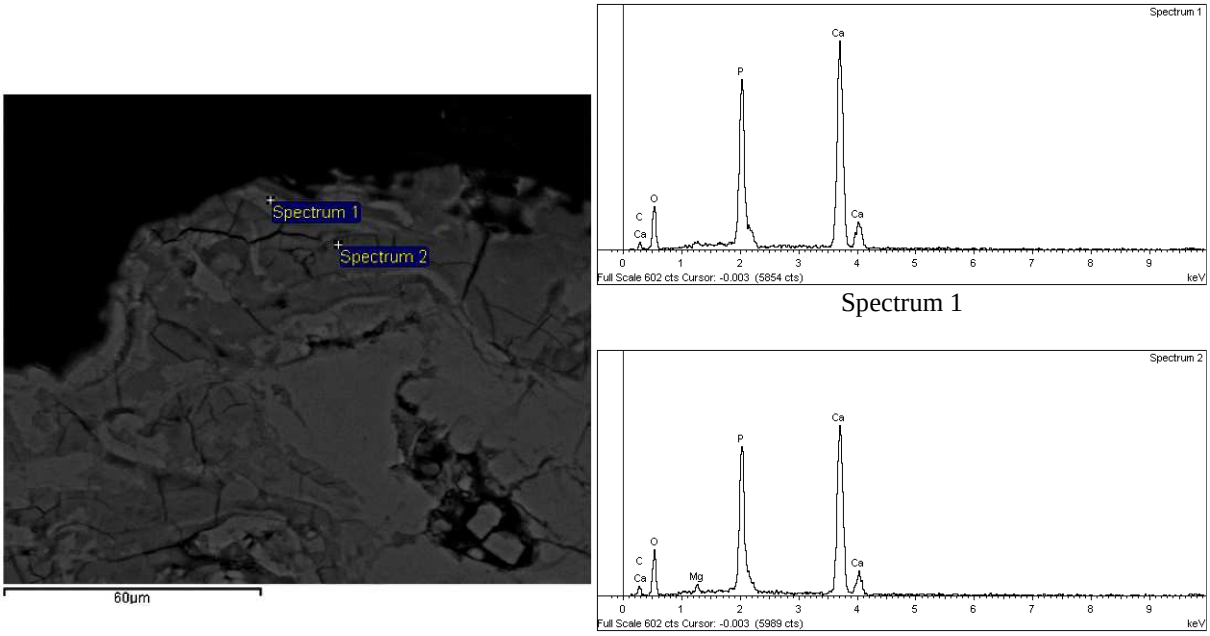

Spectrum 1

Spectrum 2

Figure 2.31: Cross section and EDS microanalysis of the PS-HA coating after 14 day in SBF
Spectrum 1: Ca/P 1.50, Spectrum 2: Ca/P 1.42

As a general consideration, the reaction kinetics were faster on the PS-HA/SPS-BGCa system than on the pure PS-HA coating. Indeed, the HCA layer grown in the PS-HA sample after 14 days in SBF was thinner than that grown on the PS-HA/SPS-BGCa system after 7 days in SBF, as it is apparent from the comparison of the corresponding SEM images in Fig. 2.30 and Fig. 2.31.

2.3.3 Conclusions

In this study HA coatings with and without a bioactive glass topcoat were tested *in vitro.*

With respect to pure HA coatings, the samples with the glass topcoat showed a greater reactivity, since the surface was entirely covered by HCA in less than one week. Nevertheless, this is only a preliminary trial, since cell tests are necessary to determine the effectiveness of the topcoat. In this way it could be possible to verify whether the high porosity of the topcoat, associated to the intrinsic bioactivity of the glass, could be able to increase the absorption of metabolites and the cellular activity.

2.4 *Suspension Plasma Sprayed hydroxyapatite/bioactive glass composite coatings. Comparison of different microstructures*

Introduction

The aim of this work was to produce different composite coatings with bioactive glass and hydroxyapatite, and then to verify which of them possessed the best properties.

Bioactive glass and hydroxyapatite were chosen since they are the most common bioactive materials, and they both have their unique characteristics. In fact, bioactive glasses have a very high index of bioactivity, while HA is stable in biological environment.

The so-called BG_Ca was selected as the bioactive glass [69], since it has good bioactivity and a limited tendency to crystallize at high temperature, due to its formulation which is relatively rich in CaO and poor in Na_2O with respect to conventional bioactive glasses based on the standard Bioglass® 45S5 developed by Hench [30]. The same BG_Ca glass has already been used to produce bioactive coatings in previous studies [141].

The suspension plasma spray technique was chosen, because it makes it possible to obtain coatings with a fine microstructure and, most of all, because it works on powder suspensions, which may result in easier mixing of different feedstock materials.

Three different types of composite coatings were produced, which were named: Composite, Duplex and Graded. The Composite coatings were produced spraying a mixture of the two raw materials and therefore the constituent phases were randomly distributed throughout the coating.

The Duplex coatings consisted in a double-layered structure: BG_Ca on the surface and HA in contact with the substrate. In this case the hydroxyapatite worked as a bond coat for the bioactive glass. The layering sequence was designed in order to take full advantage of the high bioactivity of bioactive glasses, which is superior to that of HA thus making them more suitable to interface with the biological environment. On the other hand, HA has a great *in vivo* stability, thus it provides a more stable protection to the substrate.

The Graded coatings were an evolution of the Duplex coatings, in which the composition varied gradually from HA to BG_Ca. The coatings were obtained by spraying many layers with progressively different composition. The advantage of a graded structure is that the abrupt glass/HA interface, which may be a weak point in conventional bi-layered systems, is removed.

2.4.1 Materials and methods

2.4.1.a Feedstock materials

Bioactive glass suspension:

The BG_Ca glass was produced by the conventional melt-quenching method (as described in detail in Chapter 2.1), then it was dry milled, and attrition milled in ethanol with 2 wt.% of Beycostat C213. The obtained BG_Ca powder had a mono-modal distribution with mean diameter of d_{50}=4.7 µm (Fig. 2.32), as determined with a granulometer Partica LA-950V2 (Horiba). The feedstock suspension was formulated by dispersing 20 wt% of solid phase in 80 wt% of ethanol. Ethanol was chosen as an attrition and suspension fluid since bioactive glasses are water-reactive [142].

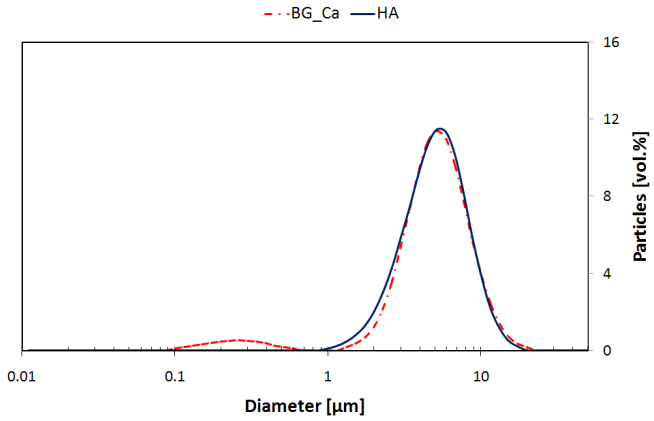

Figure 2.32: Grain size distribution of the powders

Hydroxyapatite suspension:

The starting powder was pure Hydroxyapatite (HA) with mean diameter of d_{50}=120 µm commercialized by Tomita (Japan). The powder was milled by an attrition system using 0.8 mm zirconia balls and adding the dispersant Beycostat C213 (2 wt% of the dry powder). The obtained powder had a slightly bi-modal distribution with mean diameter of d_{50}=4.6 µm, (Fig. 2.32). The feedstock suspension was formulated by dispersing 20 wt% of solid phase in 40 wt% of ethanol and 40 wt% of water. The use of a mixture of water and ethanol was chosen since water vapour prevents the decomposition of HA [17].

Moreover, it should be underlined that, in order to obtain HA-glass composite layers, it was necessary to spray the HA and the bioactive glass powders together, so the deposition conditions were set in between of those optimized for the constituent phases, BG_Ca and HA, when sprayed individually [25, 141]. Since the BG_Ca glass requires a more powerful treatment than HA, the high power may increase the decomposition of HA. Then, the addition of water, which reduces the enthalpy of the plasma [155], may preserve the structure of HA, especially during the deposition of HA-rich composite layers. On the other hand, if the HA

powder were dispersed in pure water, the enthalpy of the plasma would be reduced to such an extent that the glass particles could not be properly melted. Moreover, the mixing into the injector of a water-based suspension and the BG_Ca-ethanol one may favour the clogging of the injector.

2.4.1.b Coatings deposition

An SG-100 torch (Praxair, S.T., Indianapolis, IN, USA) was used to produce the coatings. Both the suspensions were supplied by means of peristaltic pumps (Fig. 2.33a). The pumping systems were two and independent, the suspensions were mixed only at the entrance of the injector. Two non-return valves were mounted in order to avoid undesired mixing and reflux (Fig. 2.33b). During spraying, the suspensions were continuously stirred to avoid sedimentation and agglomeration. An injector with a 500 μm-large hole was used; the injection of the suspension was internal to the torch, at 16 mm from its exit.

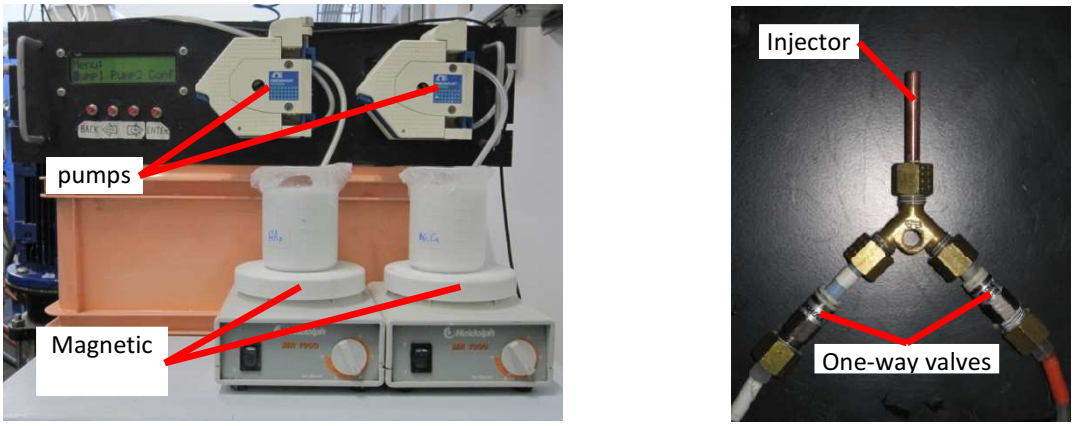

(a) (b)

Figure 2.33: Suspension feeding system: (a) peristaltic pumps, (b) injector

Various trials were made to find the deposition parameters that could combine a minimal decomposition of HA with a good cohesion of the BG_Ca particles. The final spray parameters are listed in the Table 2.7.

	Power [kW]:	34
Gases	**Ar [slpm]:**	45
	H_2 [slpm]:	7.5
	Distance [mm]:	55
	Torch speed [mm/s]:	750
	Scan step [mm]:	10
	Suspensions flowrate [g/min]:	30

Table 2.7: Spray parameters

All the coatings were obtained through 8 spraying sessions, each of which corresponded to 4 torch passages. Before each session, the sample surface was left to cool down below 80°C.
In order to obtain the different microstructures of the Composite, Duplex and Graded coatings, the flow rates of the two suspensions were properly regulated by means of the peristaltic pumps. The used values are listed in Table 2.8. The expected compositions are schematically shown in Figure 2.34.

Session	*Composite*		*Duplex*		*Graded*	
	BG_Ca	*HA*	*BG_Ca*	*HA*	*BG_Ca*	*HA*
1	15	15	-	30	-	30
2	15	15	-	30	4	26
3	15	15	-	30	9	21
4	15	15	-	30	13	17
5	15	15	30	-	17	13
6	15	15	30	-	21	9
7	15	15	30	-	26	4
8	15	15	30	-	30	-

Table 2.8: Suspensions flow rates [g/min]

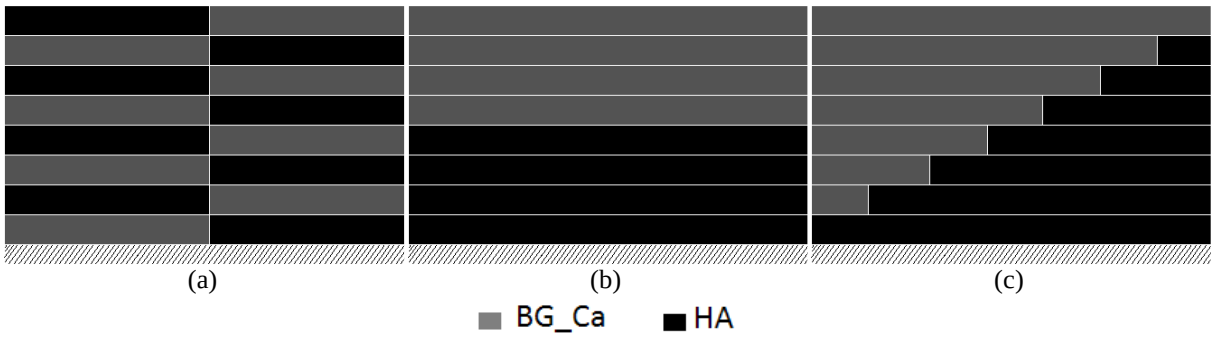

Figure 2.34: Theoretical microstructure of the composite coatings: (a) Composite, (b) Duplex, (c) Graded

Substrates were 316 l stainless steel discs (25 mm in diameter, thickness of 8 mm). They were sandblasted using 250 μm corundum powder at 5 Bar. The resulting roughness was R_a=3.5 μm. Before spraying the substrates were ultrasonically washed with ethanol and acetone.
During the deposition an optical IN 5 Plus pyrometer (Impac) was used to record the superficial temperature. The mean values of the temperature were calculated for each spray session, and they are reported in Table 2.9.

	Composite	*Duplex*	*Graded*
T_{mean}**[°C]**	321	247	297
Std. Dev. [°C]	10	53	46

Table 2.9: Mean surface temperatures measured during spraying

Coatings of pure BG_Ca and of pure HA were also sprayed using the same spraying parameters of the composites. The mono-component coatings were used as a reference. Composite, Duplex, and Graded samples in the following will be referred to as "bi-phasic" to distinguish them from mono-component coatings.

2.4.1.c *In vitro* tests

The samples were tested *in vitro* by soaking them in a simulated body fluid (SBF). According to the standard protocol defined by Kokubo and Takadama, the SBF volume-to-coating surface ratio was fixed to 20 ml/cm^2. Therefore the samples were cut to obtain a surface area of 1 cm^2 and each sample was immersed in 20 ml of SBF. The samples were removed from the SBF after time periods of 1, 7, and 14 days. During the tests the SBF was refreshed every 2 days in order to simulate the dynamic conditions of the human body. The temperature was constant at 37°C and the sealed containers were kept in a water vapour saturated environment to avoid fluid evaporation. At the extraction from SBF, the samples were carefully washed with distilled water, and dried at room temperature.

2.4.1.d Characterization

The samples were analysed before and after soaking in SBF through different techniques.

The surface of the coatings was investigated by means of X-Ray Diffraction (XRD). The used instrument was an X'pert PRO diffractometer (PANalytical, Almelo, The Netherlands) equipped with an X'Celerator detector. The diffraction patterns were collected in the 10°-70° 2θ range (step size: 0.017°, step time: 71.12 s).

An accurate microstructural analysis was carried out on the coatings' surface and polished cross section by means of an environmental scanning electron microscope ESEM (ESEM Quanta 200-FEI Company, Eindhoven, The Netherlands) equipped with an X-EDS microanalysis system (Inca, Oxford Instruments, U.K.). The microscope was operated in high-vacuum and in low-vacuum mode according to the specific sample to analyse (pressure: 0.45 Torr).

Scratch tests were performed on the surface of the as-produced bi-phasic coatings (Open platform, CSM Instruments, equipped with 100 µm Rockwell diamond tip). The parameters of the scratch were: linear load from 20 mN to 30 N, scratch length 3mm, load rate 10 N/min. Critical loads were determined by optical analysis. Three scratches were performed on each sample.

2.4.2 Results

Regardless of the composition, the obtained bi-phasic coatings appeared continuous.

To verify if the obtained microstructures corresponded to the expected ones, the polished cross-sections were analysed through EDS analysis. Compositional maps were acquired (Fig. 2.35). The silicon was selected as the marker of BG_Ca, while the phosphorous was chosen to indicate the HA.

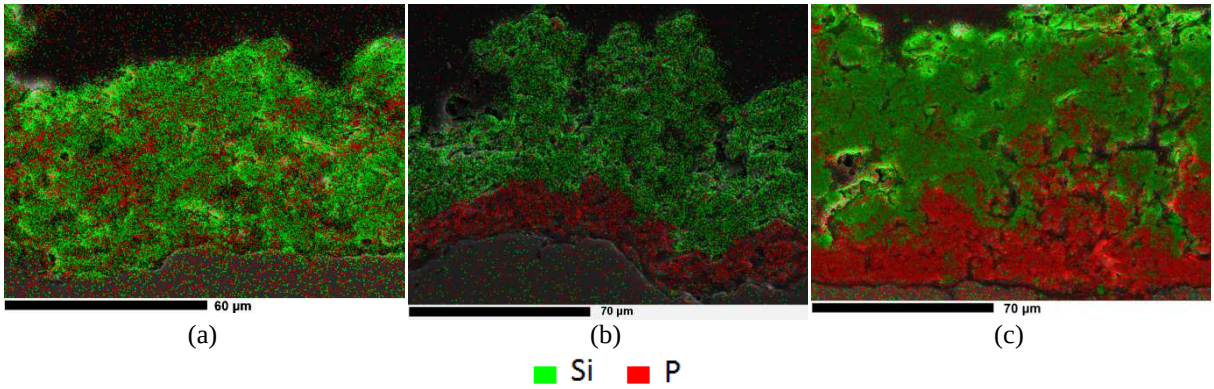

Figure 2.35: EDS maps showing the distribution of Si (in green – representative of BG_Ca glass) and P (in red – representative of HA) on the cross section: (a) Composite, (b) Duplex, (c) Graded

The microstructures, as is shown in Figure 2.35, were similar to the expected ones (Fig. 2.34). The microstructure of the Composite sample (Fig. 2.35a) appeared as a glass matrix within which zones of HA were dispersed. The cross-section of Duplex sample (Fig. 2.35b) was clearly divided into two layers. Finally, in the Graded sample (Fig. 2.35c), the composition varied along the thickness of the coating. The main difference between the expected microstructures and obtained ones was the greater presence of BG_Ca in the latter. Most likely, the higher deposition efficiency of the bioactive glass with respect to the HA was the main reason for such difference. In fact, the pure BG_Ca coating was twice as thick as the pure HA one (Fig. 2.36a), although both of them were produced using the same parameters.

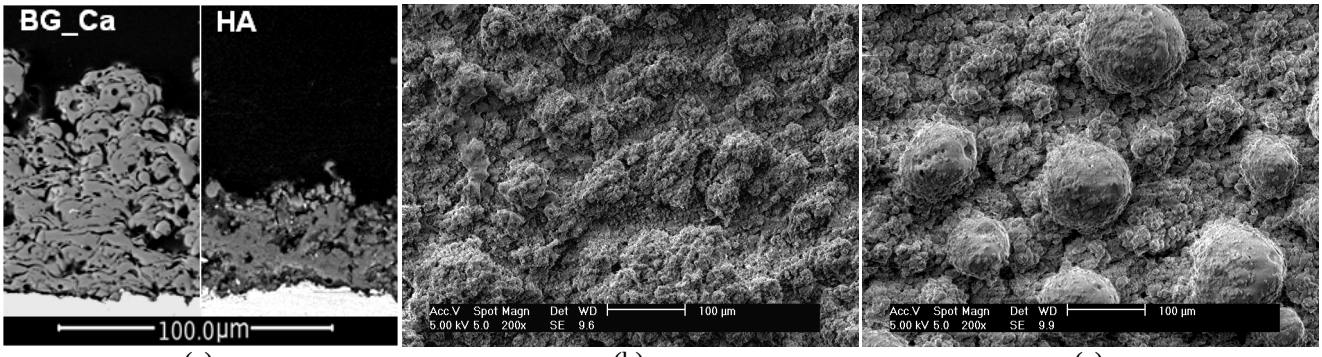

Figure 2.36: SEM images of the reference coatings:
(a) compared cross-sections, (b) HA surface, (c) BG_Ca surface

The mechanical characterization of the samples was focused on the scratch-resistance of their surface. The critical load was defined as the load at which the metal substrate was detectable. The values were mainly determined by means of optical observation, but also frictional force and acoustic emission were used for validation (Fig. 2.37). The critical load was 21.2 (1.7) N for the Duplex and 27.1 (0.8) N for the Composite. During the scratch test of the Graded sample, instead, the maximum load (30 N) allowed by the instrument was reached without uncovering the substrate. Therefore the graded microstructure provided the best adhesion between the coating and the substrate. Probably the double layer structure of the Duplex sample induced the formation of residual stresses, which were strongly reduced by the progressive change in composition of the Graded coating.

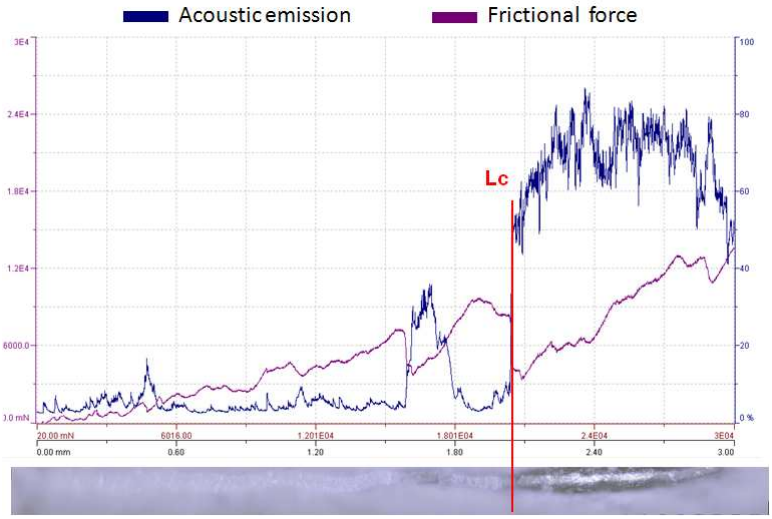

Figure 2.37: Example of a scratch test (Duplex coating):
juxtaposition of Acoustic emission graph, Frictional force graph and Optical analysis

The surface of the samples (Fig. 2.38) showed a high roughness mainly due to the presence of semi-spherical structures which derived from sintering and swelling phenomena associated to the BG_Ca particles. In fact, the morphology of the Composite coating, whose surface was the richest in HA, was quite similar to that of the pure HA coating (Fig. 2.36b), which didn't display the semi-spherical structures. Instead the surface of the Duplex and Graded samples (Fig. 2.38b-c), which was rich in glass, showed a diffused development of semi-spherical features. At a higher magnification (Fig. 2.39), both flattened splats and crystallized zones were present. The crystals were very thin and possessed an acicular morphology. As previously observed for semi-spherical structures, also the crystallizations were more evident in the glass-rich surfaces.

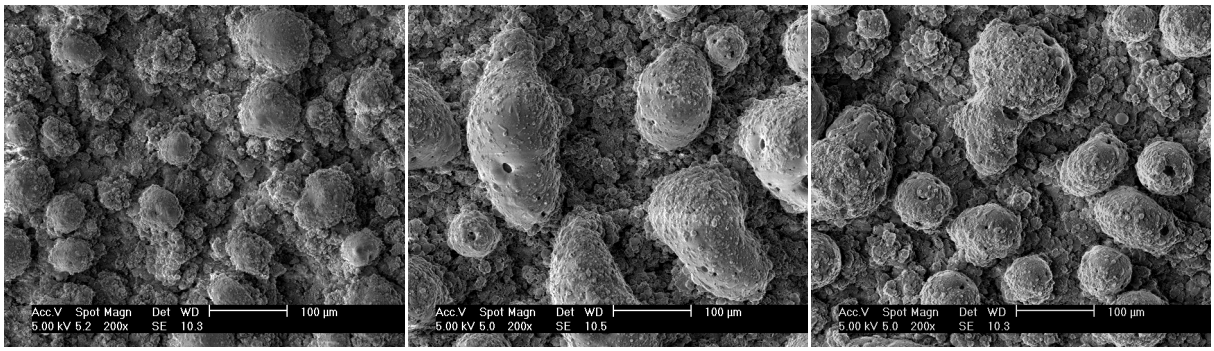

(a) (b) (c)

Figure 2.38: SEM images of the coatings' surface: (a) Composite,(b) Duplex, (c) Graded

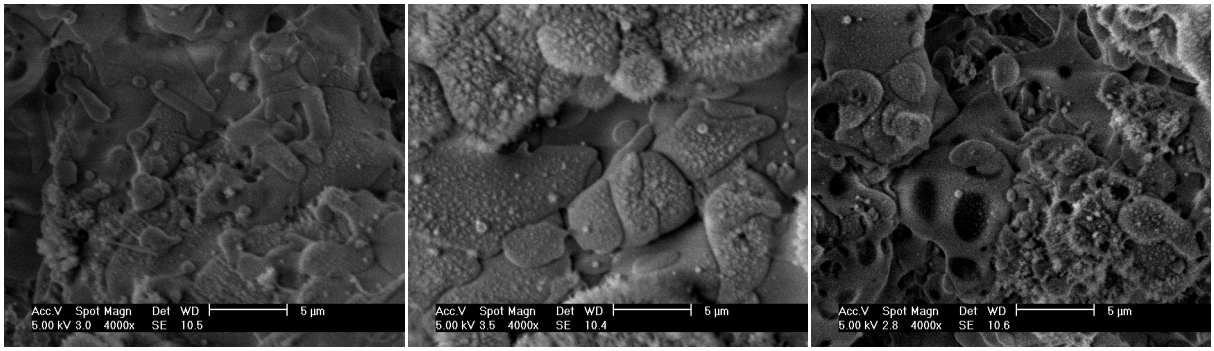

(a) (b) (c)

Figure 2.39: High magnification SEM images of the coatings' surface: (a) Composite, (b) Duplex, (c) Graded

Comparing the X-ray diffraction spectra (Fig. 2.40), a similarity between the Duplex and Graded samples was observed. They also resembled the spectrum of the pure BG_Ca coating. In the spectra, the broad band between 25° and 35° (2θ) was due to the glassy phase, and the peaks of pseudowollastonite ($CaSiO_3$) were detected. Instead, the pattern of the Composite sample was more similar to that of the pure HA coating. This is not surprising since, in this sample, a high amount of HA was present on the surface. In the spectrum of the Composite coating, the peaks of HA and the band of glass were both present, but the development of pseudowollastonite was not evident.

Finally, the diffractogram of the pure HA coating, besides the peaks of the HA itself, showed some weak peaks attributable to the decomposition phases TTCP, TCP and CaO. Since the Composite, Duplex and Graded Coatings were sprayed with the same parameters used for the pure HA sample, it is probable that also the HA present in such coatings suffered a limited decomposition even if the peaks of the secondary phases were not visible due to the presence of the bioactive glass which surrounds – in the Composite coating – or covers – in the Duplex and Graded coatings – the HA.

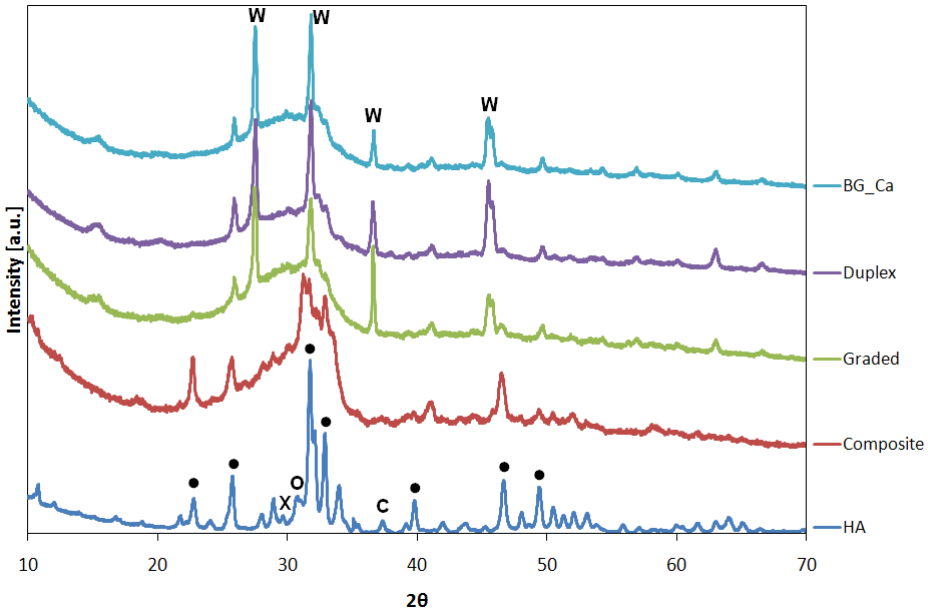

Figure 2.40: X-ray diffraction patterns of the as-produced coatings.
W: pseudowollastonite, X: TTCP, O: TCP, C: CaO, ●: HA

Comparing the evolution of the XRD spectra after *in vitro* test, a similar behaviour could be observed for the Duplex (Fig. 2.41) and Graded (Fig. 2.42) samples. The peaks of the crystallization phases disappeared after a week of immersion; at the same time the main peaks of HA became visible. A broad halo in the 20°-25° 2θ range was due to the growth of a silica gel layer and the peaks of calcium carbonate, co-precipitated with HCA, could be observed occasionally. After two weeks in SBF, the peaks in the diffraction spectra of the Duplex and Graded samples were exclusively associated to HCA. However the peaks were broad, thus confirming the low crystallinity of the HCA developed *in vitro*.

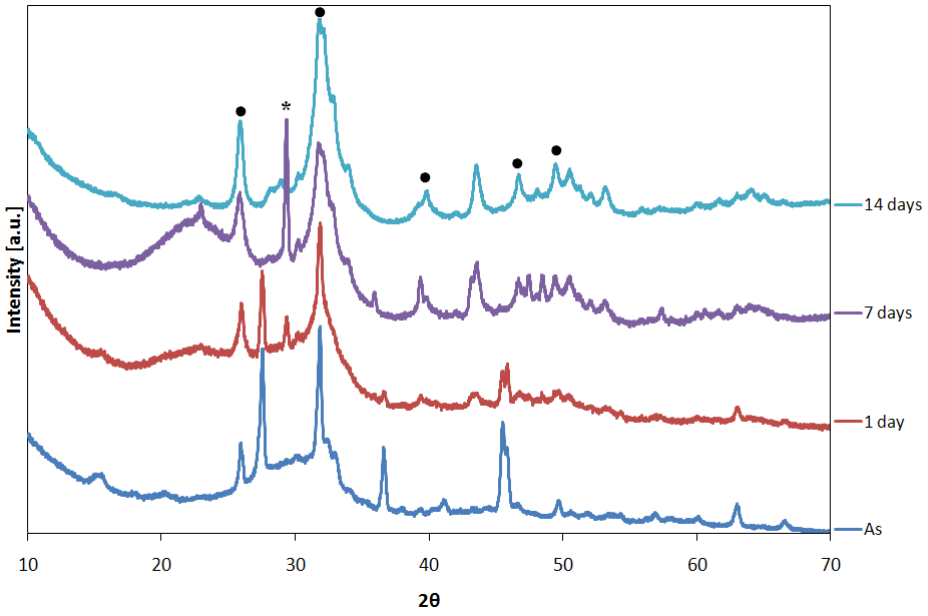

Figure 2.41: XRD, Duplex coatings, evolution of the spectra after *in vitro* tests. *: $CaCO_3$, ●: HA

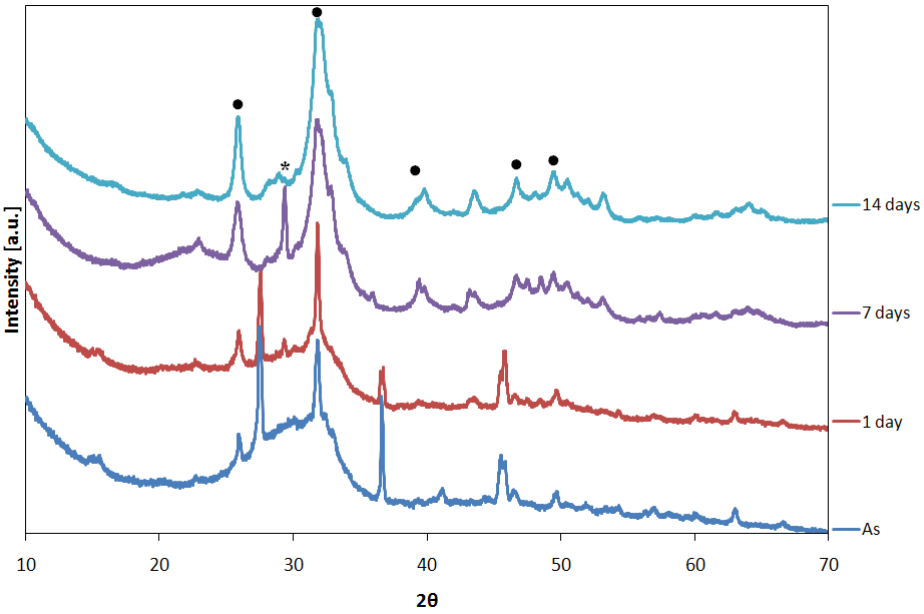

Figure 2.42: XRD, Graded coatings, evolution of the spectra after *in vitro* tests. *: $CaCO_3$, ●: HA

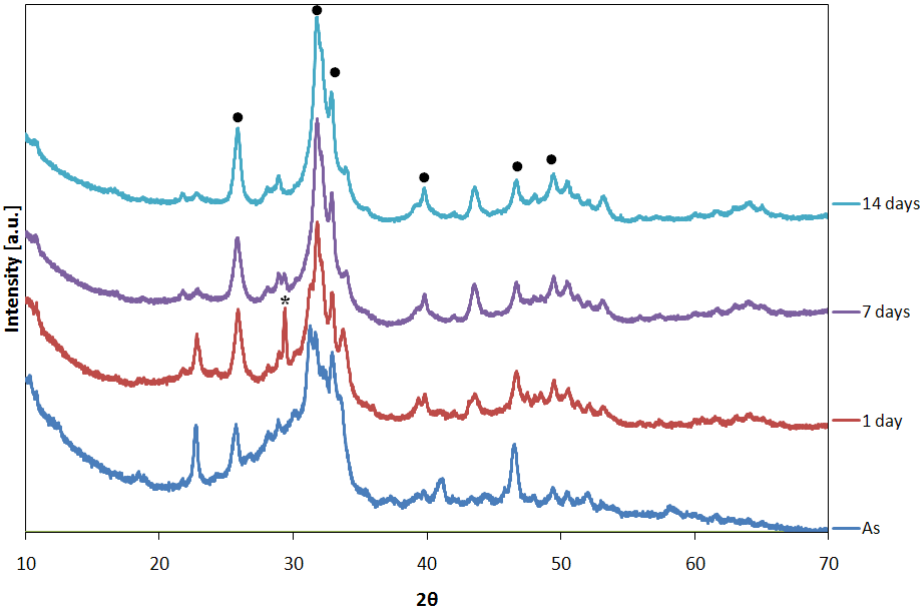

Figure 2.43: XRD, Composite coatings, evolution of the spectra after *in vitro* tests. *: $CaCO_3$, ●: HA

The diffraction spectra of the pure BG_Ca coating showed the same trend. However, in this case, after two weeks of immersion the silica gel was still detectable and the peaks of the precipitated HCA looked even broader than in the Duplex and Graded spectra. This result suggests that the presence of HA underneath the bioactive glass layer on the working surface does not compromise the reaction kinetics in the Duplex and Graded coatings.

Also the diffraction spectra of Composite coating (Fig. 2.43) showed a similar trend: starting from the first day in SBF the pattern of BG_Ca gradually disappeared and, after two weeks of immersion, only the main peaks of HCA were detectable. However in this case the HA pattern

was already present in the as produced sample. Finally, the diffraction spectra of the pure HA coating showed a slight variation as a result of immersion in SBF: the peaks associated with the secondary phases gradually disappeared starting from the first day of immersion.

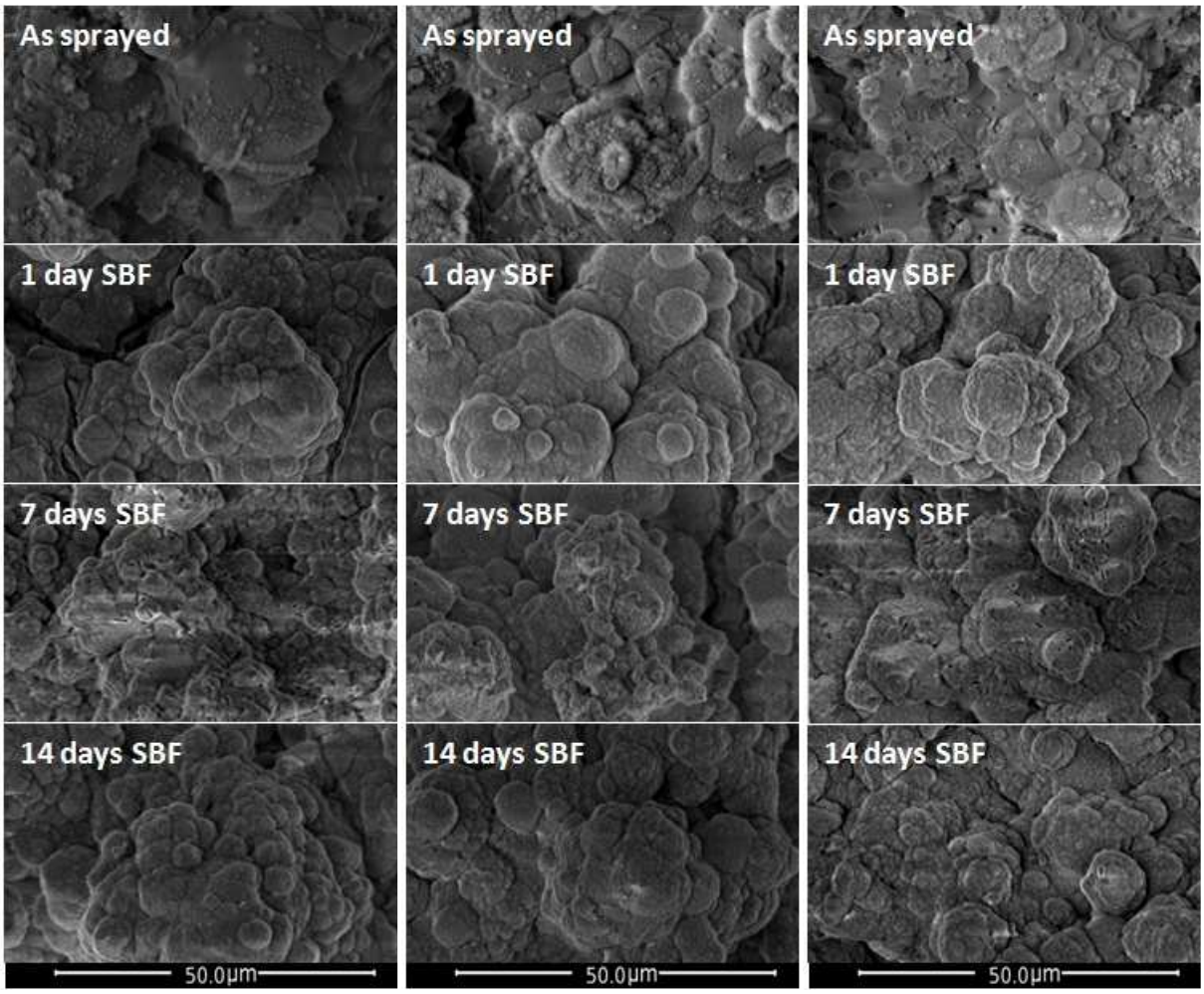

(a) (b) (c)

Figure 2.44: SEM images (secondary electrons) of the surfaces after immersion in SBF.
(a) Composite, (b) Duplex, (c) Graded

The SEM analysis of the samples corroborates the hypothesis of the HCA development *in vitro*. In fact, already after the first day of immersion in SBF, the surface morphology of the samples changed; indeed “cauliflower-like” features developed (Fig. 2.44), which are characteristic of *in vitro* grown HCA [141]. All samples showed a similar evolution. The surface of the BG_Ca coating showed the same behaviour of the bi-phasic coatings, with the development "cauliflower-like" features (Fig. 2.45a), while the bioactivity of the HA coating was less noticeable. In fact, the coating surface did not undergo significant changes as a result of the immersion in SBF (Fig. 2.45b).

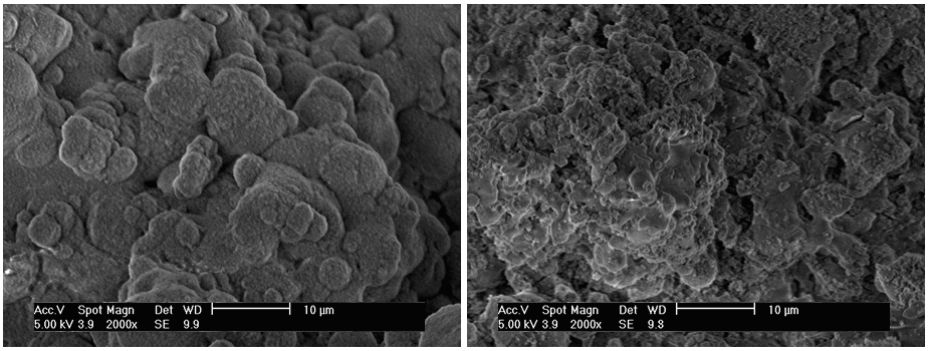

(a) (b)

Figure 2.45: SEM images of the reference coatings after 14 days in SBF:
(a) BG_Ca, (b) HA

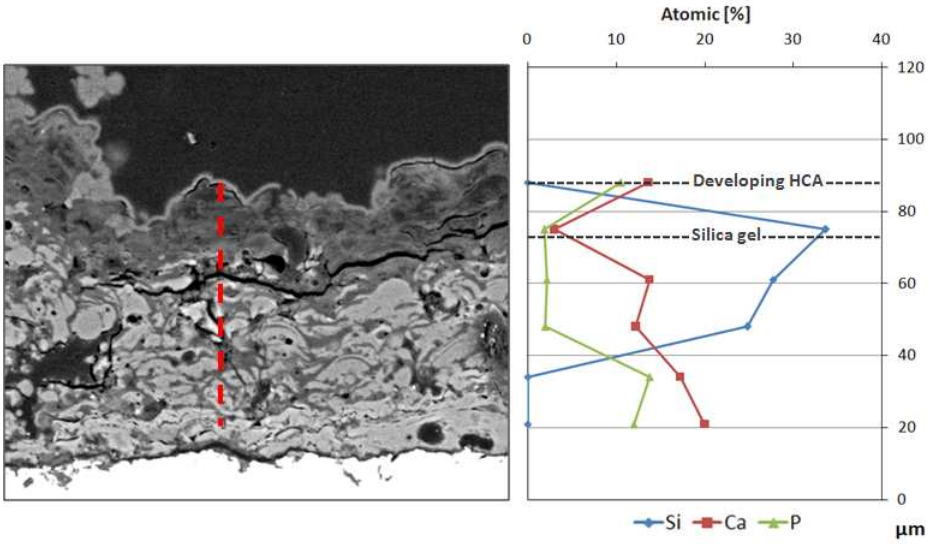

Figure 2.46: EDS analysis, Duplex coating after 1 day in SBF

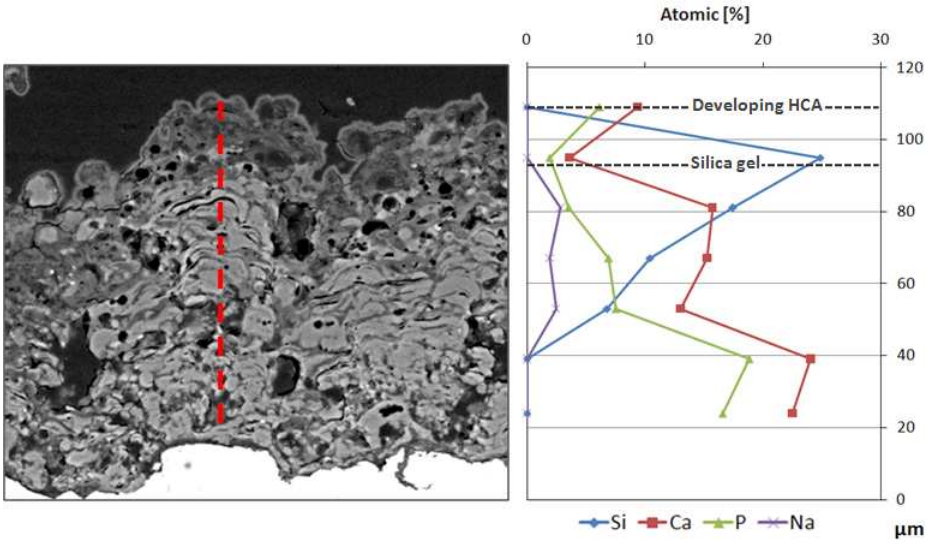

Figure 2.47: EDS analysis, Graded coating after 1 day in SBF

After one day of immersion in SBF, the cross sections of the Duplex (Fig. 2.46) and Graded (Fig. 2.47) samples showed a typical layered structure. Indeed, both samples had a surface layer

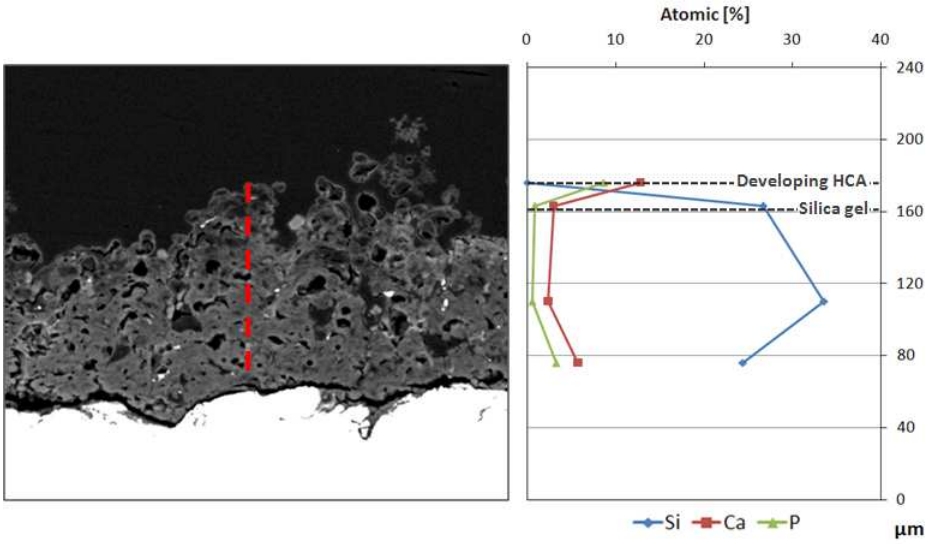

Figure 2.48: EDS analysis, BG_Ca coating after 7 days in SBF

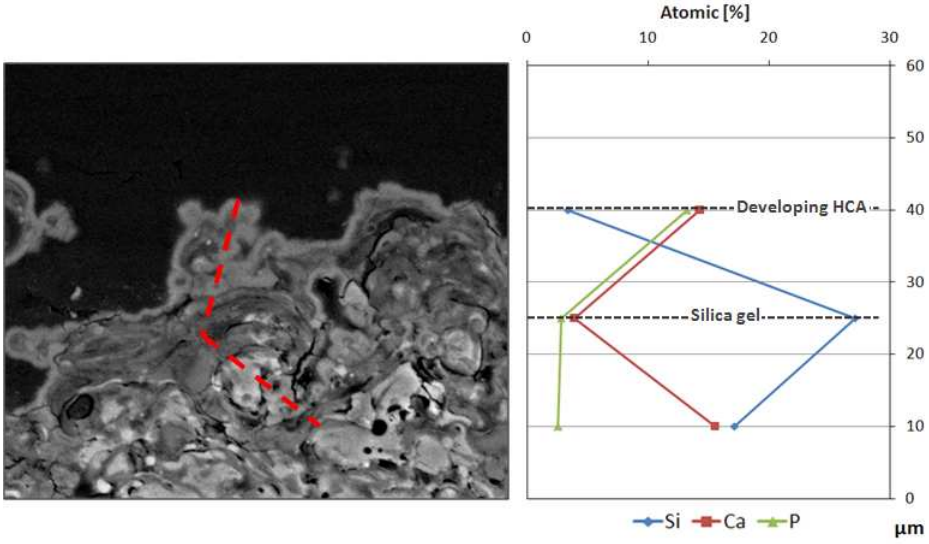

Figure 2.49: EDS analysis, Composite coating after 1 day in SBF

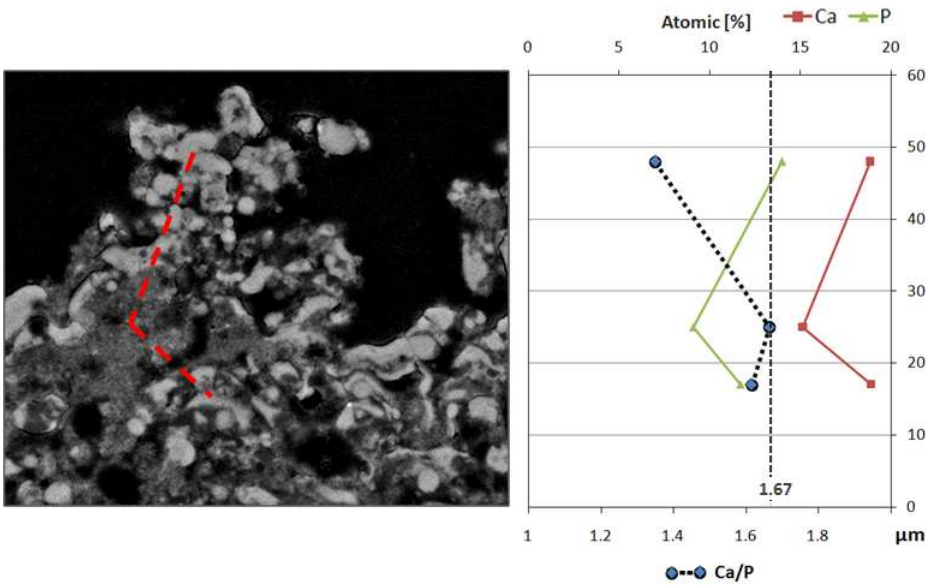

Figure 2.50: EDS analysis, HA coating after 7 days in SBF

rich in calcium and phosphorus, and a deeper layer mainly composed of silicon; below them, the deepest part of the coating was not yet altered by the SBF. On account of the data available in the literature, it is possible to conclude that the surface layer was the result of the precipitation and growth of HCA induced by the reaction between the glass and the SBF, mediated by the development of a silica gel layer [126].

The same behaviour was observed on the cross-section of BG_Ca coating, which showed the layered structure composed by HCA surface and silica gel thick zone. In fact, after one week of immersion in SBF the entire coating was converted to silica gel (Figure 2.48). Also the Composite coating (Fig. 2.49) showed a similar behaviour, since a superficial reaction zone rich in Ca and P formed. However, although silica gel zones and un-reacted glass areas were detected, in this case there was not a stratified structure, but just various spots dispersed throughout the coating thickness. This is due to the initial microstructure of the Composite coating in which areas of BG_Ca were interspersed with HA zones. As previously noted, the bioactivity of the HA coating was less marked. However area with different Ca/P ratio were observed in the cross-section of the one week soaked coating (Fig. 2.50). In particular, in the surface a Ca-poor layer was detected, which may correspond to the Ca-poor ACP mentioned in Chapter 1.2.5. However the HA coating showed good stability in SBF.

After two weeks of *in vitro* test in SBF, the Duplex (Fig. 2.51) and Graded (Fig. 2.52) samples had an anomalous microstructure. In fact they both showed the highest concentration of silicon in the deepest layers of the coating, close to the interface with the metal substrate.

This behaviour is usually observed in bioactive glasses [126], since the reaction with SBF starts at the glass surface and moves toward the deepest levels. Then, in bioactive glass coatings, the layers in contact with the substrate are normally the last part of the coating which undergoes chemical changes thus converting to silica gel and then to HCA.

Such phenomenon is difficult to explain for Duplex and Graded samples, since in the original un-reacted coatings there was not silicon at the interface with substrates (Fig. 2.35). One possible explanation is that, during the first stages of reaction in SBF, the surface zone of BG_Ca transformed to layers of silica gel and HCA (Fig. 2.46-47). Afterwards, also the process of dissolution and re-precipitation of the coatings' HA occurred. However, in this case the deepest layers of the coatings, consisting of HA, were dissolved by the SBF, and the precipitation of new HCA did not take place in the same point, but on the surface of the silica gel layer. In this way the layers below the silica gel were gradually dissolved, and new HCA developed above the silica gel. This involved a gradual migration of the silicon-rich stratum downward in the direction of the substrate. Comparing the EDS analysis of the cross-sections

(Fig. 2.51-53), the Duplex sample was the coating in which the silicon appeared more present throughout its entire thickness.

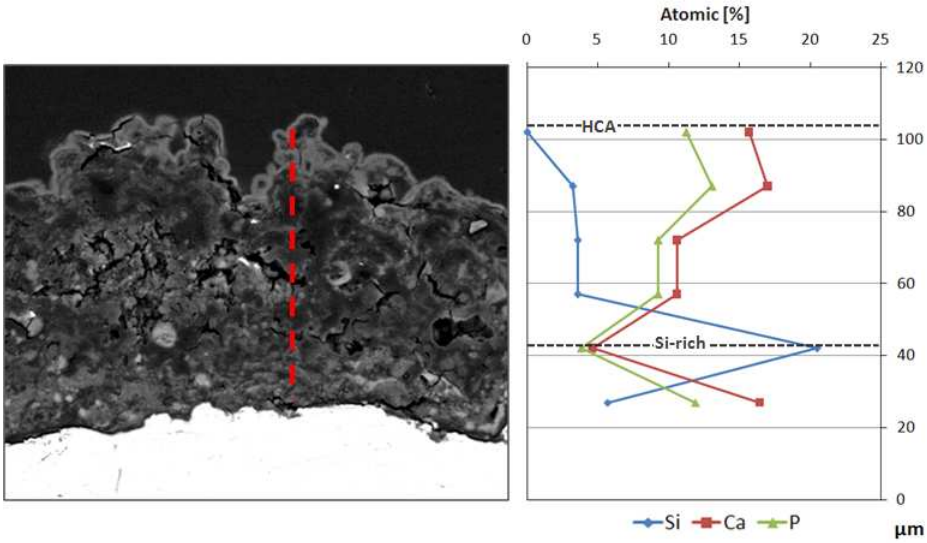

Figure 2.51: EDS analysis, Duplex coating after 14 days in SBF

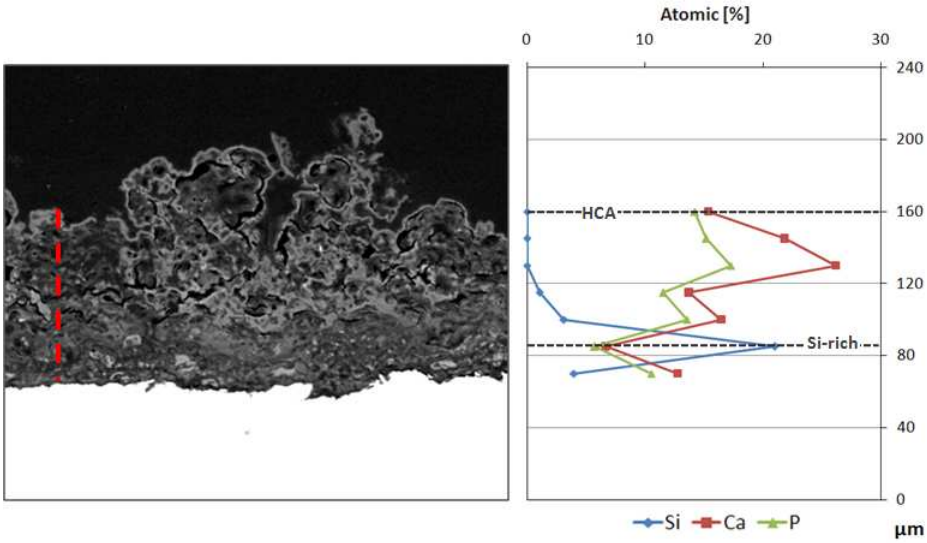

Figure 2.52: EDS analysis, Graded coating after 14 days in SBF

The silicon-rich stratum close to substrate was not observed in the Composite coating (Fig. 2.53) in which silicon-rich particles were still present throughout the thickness of the coating, even after two weeks of immersion in SBF. Once again, the different behaviour of the Composite coating may be attributed to its starting microstructure.

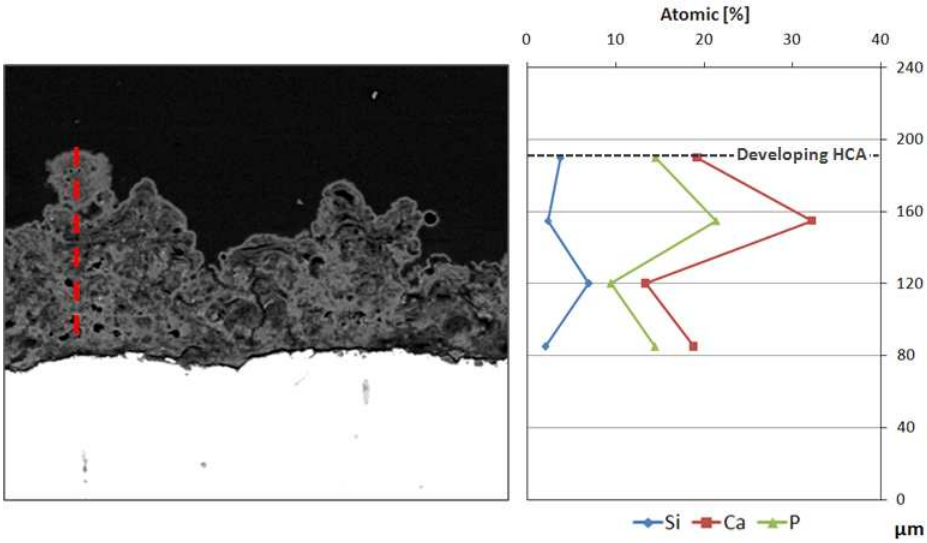

Figure 2.53: EDS analysis, Composite coating after 14 days in SBF

2.4.3 Conclusions

In this study various coatings made with BG_Ca glass and HA were produced. All the bi-phasic samples showed a high reactivity in SBF, and the ability to form HCA on their surface. The produced bi-phasic structures, which included a significant amount of HA, did not affect the bioactivity of the bioactive glass. Then, although more detailed investigations and more advanced *in vitro* test are required, it can be expected that the adhesion rate of the coatings to the bone tissue is only slightly lower to that of pure bioactive glass coatings.

The Graded sample seems to be the most promising one, since it combines a good apatite-forming ability and a strong adhesion to the substrate, as qualitatively observed by means of scratch tests.

2.5 *Production and characterization of a graded hydroxyapatite/bioactive glass coating.*

Introduction

The purpose of this research work was the production of bioactive glass/hydroxyapatite (HA) graded coatings. The constituent phases were selected to combine the high bioactivity of bioactive glasses with the long-term stability in biological environment of HA.

In a previous study (Chapter 2.4) different composite microstructures were compared, and the graded composition resulted to be the best one.

The advantage of the graded structure is that the deep layers of HA provide stability to the coating and protection to the substrate, while the bioactive glass surface ensures a great bone bonding ability to the system.

Compared to the previous coatings described in Chapter 2.4, many changes were introduced to improve the properties of the coating. First of all, micron-sized powders were used with the aim of achieving a finer microstructure, with improved mechanical properties and bioactivity. Moreover the percentage of HA was increased to improve the stability of the coatings without affecting the bioactivity. To conclude, an industrial robot was used to control the torch movement, and the number of layers having different composition was reduced. The last changes were expected to facilitate the scalability to industrial applications. In order to assess their reliability, the coatings produced in this way were characterized from a microstructural and mechanical point of view. They were also *in vitro* tested by immersion in SBF to verify their bioactivity. Finally, the adhesion of the coating to the substrate was qualitatively evaluated by scratch tests both before and after *in vitro* the tests.

2.5.1 Materials and methods

2.5.1.a Feedstock materials

Bioactive glass suspension:

The BG_Ca glass was produced by a conventional melt-quenching method, then it was dry milled and attrition milled in ethanol with 3 wt.% of the Beycostat C213 dispersant. The final BG_Ca powder had a bi-modal distribution with mean diameter of d_{50}=1.7 µm, (Fig. 2.54) as determined with a granulometer Partica LA-950V2, Horiba. The feedstock suspension was formulated by dispersing 10 wt% of solid phase in 90 wt% of ethanol.

Hydroxyapatite suspension:

The starting powder was commercial pure Hydroxyapatite (Tomita, Japan) with mean diameter of d_{50}=120 µm. The powder was attrition milled in ethanol adding 3 wt% of Beycostat C213 as dispersant. The obtained powder had a bi-modal distribution with mean diameter of d50=1.7 µm, (Fig. 2.54). The feedstock suspension was formulated by dispersing 10 wt% of solid phase in 45 wt% of ethanol and 45 wt% of water.

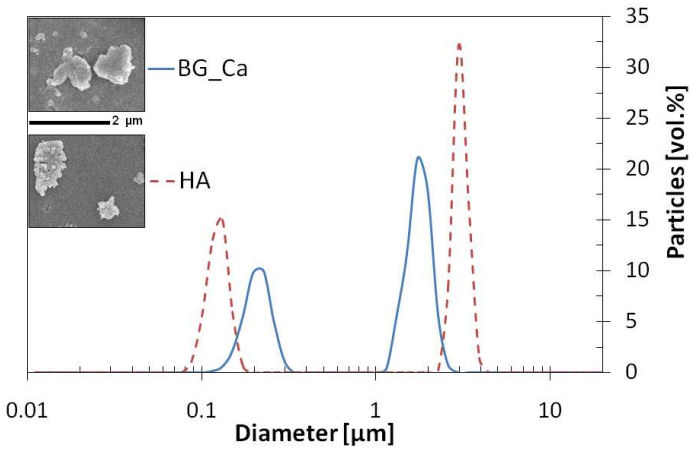

Figure 2.54: Grain size of the powders

2.5.1.b Coatings deposition

Plasma spraying was carried out using a Praxair implant including an SG-100 torch (Praxair, S.T., Indianapolis, IN, USA) configured in subsonic mode. The torch was mounted on a 5-axis ABB IRB-6 industrial robot (Fig. 2.55). The internal injection was used, with a radial 90° injection hole at 16 mm from torch's exit. A double peristaltic pump system was used to supply the suspensions. During spraying, the suspensions were continuously stirred to avoid sedimentation and agglomeration.

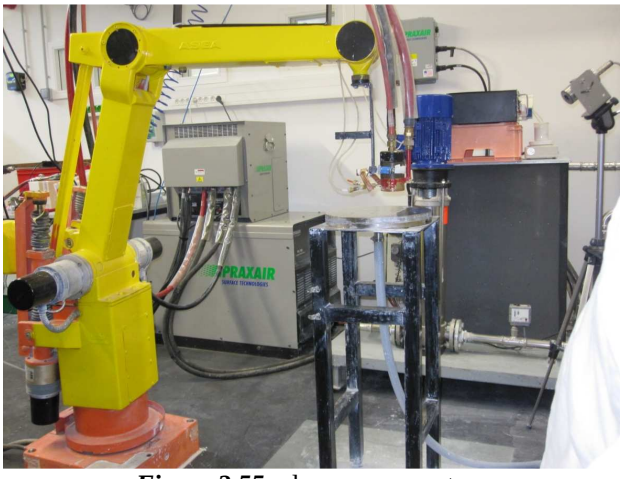

Figure 2.55: plasma spray set up

In order to ensure an appropriate momentum to the small size particles, a 300 μm injector was used. Compared to the previous study, the suspensions were diluted to a solid content of 10 wt.% to avoid clogging the injector; for the same reason the dispersant was increased up to 3 wt.% of the dry powders. The use of finer powders, more dilute suspensions, and different equipments required a new optimization of the spray parameters (Tab. 2.10).

Gases	**Power [kW]:**	38
	Ar [slpm]:	45
	H_2 [slpm]:	6
	Distance [mm]:	55
	Torch speed [mm/s]:	750
	Scan step [mm]:	3
	Suspensions flowrate [g/min]:	20

Table 2.10: Spray parameters

The coatings were produced in five sessions, and the flowrate of the feedstock suspension was varied each session (Tab. 2.11). During spraying, the suspensions were continuously stirred to avoid sedimentation and agglomeration. Since the deposition efficiency of the HA powder is lower than BG_Ca one (as previously observed in Chapter 2.4), the number of passages was adjusted (Tab. 2.11). During spraying a jet of compressed air was used to avoid excessive heating of the coating. Moreover, before each session, the sample surface was left to cool down below 80°C.

Session	***BG_Ca***	***HA***	***Passages***	T_{mean} **[°C]**
1	-	20	12	270
2	4	16	12	317
3	8	12	10	336
4	15	5	8	333
5	20	-	8	347

Table 2.11: Suspensions flows [g/min], and mean surface temperatures during spraying

Substrates were 316 l stainless steel plates sandblasted using 250 μm corundum powder at 2.5 Bar. The resulting roughness was Ra=1.6 μm. Before spraying, the substrates were ultrasonically washed with ethanol and acetone. During the coating deposition, an optical IN 5 Plus pyrometer (Impac) was used to record the superficial temperature. The mean values of the temperature were calculated for each spray session, and they are reported on Table 2.11. In order to understand better the microstructure of the coatings, single scan depositions were

performed using the same spray parameters. In this way it was possible to separately analyse the splats of the two materials. Two different kinds of substrates were used: mirror like 316 l stainless steel plate (“SS”), and microscope glass slides (“glass”). The former was used to analyse the interaction between sprayed particles and the actual substrate. The latter was employed to simulate the interaction between the sprayed particles and the superficial layers of forming coating.

2.5.1.c *In vitro* tests

In order to assess the bioactivity of the graded coatings, *in vitro* tests were performed according to the standard procedure proposed by Kokubo [34]. The SBF was refreshed every 2 days to mimic the dynamic condition of the human body. The samples were removed from the SBF after time periods of 1, 3, 7, and 14 days. The samples were carefully washed with distilled water, and after that they were dried at room temperature.

2.5.1.d Characterization

The surface of the coatings was investigated by means of X-Ray Diffraction, XRD, with an X’pert PRO diffractometer (PANalytical, Almelo, The Netherlands) equipped with the X'Celerator detector. The diffraction patterns were collected in the 10°-70° 2θ range (step size: 0.017°, step time: 71.12 s).

The coatings' surface and polished cross-section were investigated using an environmental scanning electron microscope, ESEM (ESEM Quanta 200-FEI Company, Eindhoven, The Netherlands) equipped with a X-EDS microanalysis system (Inca, Oxford Instruments, U.K.). The microscope was operated both in high-vacuum and low-vacuum mode (pressure: 0.45 Torr).

The surface and the cross-section coating were analysed by micro-Raman Spectroscopy (Jobin-Yvon Raman Microscope Spectrometer, HORIBA Jobin Yvon S.A.S., Villeneuve d’Ascq, France). The laser source emits 20 mW at 632.8 nm; 100x objective and no filters were employed.

Open platform (CSM Instruments) equipped with the nanoindenter module was used to perform depth-sensing nano-indentation tests on the cross-section of the as-produced coatings. The sample was mounted in resin, and polished to obtain a mirror like cross-section. A 50 mN force with linear loading/unloading rate of 40 mN/min was applied, the maximum load was held for 15 seconds. The indentations were performed using a Berkovich tip and the

elastic modulus and Vickers hardness were calculated according to the Oliver and Pharr method [143]. Because of the graded microstructure of the coating, the indentations were carried out in three different areas: next to the interface with the substrate (HA-rich area) at the half thickness of the coating (Middle) and in proximity to the surface (BG_Ca-rich area). 15 indentations were located on each area.

Scratch tests were performed on the surface of the coatings before and after *in vitro* tests. Open platform (CSM Instruments) equipped with 100 µm Rockwell diamond tip was used. The parameters of the scratch were: linear load from 20 mN to 30 N, scratch length 3mm, load rate 10 N/min. Critical loads were determined by optical analysis. Three scratches were performed on each sample.

2.5.2 Results and Discussion

Splat investigation:

First of all, the splats obtained from a single scan were analysed (Fig. 2.56).

Both the constituent phases, BG_Ca and HA, showed a different behaviour on different substrates. This was mainly due to the intrinsic properties of the substrate materials, especially the wettability and the thermal diffusion coefficient.

The BG_Ca particles impinging on the SS substrates formed various structures (Fig. 2.56a), including "pancake" splats, "drop-like" particles, and irregularly shaped ones. The latter probably resulted from incompletely molten particles. The "drop-like" splats probably derived from the splashing of larger particles. Some particles resolidified in-flight and they retained a spherical shape when they reached the substrate. The pancake structures are typically observed in coatings deposited by SPS [2].

On the glass substrate, instead, the BG_Ca particles generated flattened splats (Fig. 2.56c). This fact was due to the great chemical affinity between the particles and the substrate. Beside, also the low thermal conductivity of the glass, with the consequent slow cooling of the particles, could play a significant role. It is worth noting that some splats had a "shell-like" shape, that seemed to derive from gas bubbles trapped under the splat. This structure may explain the porosity that was previously observed on the bioactive glass coatings (Chapter 2.2-2.3)[141]. The HA powder showed a more classical behaviour: flower-like lamellae were formed on the metal substrate (Fig. 2.56b), while particles gave rise to well flattened splats on the glass substrate (Fig. 2.56d). Moreover, on both substrates, small irregular particles could be observed. As already proposed for the BG_Ca powder, such irregular splats could derive

from particles that were dragged in the plasma periphery [20].

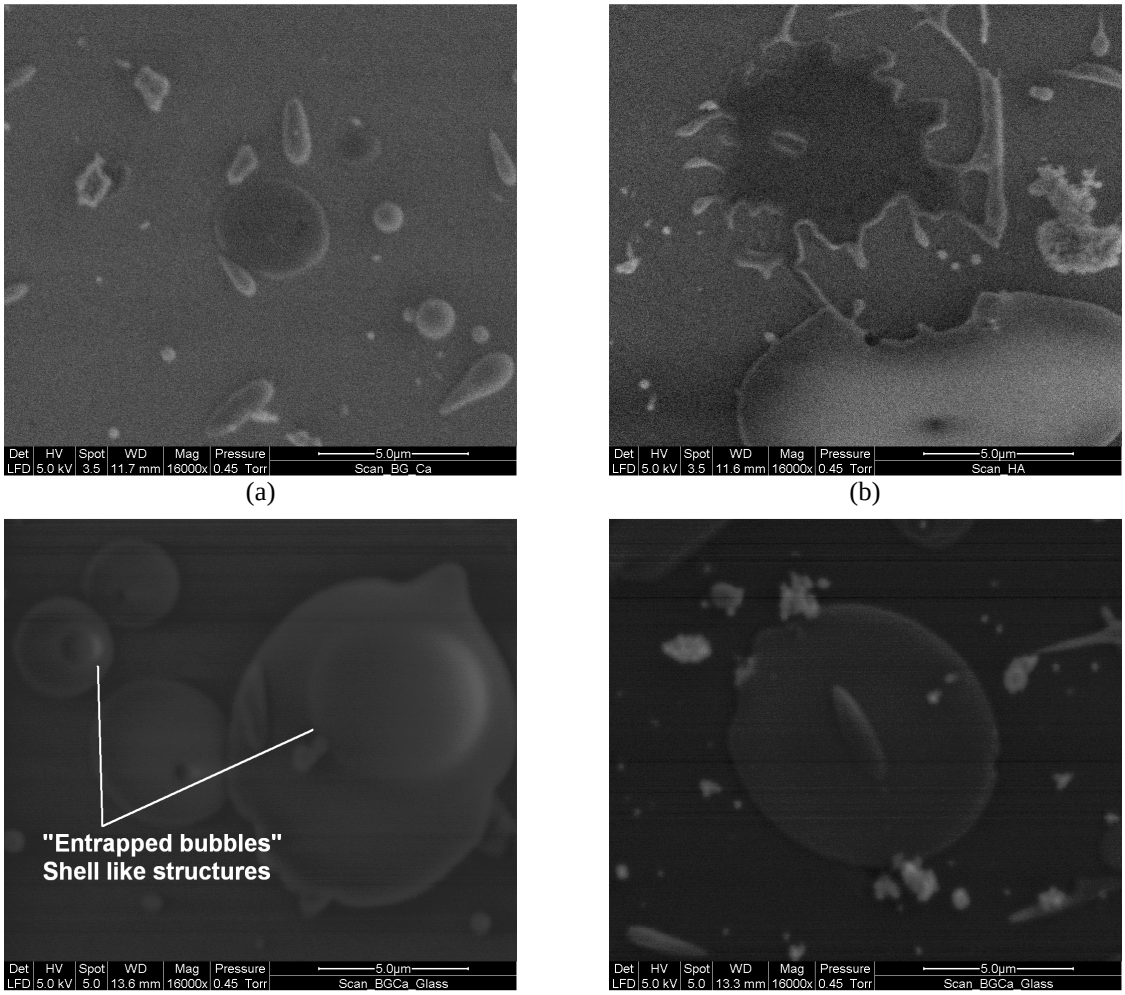

Figure 2.56: SEM images (secondary electrons) of single scan splats:
(a) BG_Ca on SS, (b) HA on SS, (c) BG_Ca on glass, (d) HA on glass

Coating analysis:

The final graded coating was compact and continuous, and the compositional gradient was the expected one as proved by the EDS map in Figure 2.57 (where Si was the BG_Ca marker, whereas P was the HA marker).

The surface of the sample was rough (Fig. 2.58a), with very fine acicular crystallization (Fig. 2.58b). This is consistent with the surface features previously detected on pure BG_Ca coatings, as well as on Duplex and preliminary Graded coatings having a pure glass layer on the working surface.

The cross-section of the sample was analysed by Raman spectroscopy as shown in Figure 2.59. Coherently with the planned microstructure, the Spectrum 1 showed the HA pattern while the Spectrum 7 had the BG_Ca peaks; the spectra collected on the intermediate layers

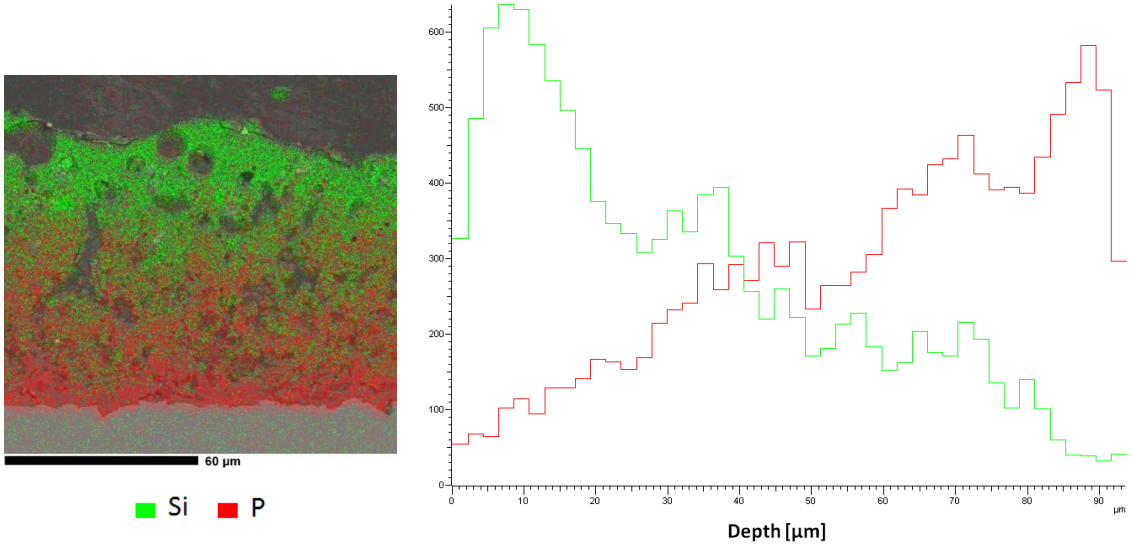

Figure 2.57: EDS map of as produced coating cross section and composition profile

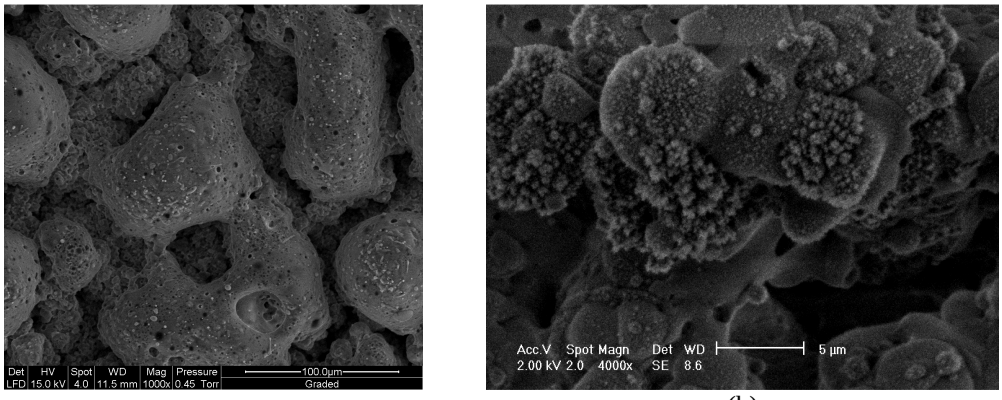

(a) (b)

Figure 2.58: SEM images (secondary electrons) of surfaces at different magnifications

were a combination of the patterns of the constituent phases. Although the identification of the patterns was reliable, some differences between the spectra acquired on the coating and those of the feedstock materials [130] were detectable. The variations were attributable to the spraying process. In particular, in the Spectrum 1 the peak at about 960 cm^{-1}, which is associated to symmetrical stretching of PO_4 group, was formed by two peaks. The first one was a sharp peak related to the HA, while the second peak was broad and it was probably caused by the decomposition phases, mainly ACP [154]. Instead, in the Spectrum 7 the peak centred at about 860 cm^{-1} was more intense than in bulk BG_Ca [130]. This peak is associated with the presence of non-bridging oxygens, which suggests the glass network had an open structure. The Spectrum 4 deviated from the simple superposition of the HA and BG_Ca patterns. In fact, weak secondary peaks at about 640, 1115 and 1185 cm^{-1} appeared in the spectrum. The new peaks were probably due to a new phase which resulted from a reaction

between HA and BG_Ca. Unfortunately the identification of the new compound was not possible.

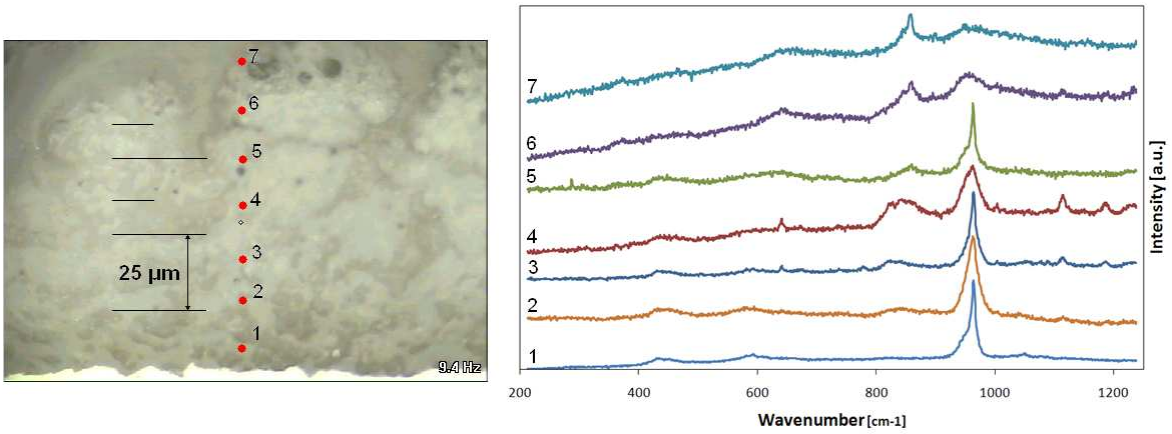

Figure 2.59: Raman spectra acquired on coating's cross section

The coating cross-section was tested by depth-sensing nano-indentations (Fig. 2.60). The mechanical properties were measured at three different depth levels (Fig. 2.61): next to the substrate (HA-rich area), at mid-thickness (Middle) and on the surface (BG_Ca-rich area).

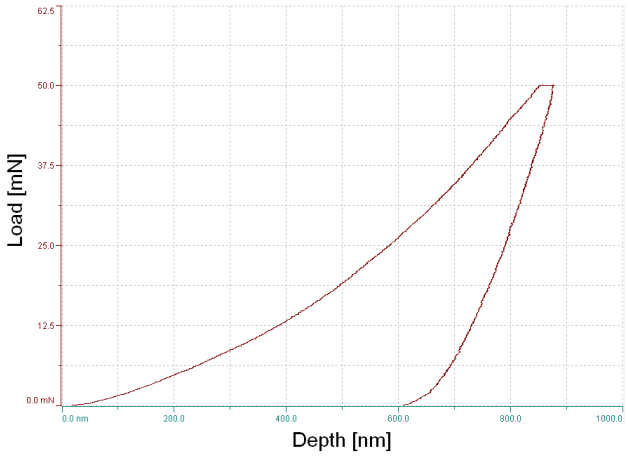

Figure 2.60: Load/unload curve recorded during depth-sensing nanoindentation, HA-rich area

The obtained values had a relevant standard deviation. This was due to the ceramic nature of the coatings, to the composite microstructure, and to the porosity. The hardness and elastic modulus values of the BG_Ca-rich area were much better than those previously measured on pure BG_Ca coatings which were produced by the same technique (Chapter 2.2). Such improvement might be due to the addition of HA, however the most important reasons were surely the smaller size of the feedstock powders and the refined optimization of the spray parameters. The mechanical properties of this area were comparable to those of pure Bioglass® coatings obtained by means of HVSFS [24]. The HA-rich layers showed the

highest elastic modulus and great hardness, confirming the high compactness and adhesion of the HA particles. The measured values were even better than those of pure HA SPS coatings [156]. To conclude, the intermediate zone exhibited an elastic modulus similar to that of the BG_Ca-rich area, while the hardness was the lowest among the three areas. The relatively low value of hardness could be attributed to a not perfect adhesion between HA and BG_Ca lamellae. Furthermore the new phase, which was detected in this area, may have contributed to a reduction of hardness.

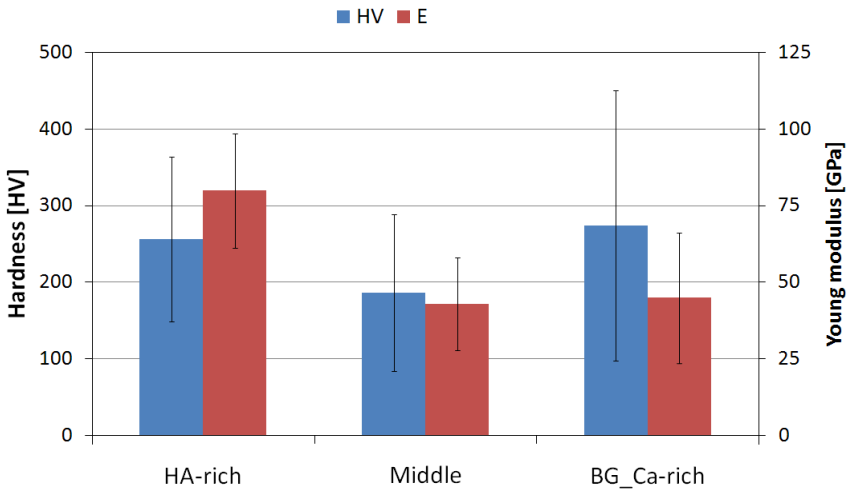

Figure 2.61: Mechanical properties calculated by means of nano indentations on coating cross section

The samples were tested *in vitro* to assess their bioactivity. The SEM inspection (Fig. 2.62) showed that the morphology changed starting from the first day of immersion, with the formation of "cauliflower-like" deposits. This morphology is typical of HCA which develops *in vitro* [157].

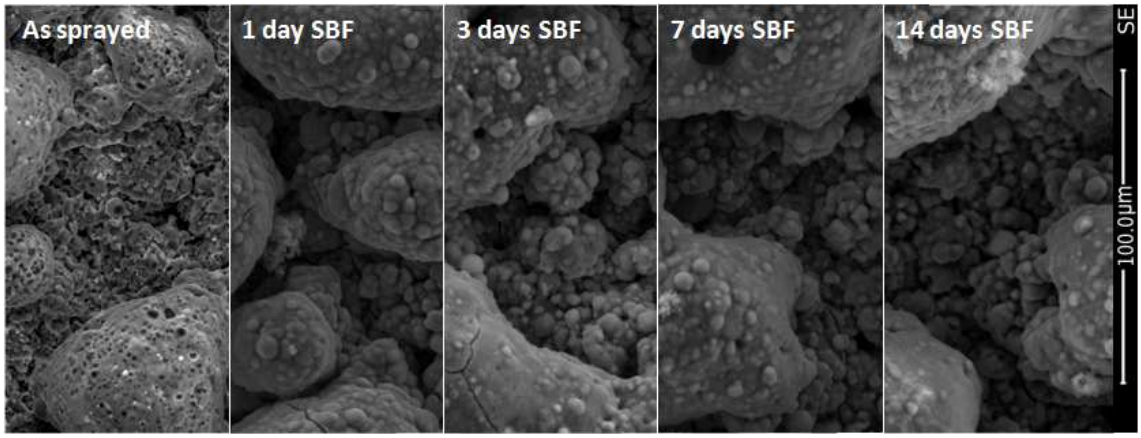

Figure 2.62: SEM images (secondary electrons) of samples' surface after in vitro tests.

Furthermore, the composition of the coatings' surface was monitored by means of EDS analysis (Fig. 2.63). The elementary composition confirmed that, after one day of immersion

in SBF, the silicon percentage dropped while the amount of phosphorus increased. The analysis also revealed that the main changes occurred within the first week.

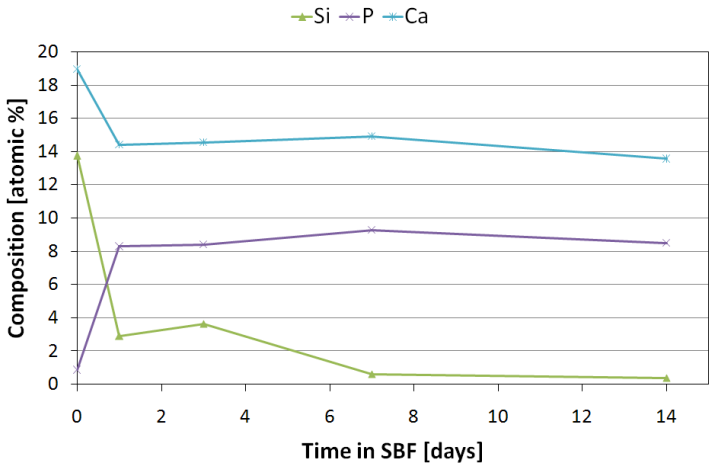

Figure 2.63: Coatings' surface composition determined by EDS on a 6 mm^2 area

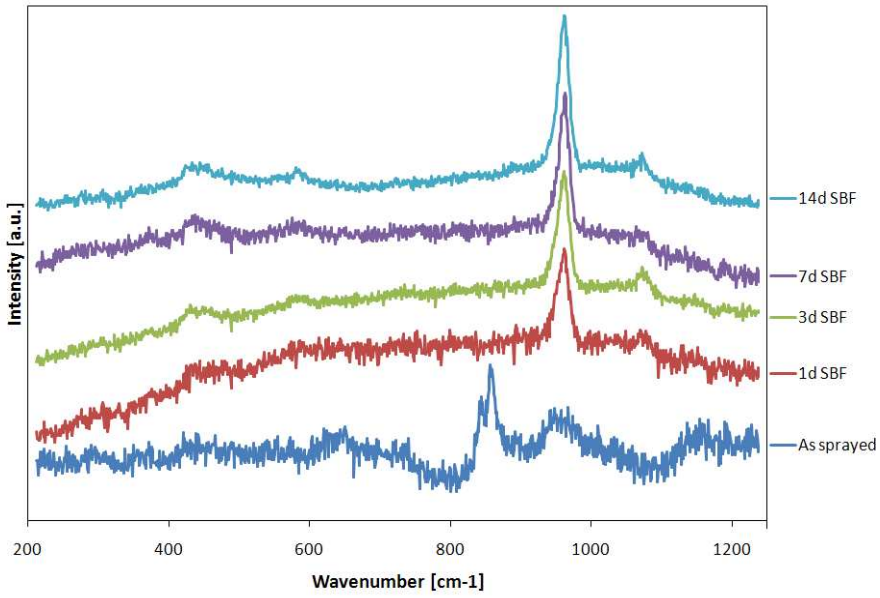

Figure 2.64: Raman, evolution of the spectra as result of *in vitro* test.

The Raman investigation carried out on the surface (Fig. 2.64) agreed with previous analyses: the main peak of HA could be detected already after one day in SBF. Besides the peak at about 960 cm^{-1}, which is due to the vibration of the PO_4 group in HA, another peak at about 1070 cm^{-1} was present. This peak is commonly related to the carbonate group [139]; accordingly the *in vitro* developed HA was carbonated, i.e. HCA. With increasing immersion time in SBF, the pattern of HCA was more evident and its secondary peak groups occurred at about 430 and 600 cm^{-1}.

The evolution of the X-ray diffraction pattern (Fig. 2.65) confirmed the results of the Raman

analysis: after one day of immersion, the peaks of HA could be identified and, with increasing immersion time, the peaks became sharper. It is interesting to note that the XRD spectrum of the as produced sample showed some peaks due to crystallization phases. Indeed, in this pattern the peaks of pseudowollastonite ($CaSiO_3$) and larnite (Ca_2SiO_4) were detected. The development of such crystalline phases was certainly due to the spray process, and they were still present after one day of immersion in SBF. After three days of *in vitro* test the peaks of the crystalline phases completely disappeared.

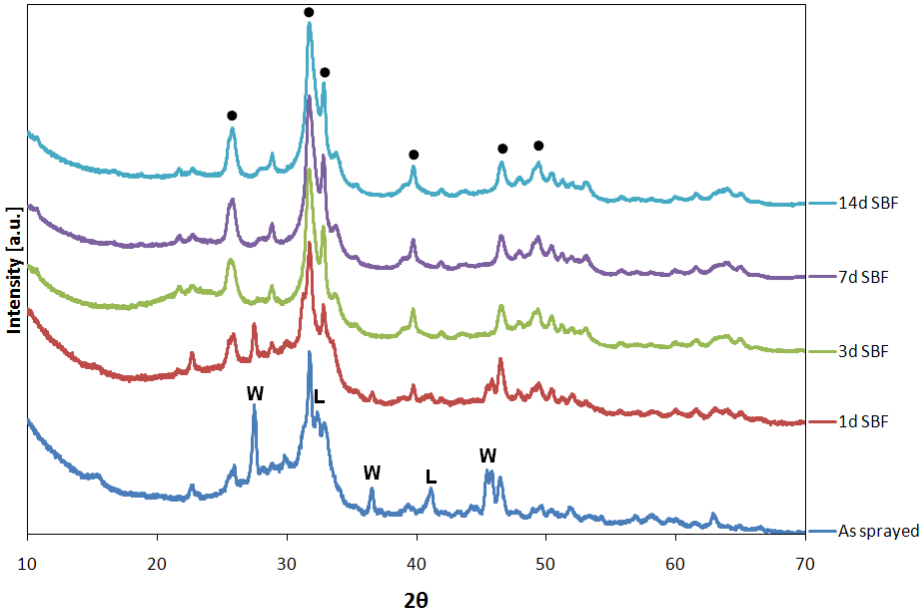

Figure 2.65: XRD, evolution of the spectra as result of *in vitro* test.
W: pseudowollastonite, L: larnite, ●: HA

In order to verify what happened during the immersion in SBF, the cross-section of the samples was analysed (Fig. 2.66-67). The maps of the elements were acquired, and compositional profiles as a function of depth were calculated. After one day of immersion in SBF (Fig. 2.66a), a superficial layer rich in calcium and phosphorus formed. In addition, under this layer, an area mainly composed of silicon was observable. According to the available literature [33], the former was the growing HCA, while the latter was a silica gel layer. Below these areas, a zone composed by silicon and calcium may be attributed to some BG_Ca glass survived during the first day in SBF.

After three days in SBF (Fig. 2.66b), the HCA layer was thicker, while the glass was completely replaced by the silica gel. Moreover, some HCA formed within the silica gel matrix. After one week of immersion in SBF the HCA layer further thickened (Fig. 2.67a), and the silicon rich area concentrated at the surface. This phenomenon was more prominent

after two weeks (Fig. 2.67b) when a silicon-rich layer was clearly detectable. A similar but opposite behaviour was observed in preliminary graded coatings (Chapter 2.4). In the previous case the silica gel accumulated close to the substrate, while in this case the silica gel migrated on coating's surface, below the HCA layer. In agreement with what was hypothesized in Chapter 2.4, the HCA grew preferentially on one of the surface of the silica gel, resulting in a gradual migration of the silicon-rich stratum. In this case it can be assumed that, in the layers below the silica gel, the HCA growth rate was greater than the dissolution rate of the coating's HA. Consequently the silica gel was led to move towards the superficial

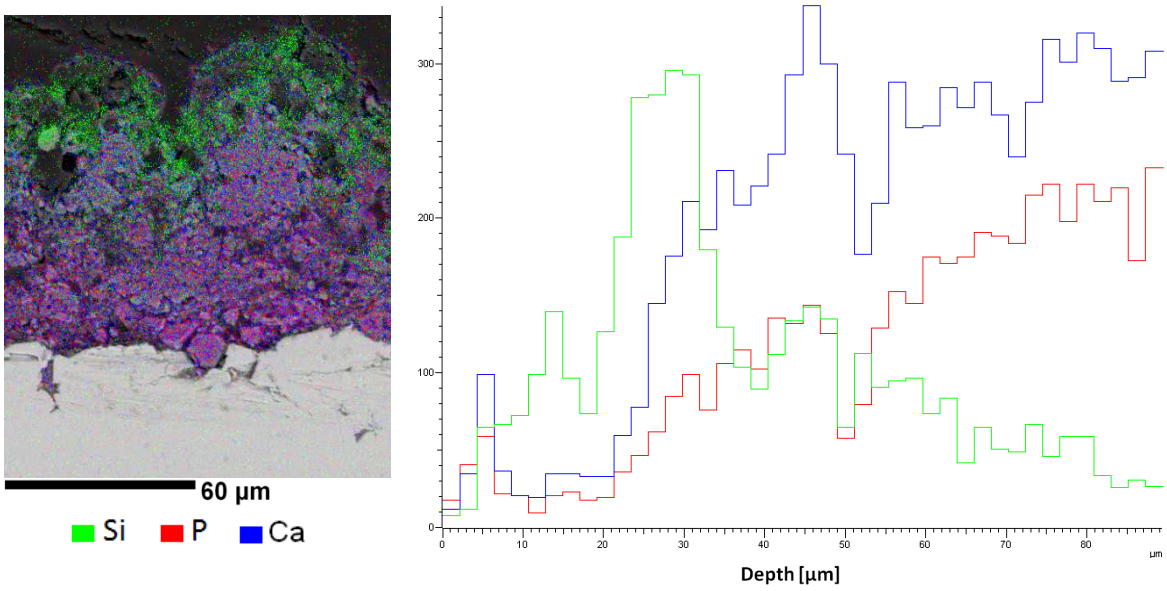

(a)

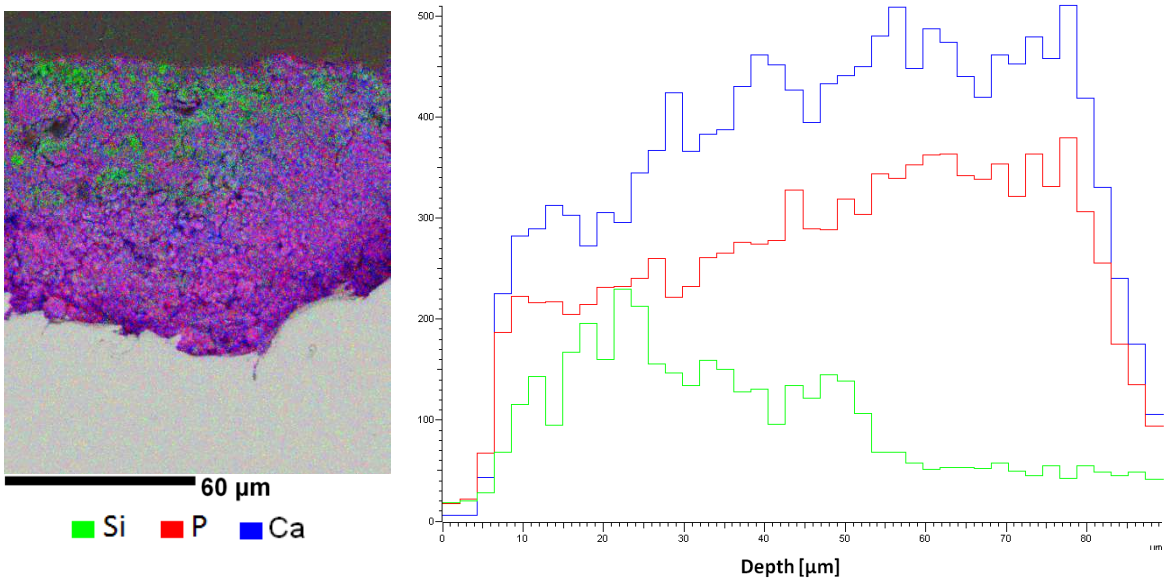

(b)

Figure 2.66: EDS maps and compositional profile of samples after *in vitro* test.
(a) sample immersed one day in SBF, (b) sample immersed three days in SBF

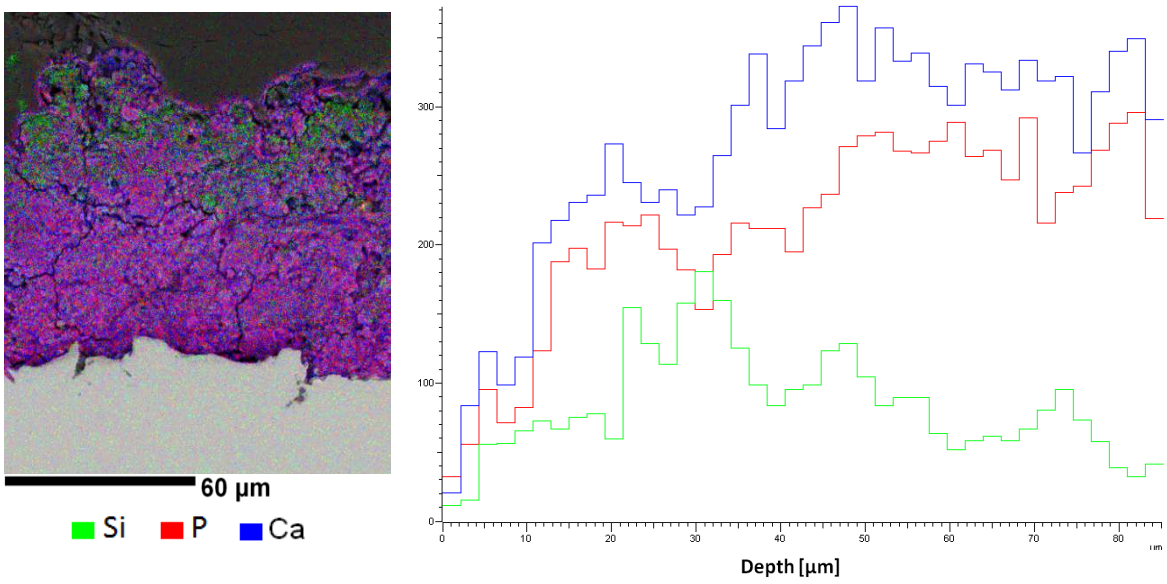

(a)

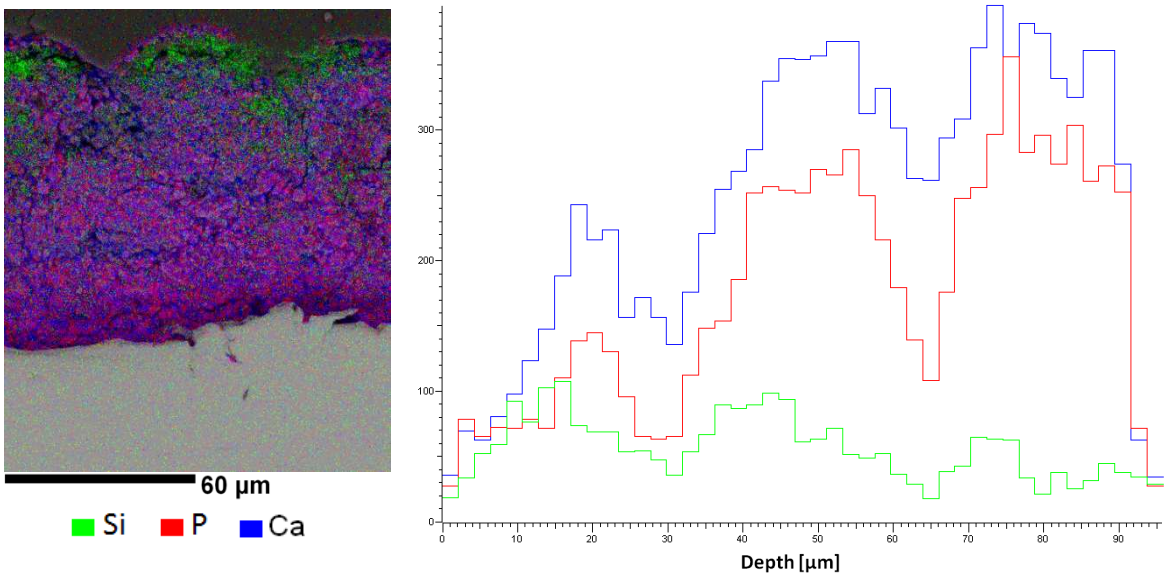

(b)

Figure 2.67: EDS maps and compositional profile of samples after *in vitro* test.
a) sample immersed one week in SBF, (b) sample immersed two weeks in SBF

layers. The high stability and compactness of HA-rich area were probably the reason for this behaviour. In order to determine the adhesion of the coating to the substrate and to test the interface stability as a function of the immersion time in SBF, scratch tests were carried out. During all the scratch test the maximum load allowed by the instrument (30 N) was reached without the detachment of the coating (Fig. 2.68). Even in the sample soaked two weeks, the detection of the substrate was not possible, as confirmed by optical and SEM analysis (Fig. 2.69a).

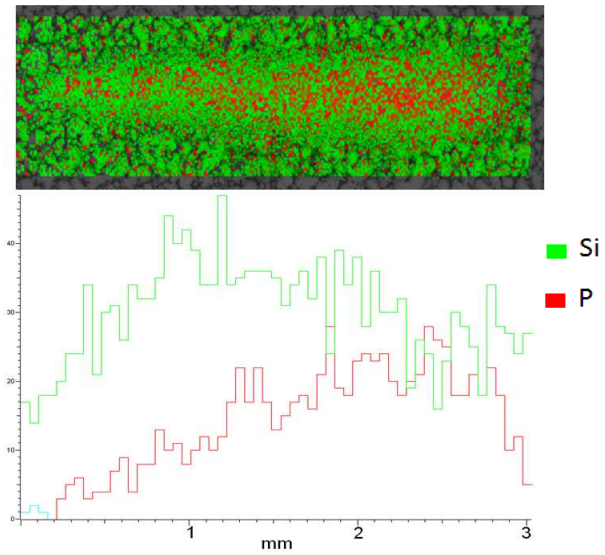

Figure 2.68: EDS map of scratch track, as produced coating

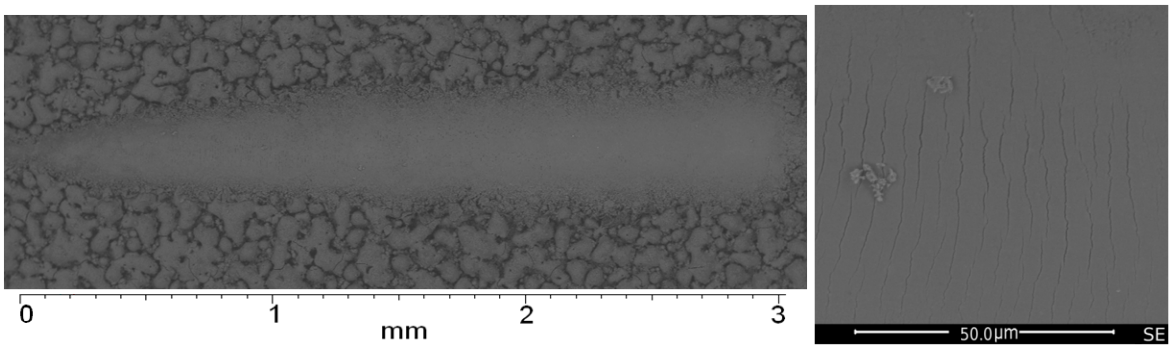

(a) (b)

Figure 2.69: SEM immages (secondary electrons) of scratch:
(a) Scratch track of 14 day SBF sample, (b) cracks in scratch track of as produced coating

Although the detachment of the coating never happened during the tests, transversal cracks formed inside the scratch track (Fig. 2.69b). The load at which the cracks formed decreased for increasing time of immersion in SBF (Fig. 2.70). Thus the reactions occurred with the SBF worsened the properties of the coating; in fact the "cracking load" was almost 9 N for the as-sprayed coating, while it was about 5.2 N after one day in SBF. It is worth noting that bioactive glasses are transformed into hydrated silica gel during the reaction with SBF [33]. This implies that the surface of bulk bioactive glasses often cracks after the extraction from the SBF because of drying processes [130] and this undermine the surface integrity. Accordingly, if the aim is to measure the mechanical properties of a sample containing bioactive glass in operative conditions, the tests should be completed in situ directly during the *in vitro* tests, prior to the drying process. In this way the artifacts due to the samples' drying, which does not occur in the human body, can be avoided.

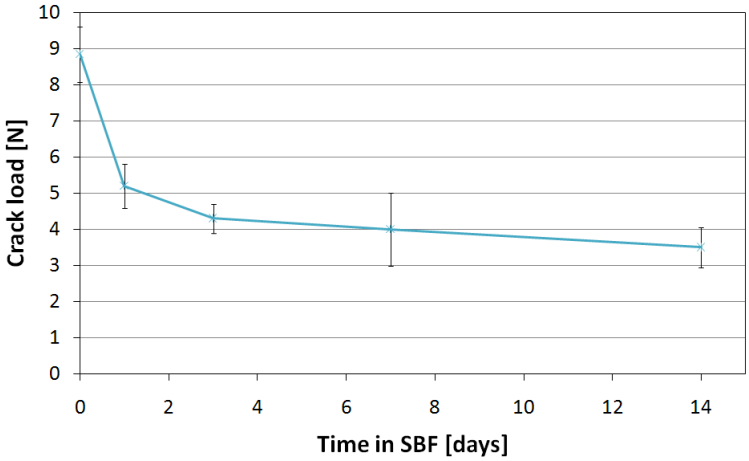

Figure 2.70: Loads at which transversal crack appeared inside the scratch track as a function of time in SBF

2.5.3 Conclusions

In this study a bioactive glass/HA graded coating was produced and characterised.

The coating showed good mechanical properties and a remarkable bioactivity. Furthermore, the adhesion of the coating to the substrate was high even after *in vitro* tests.

Further long-term *in vitro* tests and cytotoxicity tests must be carried out to check the properties of the coating. However, the coating was very promising, especially because it can be produced with a protocol easily scalable to industrial applications.

Chapter 3:

Conclusions and Future Perspectives

3.1 *Conclusions*

The production of prosthetic implants is a well-established practice, nevertheless research is constantly evolving to enhance the prosthesis performances. In order to promote osteointegration of implants, a common practice is to cover them with a bioactive coating, usually composed of hydroxyapatite (HA).

This approach has been proved to increase the compatibility of prosthesis with bone and extend their lifespan expectancy. However, revision surgeries are common, and implants failure still occurs. In addition, in some applications, fixing times shorter than HA coated implants ones would be preferable. For this reasons, many studies are ongoing to apply new materials and coatings production techniques to prosthetic.

The aim of this research project was the production of innovative coatings of bioactive glasses and HA for biomedical applications. The suspension plasma spray process was employed to produce the coatings.

In the first part of the work, bulk bioactive glasses were *in situ* analysed during *in vitro* test with the purpose of compare their bioactivity. As a result of this study, and other previous analysis , the bioactive glass BG_Ca was selected as suitable for the production of coatings.

Following, the technique SPS was used to produce coatings with this bioactive glass. A preliminary screening of processing parameters revealed that the microstructure was mainly governed by the spray distance and the power input to plasma. Bioactive glass coatings suitable for biomedical applications were obtained spraying with power from 36 to 40 kW and spray distance from 50 to 70 mm. The obtained coatings showed bioactivity in SBF, and their porosity and degree of crystallinity were proved to be the major factors affecting system reactivity.

Accordingly, a highly porous and nearly amorphous topcoat was produced with BG_Ca to increase the bioactivity of traditional HA coatings. The topcoat was considered effective to increase the *in vitro* reactivity of HA coatings. Then, since beneficial effects from the introduction of BG_Ca in HA coatings were observed, the study progressed with the realization of specific composite systems using both the materials.

Therefore SPS process was used to spray bi-phasic coatings of HA and BG_Ca. The coatings

were produced with different microstructures: standard composite, double layered coatings, and compositionally graded ones. The aim of the bi-phasic coatings was to merge the high bioactivity of bioactive glasses with the superior stability of HA. The bi-phasic coatings were compared, and the coating with compositional gradient seemed to be the most promising one. In fact it showed high bioactivity and the strongest adhesion to the substrate respect to the other coatings. Then graded microstructure was selected for the production of an optimized second series of coatings. The new coatings were sprayed using smaller size powders and higher content of HA respect to the previous series. Moreover the suspension feeding protocol was simplified and an industrial robot was used for torch movement. Then the coating production was expected to be easily scalable to industrial applications. The coating showed good mechanical properties and a remarkable bioactivity. Furthermore, even if *in vitro* tests affected its properties, the adhesion of the coating to the substrate was not compromised by SBF tests.

3.2 *Future Perspectives*

There is potential for further research on coatings produced in this study.

First, the bioactive glass coatings (Chapter 2.2) may be tested with more advanced *in vitro* test to asses cell response. Moreover, the composition of the glass could be refined in order to further adapt it to the deposition process.

The bioactive glass topcoat (Chapter 2.3) would be tested with cell cultures in order to verify if its beneficial effect on cell adhesion and metabolite absorption is the expected one. Moreover this layer may be applied on commercial coatings. A further evolution of the topcoat may be the post-spraying impregnation with drug release agents, in order to further facilitate the implants osteointegration and provide new functionality to the coatings.

The submission of Graded coating (Chapter 2.5) to long term *in vitro* test could be useful. Moreover, the properties of these coatings can be further improved with the introduction of a third component, such as TiO_2, which act as a bond coat.

However the proposed coatings were developed for prosthetic use, then, before a clinical use further analysis must be performed. Specifically, in order to certify the effectiveness and non-toxicity of the coatings, *in vivo* test and clinical trial must be carried out.

References

[1] Robert B. Heimann. Plasma Spray Coating: Principles and Applications. (2008) Wiley-VCH.

[2] L. Pawłowski, The Science and Engineering of Thermal Spray Coatings, (2008) Wiley, Chichester

[3] H. Herman, S. Sampath and R. McCune. Thermal spray: current status and future trends. MRS Bulletin. 25 (2000) pp.17-25.

[4] J. Schein, J. Zierhut, M. Dzulko, G. Forster, and K. D. Landes. Improved Plasma Spray Torch Stability Through Multi-Electrode Design. Contributions to Plasma Physics. 47 (2007) pp.498-504.

[5] R.A. Miller. Current status of thermal barrier coatings -An overview. Surface and Coatings Technology. 30 (1987) pp.1-11.

[6] E. Lugscheider, C. Barimani, P. Eckert, and U. Eritt. Modeling of the APS plasma spray process. Computational Materials Science. 7 (1996) pp.109-114.

[7] P. Fauchais. Understanding Plasma Spraying. Journal of Physics D: Applied Physics, Vol. 37, (2004), pp.R86-R108.

[8] Y.J. Su, T.F. Berencki, K.T. Faber. *In Situ* Characterization of Small-Particle Plasma Sprayed Powders. Journal of Thermal Spray Technology. 11 (2002) pp.52-61.

[9] L. Pawłowski. Suspension and solution thermal spray coatings. Surface and Coatings Technology. 203 (2009) pp.2807-2829.

[10] R. Tomaszek, L. Pawłowski, L. Gengembre, J. Laureyns, and A. Le Maguer. Microstructure of suspension plasma sprayed multilayer coatings of hydroxyapatite and titanium oxide. Surface and Coatings Technology. 201 (2007) pp.7432-7440.

[11] E. Bouyer, F. Gitzhofer, and M.I. Boulos. Suspension plasma spraying for hydroxyapatite powder preparation by RF plasma. IEEE Trans. Plasma Sci. 25 (5) (1997) pp.1066.

[12] G. Schiller, M. Müller and F. Gitzhofer. Preparation of perovskite powders and coatings by radio frequency suspension plasma spraying. Journal of Thermal Spray Technology. 8 (1999) pp.389-392.

[13] K. Wittmann, F. Blein, J.F. Coudert, and P. Fauchais. Control of the Injection of an Alumina Suspension Containing Nanograins in a dc Plasma Proceedings of the International Thermal Spray Conference. (2001) pp.375-382.

[14] P. Blazdell, and S. Kuroda. Plasma spraying of submicron ceramic suspensions using a continuous ink jet printer. Surface and Coatings Technology. 123: 2-3 (2000) pp.239-246

[15] A. Killinger, R. Gadow, G. Mauer, A. Guignard, R. Vaßen, and D. Stöve. Review of New

Developments in Suspension and Solution Precursor Thermal Spray Processes . Journal of Thermal Spray Technology. 20 (2011) pp.677-695.

[16] Z. Chen, and R.W. Trice. Air-plasma spraying colloidal solutions of nanosized ceramic powders. Journal of Materials Science. 39 (2004) pp.4171-78.

[17] H. Li, K.A. Khor, and P. Cheang. Effect of Steam Treatment During Plasma Spraying on the Microstructure of Hydroxyapatite Splats and Coatings. Journal of Thermal Spray Technology. 15 (2006) pp.610-616.

[18] Y. Shan, T.W. Coyle, and J. Mostaghimi, Modeling the Influence of Injection Modes on the Evolution of Solution Sprays in a Plasma Jet. Journal of Thermal Spray Technology. 19 (2010), pp.248-254.

[19] J. Fazilleau, C. Delbos, V. Rat, J. F. Coudert. P. Fauchais, and B. Pateyron. Phenomena Involved in Suspension Plasma Spraying Part 1: Suspension Injection and Behavior . Plasma Chemistry and Plasma Processing. 26 (2006) pp.371-391.

[20] L. Łatka, S.B. Goryachev, S. Kozerski, and L. Pawłowski. Sintering of Fine Particles in Suspension Plasma Sprayed Coatings. Materials 3 (2010) pp.3845.

[21] V. Hurevich, I. Smurov, and L. Pawłowski. Theoretical study of the powder behavior of porous particles in a flame during plasma spraying. Surface and Coatings Technology. 151-152 (2002) pp.370.

[22] A. Bacciochini, G. Montavon, J. Ilavsky, A. Denoirjean, and P. Fauchais. Porous Architecture of SPS Thick YSZ Coatings Structured at the Nanometer Scale. Journal of Thermal Spray Technology. 19 (2010) pp.198-206.

[23] R. Jaworski, C. Pierlot, L. Pawłowski, M. Bigan, and M. Quivrin. Synthesis and Preliminary Tests of Suspension Plasma praying of Fine Hydroxyapatite Powder. Journal of Thermal Spray Technology. 17 (2008) pp.679-684.

[24] L. Altomare, D. Bellucci, G. Bolelli, B. Bonferroni, V. Cannillo, L. De Nardo, R. Gadow, A.
Killinger, L. Lusvarghi, A. Sola and N. Stiegler. Microstructure and *in vitro* behaviour of 45S5 bioglass coatings deposited by high velocity suspension flame spraying (HVSFS). Journal of Materials Science: Materials in Medicine. 22 (2011) pp.1303.

[25] S. Kozerski, L. Pawłowski, R. Jaworski, F. Roudet, F. Petit. Two zones microstructure of suspension plasma sprayed hydroxyapatite coatings. Surface and Coatings Technology. 204 (2010) pp.1380.

[26] B. D. Ratner, A. S. Hoffman, F. J. Schoen, J. E. Lemons. Biomaterials Science: An Introduction to Materials in Medicine (2nd Edition). Elsevier Academic Press 2004.

[27] M. Vallet-Regì. Evolution of bioceramics within the field of biomaterials. Comptes Rendus Chimie. 13 (2009) pp.174-185.

[28] L. L. Hench. Biomaterials: a forecast for the future. Biomaterials. 19 (1998) pp.1419-1423.

[29] A. A. Hofmann, T. D. Goldberg, A. M. Tanner and T. M. Cook. Surface cementation of stemmed tibial components in primary total knee arthroplasty. The Journal of Arthroplasty. 21 (2006) pp.353-357.

[30] L. L. Hench. The story of bioglass.Journal of Materials Science: Materials in Medicine. 17 (2006) pp.967-978.

[31] L.L. Hench, R.J. Splinter, T.K. Geenlee, and W.C. Allen. Bonding mechanisms at the interface of ceramic prosthetic materials. Journal of Biomedical Materials Research. 5 (1971) pp.117-141.

[32] L. L. Hench. Bioceramics: from concept to clinic. Journal of the American Ceramic Society. 74 (1991) pp.1487-1510.

[33] L.L Hench. Bioceramics. Journal of the American Ceramic Society. 81 (1998) 1705-1028.

[34] T. Kokubo and H. Takadama. How useful is SBF in predicting *in vivo* bone bioactivity?. Biomaterials. 27 (2006) pp.2907-2915.

[35] M. Bohner, and J. Lemaitre. Can bioactivity be tested *in vitro* with SBF solution? Biomaterials. 30 (2009) pp.2175-2179.

[36] M. Bohener. Resorbable biomaterials as bone graft substitutes. Materials Today. 13 (2010) pp.24-30.

[37] L. L. Hench and J. Wilson . An introduction to bioceramics.1993, Singapore, World Scientific Publishing Co Pte Ltd.

[38] L. L. Hench. Genetic design of bioactive glass. Journal of the European Ceramic Society. 29 (2009) pp.1257-1265.

[39] D.S Metsger, T.D. Driskell, and J.R. Paulsrud. Tricalcium phosphate ceramic-a resorbable bone implant: review and current status. The Journal of the American Dental Association. 105 (1982) pp.1035.

[40] K. S. Katti. Biomaterials in total joint replacement. Colloids and Surfaces B: Biointerfaces. 39B (2004) pp.133-142.

[41] H.M. Kim, T. Himeno, T. Kokubo, and T. Nakamura. Process and kinetics of bonelike apatite formation on sintered hydroxyapatite in a simulated body fluid. Biomaterials. 26 (2005) pp.4366-4373.

[42] F. Fazan and P. M. Marguis. Dissolution behaviour of plasma-sprayed hydroxyapatite coatings. Journal of Materials Science: Materials in Medicine. 11 (2000) pp.787-792.

[43] M. Nagano, T. Nakamura, T. Kokubo, M. Tanahashi and M. Ogawa. Differences of bone bonding ability and degradation behaviour *in vivo* between amorphous calcium phosphate and highly crystalline hydroxyapatite coating. Biomaterials. 17 (1996) pp.1771-1777.

[44] L. Sun, C.C. Berndt, K.A. Gross, and A. Kucuk. Material fundamentals and clinical performance of plasma-sprayed hydroxyapatite coatings: A review. Journal of Biomedical Materials Research. 58 (2001) pp.570-592.

[45] F.H. Lin, L. Chun-Jen, C. Ko-Shao, and S. Jui-Sheng . Thermal reconstruction behavior of the quenched hydroxyapatite powder during reheating in air. Materials Science and Engineering C. 13 (2000) pp.97-104.

[46] R.B. Heimann . Thermal spraying of biomaterials . Surface and Coatings Technology 201 (2006) pp.2012-2019.

[47] X. Zhang, X. Li, H. Fan, and X. Liu. Effect of Ca/P Molar Ratio and Heat Treatment on Thermal Decomposition and Reconstitution of Hydroxyapatite Key Engineering Materials. 330-332 Bioceramics 19 (2007) pp.107-110.

[48] J. W. Nicholson, The Chemistry of Medical and Dental Materials, Cambridge, UK. Royal Society of Chemistry, 2002.

[49] A.J. Ruys, M. Wei, C.C. Sorrell, M.R. Dickson, A. Brandwood, and B.K. Milthorpe. Sintering effects on the strength of hydroxyapatite. Biomaterials. 16 (1995) pp.409-415.

[50] S. Raynaud, E. Champion, D. Bernache-Assollant, and P. Thomas. Calcium phosphate apatites with variable Ca/P atomic ratio I. Synthesis, characterisation and thermal stability of powders. Biomaterials. 23 (2002) pp.1065-1072.

[51] Y. Chen, and X. Miao. Thermal and chemical stability of fluorohydroxyapatite ceramics with different fluorine contents. Biomaterials. 26 (2005) pp.1205-1210.

[52] K.A. Gross and C.C. Berndt. Thermal processing of hydroxyapatite for coating production. Journal of Biomedical Materials Research. 15 (1998) pp.580-587.

[53] Y. Lin, Z. Yang, and J. Cheng. Preparation, Characterization and Antibacterial Property of Cerium Substituted Hydroxyapatite Nanoparticles. Journal of Rare Earths. 25 (2007) pp.452-456.

[54] N. Patel, S. M. Best, W. Bonfield, I. R. Gibson, K. A. Hing, E. Damien, and P. A. Revell. A comparative study on the *in vivo* behavior of hydroxyapatite and silicon substituted hydroxyapatite granules. Journal of Materials Science: Materials in Medicine. 13 (2002) pp.1199-1206.

[55] Y. Shen, J. Liu, K. Lin, and W. Zhang. Synthesis of strontium substituted hydroxyapatite whiskers used as bioactive and mechanical reinforcement material. Materials Letters. 70 (2012) pp.76-79.

[56] A.E. Porter, N. Patel, J.N. Skepper, S.M. Best, W. Bonfield. Effect of sintered silicate-

substituted hydroxyapatite on remodelling processes at the bone-implant interface. Biomaterials. 25 (2004) pp.3303-3314.

[57] K.A. Hing, P.A. Revell, N. Smith, and T. Buckland. Effect of silicon level on rate, quality and progression of bone healing within silicate-substituted porous hydroxyapatite scaffolds. Biomaterials. 27 (2006) pp.5014-5026.

[58] L.T. Bang, K. Ishikawa, and R. Othman. Effect of silicon and heat-treatment temperature on the morphology and mechanical properties of silicon - substituted hydroxyapatite. Ceramics International. 37 (2011) pp.3637-3642.

[59] F.J. Xiao, L. Peng, Y. Zhang, and L.J. Yun. Silicon-substituted hydroxyapatite composite coating by using vacuum-plasma spraying and its interaction with human serum albumin. Journal of Materials Science: Materials in Medicine. 20 (2009) pp.1653-1658.

[60] P.S. Gomes, C. Botelho, M.A. Lopes, J.D. Santos, and M.H. Fernandes. Evaluation of human osteoblastic cell response to plasma-sprayed silicon-substituted hydroxyapatite coatings over titanium substrates. Journal of Biomedical Materials Research Part B: Applied Biomaterials. 94B (2010) pp.337-346.

[61] I. D. Xynos, M. V. J. Hukkanen, J. J. Batten, L. D. Buttery, L. L. Hench and J. M. Polak. Bioglass® 45S5 stimulates osteoblast turnover and enhances bone formation *in vitro*: Implications and applications for bone tissue engineering. Calcified Tissue International. 67 (2000) pp.321-329.

[62] U. Vijayalakshmi, A. Balamurugan and S. Rajeswari. Synthesis and characterization of porous silica gels for biomedical applications. Trends in Biomaterials & Artificial Organs. 18 (2005) pp.101-105.

[63] O. Bretcanu, X. Chatzistavrou, K. Paraskevopoulos, R. Conradt, I. Thompson, and A.R. Boccaccini. Sintering and crystallisation of 45S5 Bioglass® powder. Journal of the European Ceramic Society. 29 (2009) pp.3299-3306.

[64] O.P. Filho, G.P. LaTorre, ND L.L. Hench. Effect of crystallization on apatite-layer formation of bioactive glass 45S5. Journal of Biomedical Materials Research. 30 (1996) pp.509-14.

[65] P. Li, F. Zhang, and T. Kokubo. The effect of residual glassy phase in a bioactive glassceramic on the formation of its surface apatite layer *in vitro*. Journal of Materials Science: Materials in Medicine. 3 (1992) pp.452-6.

[66] V. Cannillo, and A. Sola. Potassium-based composition for a bioactive glass. Ceramics International. 35 (2009) pp.3389-3393.

[67] D. Bellucci, V. Cannillo, and A. Sola. Low Temperature Sintering of Innovative Bioactive Glasses. Journal of the American Ceramic Society.
95 (2012) pp.1313-1319.

[68] D. Bellucci, V. Cannillo, and A. Sola. Calcium and potassium addition to facilitate the

sintering of bioactive glasses. Materials Letters. 65 (2011) pp.1825-1827.

[69] A. Sola, D. Bellucci, M.G. Raucci, S. Zeppetelli, L. Ambrosio, and V. Cannillo. Heat treatment of Na2O-CaO-P2O5-SiO2 bioactive glasses: Densification processes and postsintering bioactivity. Journal of Biomedical Materials Research Part A. 100A (2012) pp.305-322.

[70] R. Xin, Q. Zhang, and J. Gao. Identification of the wollastonite phase in sintered 45S5 bioglass and its effect on *in vitro* bioactivity. Journal of Non-Crystalline Solids. 356 (2010) pp.1180-1184.

[71] T. Nakamura, T. Yamamuro, S. Higashi, T. Kokubo and S. Itoo. A new glass ceramic for bone replacement: evaluation of its bonding to bone tissue. Journal of Biomedical Materials Research. 19 (1985) pp.685-698.

[72] K. Ohura, M. Ikenaga, T. Nakamura, T. Yamamuro, Y. Ebisawa, T. Kokubo, Y. Kotoura, and M. Oka. A heat-generating bioactive glass-ceramic for hyperthermia. Journal of Applied Biomaterials. 2 (1991) pp.153-159

[73] T. Kokubo, S. Ito, M. Shigematsu, S. Sakka, and T. Yamamuro. Mechanical properties of a new type of apatite-containing glass-ceramic for prosthetic application. Journal of Materials Science. 20 (1985) pp.2001-2004.

[74] J.-A. Epinette and M. T. Manley. Fifteen years of clinical experience with hydroxyapatite coatings in joint arthroplasty. 2003, Paris, Springer Editions.

[75] G. Iezzi, A. Scarano, G. Petrone, and A. Piattelli. Two human hydroxyapatite-coated dental implants retrieved after a 14-year loading period: a histologic and histomorphometric case report. Journal of Periodontology. 78 (2007) pp.940-947.

[76] J.M. Fernández-Pradas, P. Serra, J.L. Morenza, and P.N. De Aza. Pulsed laser deposition of pseudowollastonite coatings. Biomaterials. 23 (2002) pp.2057-2061.

[77] C. Vitale-Brovarone, F. Baino, F. Tallia, C. Gervasio, and E. Verné. Bioactive glass-derived trabecular coating: a smart solution for enhancing osteointegration of prosthetic elements. Journal of Materials Science: Materials in Medicine. 23 (2012) 2369-2380.

[78] Y.C. Tsui, C. Doyle, T.W. Clyne. Plasma sprayed hydroxyapatite coatings on titanium substrates. Part 1: Mechanical properties and residual stress levels. Biomaterials. 19 (1998) pp.2015-2029.

[79] M. Rouahi, E. Champion, P. Hardouin, and K. Anselme. Quantitative kinetic analysis of gene expression during human osteoblastic adhesion on orthopaedic materials. Biomaterials, 27 (2006) pp.2829-2844.

[80] M.B. Schaffler, and D.B. Burr. Stiffness of compact bone: Effects of porosity and density. Journal of Biomechanics. 21 (1988) pp.13-16.

[81] A.J. Tonino, M. Thèrin, and C. Doyle. Hydroxyapatite-coated femoral stems. The Journal

of Bone & Joint Surgery. 81-B (1999) pp.148-54.

[82] D.D. Deligianni, N.D. Katsala, P.G. Koutsoukos, and Y. F. Missirlis. Effect of surface roughness of hydroxyapatite on human bone marrow cell adhesion, proliferation, differentiation and detachment strength Biomaterials. 22 (2001) pp.87-96

[83] A.K. Lynn, and D.L. DuQuesnay. Hydroxyapatite-coated Ti-6Al-4V: Part 1: the effect of coating thickness on mechanical fatigue behaviour. Biomaterials. 23 (2002) pp.1937-1946.

[84] C.Y. Yang, B.C. Wang, T.M. Lee, E. Chang, and G.L. Chang. Intramedullary implant of plasma-sprayed hydroxyapatite coating: An interface study. Journal of Biomedical Materials Research. 36 (1997) pp.39-48.

[85] J.P. Borrajo, P. González, S. Liste, J. Serra, S. Chiussi, B. León, and M. Pérez-Amor. The role of the thickness and the substrate on the *in vitro*bioactivity of silica-basedglasscoatings. Materials Science and Engineering: C. 25 (2005) pp.187-193.

[86] R.J. Furlong, and J.F. Osborn. Fixation of hip prostheses by hydroxyapatite ceramic coatings. The Journal of Bone and Joint Surgery. 73-B (1991) pp.741-745.

[87] B. Sandén, C. Olerud, M. Petrén-Mallmin, and S. Larsson. Hydroxyapatite coating improves fixation of pedicle screws A CLINICAL STUDY. The Journal of Bone and Joint Surgery. 84-B (2002) pp.387-391.

[88] S.S. Rajaratnam, C. Jack, A. Tavakkolizadeh, M.D. George, R.J. Fletcher, M. Hankins, and J.A. Shepperd. Long-term results of a hydroxyapatite-coated femoral component in total hip replacement: a 15- to 21-year follow-up study. The Journal of Bone and Joint Surgery. 90-B (2008) pp.27-30.

[89] J.T Melton, R. Mayahi, S.E. Baxter, M. Facek, and C. Glezos. Long-term outcome in an uncemented, hydroxyapatite-coated total knee replacement: a 15- to 18-year survivorship analysis. The Journal of Bone and Joint Surgery. 94-B (2012) pp.1067-1070.

[90] T.K. Pal, and S. Pal. Long term clinical evaluation of Ha-coated titanium dental implant for single tooth. Engineering in Medicine and Biology Society, 1995 and 14th Conference of the Biomedical Engineering Society of India. An International Meeting, Proceedings of the First Regional Conference. IEEE. pp.3/71-3/72.

[91] A. Simunek, D. Kopecka, M. Cierny, and I. Krulichova. A six-year study of hydroxyapatite-coated root-form dental implants. West Indian Medical Journal. 54 (2005) pp.393-397.

[92] M. Vilotijević, P. Marković, S. Zec, S. Marinković, and V. Jokanović. Hydroxyapatite coatings prepared by a high power laminar plasma jet. Journal of Materials Processing Technology. 211 (2011) pp.996-1004.

[93] S. Yugeswaran, C.P. Yoganand, A. Kobayashi, K.M. Paraskevopoulos, and B. Subramanian. Mechanical properties, electrochemical corrosion and in-vitro bioactivity of yttria stabilized zirconia reinforced hydroxyapatite coatings prepared by gas tunnel type

plasma spraying. Journal of the Mechanical Behavior of Biomedical Materials. 9 (2012) pp.22-33.

[94] I. Demnati, M. Parco, D. Grossin, I. Fagoaga, C. Drouet, G. Barykin, C. Combes, I. Braceras, S. Goncalves, and C. Rey. Hydroxyapatitecoating on titanium by a low energy plasma spraying mini-gun. Surface and Coatings Technology. 206 (2012) pp.2346-2353.

[95] H. Podlesak, L. Pawłowski, R. d'Haese, J. Laureyns, T. Lampke, and S. Bellayer. Advanced Microstructural Study of Suspension Plasma Sprayed Hydroxyapatite Coatings. Journal of Thermal Spray Technology. 19 (2010) pp.657-664.

[96] R. d'Haese, L. Pawłowski, M. Bigan, R. Jaworski, and M. Martel. Phase evolution of hydroxapatite coatings suspension plasma sprayed using variable parameters in simulated body fluid. Surface and Coatings Technology. 204 (2010) pp.1236-1246.

[97] Y. Lu, Y. Song, R. Zhu, M. Li and T. Lei. Factors influencing phase compositions and structure of plasma sprayed hydroxyapatite coatings during heat treatment. Applied Surface Science. 206 (2003) pp.345-354.

[98] Y.-C. Yang. Influence of residual stress on bonding strength of the plasma-sprayed hydroxyapatite coating after the vacuum heat treatment. Surface and Coatings Technology. 201 (2007) pp.7187-7193.

[99] S. Dyshlovenko, C. Pierlot, L. Pawłowski, R. Tomaszek, and P. Chagnon. Experimental design of plasma spraying and laser treatment of hydroxyapatite coatings. Surface and Coatings Technology. 201 (2006) pp.2054-2060.

[100] S. Dyshlovenko, L. Pawłowski, I. Smurov, and V. Veiko. Pulsed laser modification of plasma-sprayed coatings: Experimental processing of hydroxyapatite and numerical simulation. Surface and Coatings Technology. 201 (2006) pp.2248-2255.

[101] Y. Cao, J. Weng, J. Chen, J. Feng, Z. Yang, and X. Zhang. Water vapour-treated hydroxyapatite coatings after plasma spraying and their characteristics. Biomaterials. 17 (1996) pp.419-424.

[102] S.W.K. Kweh, K.A. Khor, and P. Cheang. An *in vitro* investigation of plasma sprayed hydroxyapatite (HA) coatings produced with flame-spheroidized feedstock. Biomaterials. 23 (2002) pp.775-785.

[103] V. Cannillo, L. Lusvarghi, F. Pierli, and A. Sola. In-vitro behaviour of titania-hydroxyapatite functionally graded coatings. Advances in Applied Ceramics. 107 (2008) pp.259-267.

[104] K.A. Khor, C.S. Yip, and P. Cheang. Post-spray hot isostatic pressing of plasma sprayed Ti-6Al-4V/hydroxyapatite composite coatings. Journal of Materials Processing Technology. 71 (1997) pp.280-287.

[105] C.H. Quek, K.A. Khor, and P. Cheang. Influence of processing parameters in the plasma spraying of hydroxyapatite/Ti-6Al-4V composite coatings. Journal of Materials Processing

Technology. 89-90 (1999) pp.550-555.

[106] Z.L. Dong, K.A. Khor, C.H. Quek, T.J. White, and P. Cheang. TEM and STEM analysis on heat-treated and *in vitro* plasma-sprayed hydroxyapatite/Ti-6Al-4V composite coatings. Biomaterials. 24 (2003) pp.97-105.

[107] V.J.P Lim, K.A. Khor, L. Fu, P. Cheang. Hydroxyapatite-zirconia composite coatings via the plasma spraying process. Journal of Materials Processing Technology. 89-90 (1999) pp.491-496.

[108] F.L.S Carvalho, C.S. Borges, J.R.T. Branco, and M.M. Pereira. Structural analysis of hydroxyapatite/bioactive glass composite coatings obtained by plasma spray processing. Journal of Non-Crystalline Solids. 247 (1999) pp.64-68.

[109] Y.P. Lu, M.S. Li, S.T. Li, Z.G. Wang, and R.F. Zhu. Plasma-sprayed hydroxyapatite+titania composite bond coat for hydroxyapatite coating on titanium substrate. Biomaterials. 25 (2004) pp.4393-4403

[110] H. Kurzweg, R. B. Heimann, T. Troczynski, and M. L. Wayman. Development of plasma-sprayed bioceramic coatings with bond coats based on titania and zirconia. Biomaterials. 19 (1998) pp.1507-1511.

[111] K.A. Khor, Y.W. Gu, C.H. Quek, and P. Cheang. Plasma spraying of functionally graded hydroxyapatite/Ti-6Al-4V coatings. Surface and Coatings Technology. 168 (2003) pp.195-201.

[112] V. Cannillo, L. Lusvarghi, and A. Sola. Production and characterization of plasma-sprayed TiO2-hydroxyapatite functionally graded coatings. Journal of the European Ceramic Society. 28 (2008) pp.2161-2169.

[113] J.A. Davidson, R.A. Poggie, and A.K. Mishra. Abrasive Wear of Ceramic, Metal, and UHMWPE Bearing Surfaces from Third-Body Bone, PMMA Bone Cement, and Titanium Debris. Bio-Medical Materials and Engineering. 4 (1994) pp.213-229.

[114] J.A. Alonso-Barrio, S. Sánchez-Herraez, O. Fernández-Hernández, J. Betegón-Nicolás, J.J. González-Fernández, and A. López-Sastre. Bioglass-coated femoral stem. The Journal of Bone & Joint Surgery. 86-B:*SUpp.II* (2004) pp.138.

[115] C. Gabbi, A. Cacchioli, B. Locardi, and E. Guadagnino. Bioactive glass coating: physicochemical aspects and biological findings. Biomaterials. 16 (1995) pp.512-520.

[116] G. Goller. The effect of bond coat on mechanical properties of plasma sprayed bioglass-titanium coatings. Ceramic International. 30 (2004) pp.351-355.

[117] T.M. Lee, E.Chang, B.C. Wang, and C.Y. Yang. Characteristics of plasmasprayed bioactive glass coatings on Ti-6A1-4V alloy: an *in vitro* study. Surface and Coatings Technology. 79 (1996) pp.170-177.

[118] J.A. Helsen, J. Proost, J. Schrooten, G. Timmermans, E. Brauns, and J. Vanderstraeten.

Glasses and bioglasses: synthesis and coatings. Journal of the European Ceramic Society. 17 (1997) pp.147-152.

[119] E. Verne`, M. Ferraris, A. Ventrella, L. Paracchini, and A. Krajewski. Sintering and plasma spray deposition of bioactive glass-matrix composite for medical applications. Journal of the European Ceramic Society. 18 (1998) pp.363-372.

[120] J. Schrooten, H. van Oosterwyck, J. Vander Sloten, and J.A. Helsen. Adhesion of new bioactive glass coating. Journal of Biomedical Materials Research. 44 (1999) pp.243-252.

[121] J. Schrooten and J.A. Helsen. Adhesion of bioactive glass coating to Ti6Al4V oral implant. Biomaterials. 21 (2000) pp.1461-1469.

[122] D. Bellucci, G. Bolelli, V. Cannillo, R. Gadow, A. Killinger, L. Lusvarghi, A. Sola, and N. Stiegler. High velocity suspension flame sprayed (HVSFS) potassium-based bioactive glass coatings with and without TiO2 bond coat. Surface and Coatings Technology. 206 (2012) pp.3857-3868.

[123] G. Bolelli, V. Cannillo, R. Gadow, A. Killinger, L. Lusvarghi, A. Sola and N. Stiegler. Microstructure and in-vitro behavior of a novel high velocity suspension flame sprayed (HVSFS) bioactive glass coating. Surface and Coatings Technology. 205 (2010) pp.1145-1149

[124] G. Bolelli, V. Cannillo, R. Gadow, A. Killinger, L. Lusvarghi, and J. Rauch. Microstructural and *in vitro* characterisation of high velocity suspension flame sprayed (HVSFS) bioactive glass coatings. Journal of the European Ceramic Society. 29 (2009) pp.2249-2257.

[125] Y. Xiao, L. Song, X. Liu, Y. Huang, T. Huang, Y. Wu, J. Chen, and F. Wu . Nanostructured bioactive glass-ceramic coatings deposited by the liquid precursor plasma spraying process . Applied Surface Science. 257 (2011) pp.1898-1905.

[126] A. Sola, D. Bellucci, V. Cannillo and A. Cattini. Bioactive glass coatings: a review. Surface Engineering. 27 (2011) pp.560-572.

[127] A. Lopez-Sastre, J.M. Gonzalo-Orden, J.A.R. Altónaga, J.R. Altónaga and M. A. Orden. Coating titanium implants with bioglass and with hydroxyapatite. International Orthopaedics. 22 (1998) pp.380-383.

[128] J.H. Chern Lin, K.S. Chen, and C.P. Ju. Biocorrosion behavior of hydroxyapatite/bioactive glass plasma sprayed on Ti6Al4V. Materials Chemistry and Physics. 41 (1995) pp.282-289.

[129] J.H. Chern Lin, H.J. Lin, S.J. Ding, and C.P. Ju. Characterization of immersed hydroxyapatite-bioactive glass coatings in Hank’s solution. Materials Chemistry and Physics. 64 (2000) pp.229-240.

[130] D. Bellucci, G. Bolelli, V. Cannillo, A. Cattini, and A. Sola. In situ Raman spectroscopy investigation of bioactive glass reactivity: Simulated body fluid solution vs TRIS-buffered solution. Materials Characterization. (2011) pp.1021-1028.

[131] M.G.W. Lockyer, D. Holland, and R. Dupree. NMR investigation of the structure of some bioactive and related glasses. Journal of Non-Crystalline Solids. 188 (1995) pp.207-219.

[132] F. Bonino, A. Damin, V. Aina, M. Miola, E. Vernè, O. Bretcanu, S. Bordiga, A. Zecchina, and C. Morterra. In situ Raman study to monitor bioactive glasses reactivity. Journal of Raman Spectroscopy. 39 (2008) pp.260-264.

[133] D. Zhang, M. Hupa, H.T. Aro, and L. Hupa. Influence of fluid circulation on in vitro reactivity of bioactive glass particles. Materials Chemistry and Physics. 111 (2008) pp.497-502.

[134] D. Bellucci, V. Cannillo, A. Sola. A new potassium-based bioactive glass: sintering behaviour and possible applications for bioceramic scaffolds. Ceramic International. 37 (2011) pp.145-157.

[135] A. Antonakosa, E. Liarokapisa, and T. Leventouri. Micro-Raman and FTIR studies of synthetic and natural apatites. Biomaterials. 28 (2007) pp.3043–3054.

[136] C.C. Lin, L.C. Huang, and P. Shen. $Na_2CaSi_2O_6$–P_2O_5 based bioactive glasses. Part 1: elasticity and structure. Journal of Non-Crystalline Solids. 351 (2005) p.3195-3203.

[137] E.C. Ziemath, and M.A. Aegerter. Raman and infrared investigations of glass and glass-ceramics with composition 2Na2O 1CaO 3SiO2. Journal of Materials Research. 1 (1994) p.216-225.

[138] P. Gonzalez, J. Serra, S. Liste, S. Chiussi, B. Leon, and M. Perez-Amor. Raman spectroscopic study of bioactive silica based glasses. Journal of Non-Crystalline Solids. 320 (2003) pp.92-99.

[139] A. Awonusi, M.D. Morris, and M.M.J. Tecklenburg. Carbonate assignment and calibration in the Raman spectrum of apatite. Calcified Tissue International. 81 (2007) pp.46-52.

[140] H. Liu, H. Yazici, C. Ergun, T.J. Webster, H. Bermek. An in vitro evaluation of the Ca/P ratio for the cytocompatibility of nano-to-micron particulate calcium phosphates for bone regeneration. Acta Biomaterialia. 4 (2008) pp.1472-1479.

[141] A. Cattini, L. Łatka, D. Bellucci, G. Bolelli, A. Sola, L. Lusvarghi, L. Pawłowski, and V. Cannillo. Suspension plasma sprayed bioactive glass coatings: Effects of processing on microstructure, mechanical properties and *in-vitro* behaviour. Surface and Coatings Technology. 2012. In Press. DOI: 10.1016/j.surfcoat.2012.10.076

[142] Y.-P. Zeng, D.-l. Jiang, J.-P. Werner, and P. Greil. Fabrication of Al2O3–A/W bioglass bioactivity tapes by tape casting. Materials Letters. 57 (2002) pp.463-468.

[143] W.C. Oliver and G.M. Pharr. An improved technique for determining hardness and elastic modulus using load and displacement sensing indentation experiments. Journal of Materials Research. 6 (1992) pp.1564-1583.

[144] H. Arstila, L. Hupa, K.H. Karlsson, and M. Hupa. Influence of heat treatment on crystallization of bioactive glasses. Journal of Non-Crystalline Solids. 354 (2008) pp.722-728.

[145] K.A. Gross, and C.C. Berndt. Biomedical Application of Apatites. Reviews in Mineralogy and Geochemistry. 48 (2002) pp.631-672.

[146] X. Liu, C. Ding, and P.K. Chu. Mechanism of apatite formation on wollastonite coatings in simulated body fluids. Biomaterials. 25 (2004) pp.1755-1761.

[147] T. Kokubo, H.-M. Kim, and M. Kawashita. Novel bioactive materials with different mechanical properties. Biomaterials. 24 (2003) pp.2161-2175.

[148] D.K. Pattanayak. Apatite wollastonite–poly methyl methacrylate bio-composites. Materials Science and Engineering: C. 29 (2009) pp.1709-1714.

[149] E. Saiz, M. Goldman, J.M. Gomez-Vega, A.P. Tomsia, G.W. Marshall, and S.J. Marshall. In vitro behavior of silicate glass coatings on Ti6Al4V. Biomaterials. 23 (2002) pp.3749-3756.

[150] C. Vitale-Brovarone, E. Verné, and P. Appendino. Macroporous bioactive glass-ceramic scaffolds for tissue engineering. Journal of Materials Science: Materials in Medicine. 17 (2006) pp.1069-1078.

[151] S. Dyshlovenko, B. Pateyron, L. Pawłowski, and D. Murano. Surface and Coatings Technology. 179 (2004) pp.110-117.

[152] S. Dyshlovenko, L. Pawłowski, P. Roussel, D. Murano, and A. Le Maguer. Relationship between plasma spray operational parameters and microstructure of hydroxyapatite coatings and powder particles sprayed into water. Surface and Coatings Technology. 200 (2006) pp.3845-3855.

[153] Z. Mohammadi, A.A. Ziaei-Moayyed, and A. Sheikh-Mehdi Mesgar. Adhesive and cohesive propieties by indentation method of plasma-sprayed hydroxyapatite. Applied Surface Science. 253 (2007) pp.4960-4965.

[154] H Li, B.S Ng, K.A Khor, P Cheang, and T.W Clyne. Raman spectroscopy determination of phases within thermal sprayed hydroxyapatite splats and subsequent *in vitro* dissolution examination. Acta Materialia. 52 (2004) pp.445-453.

[155] B. Pateyron, N. Calve, and L. Pawłowski. Influence of water and ethanol on transport properties of the jets used in suspension plasma spraying.Surface and Coatings Technology. 2012. In Press. DOI: 10.1016/j.surfcoat.2012.10.010.

[156] L. Łatka, L. Pawłowski, D. Chicot, C. Pierlot, F. Petit. Mechanical properties of suspension plasma sprayed hydroxyapatite coatings submitted to simulated body fluid. Surface & Coatings Technology. 205 (2010) pp.954-960.

[157] A. Vallés Lluch, G. Gallego Ferrera, and M. Monleón Pradas. Biomimetic apatite

coating on P(EMA-co-HEA)/SiO2 hybrid nanocomposites. Polymer. 50 (2009) pp.2874-2884.

List of Andrea Cattini's Publications

Journal Publications

1. D. Bellucci, V. Cannillo, **A. Cattini** and A. Sola. A New Generation of Scaffolds for Bone Tissue Engineering. Industrial Ceramics. Vol. 31 (2011), 1: 1-4. ISSN: 0272-8842.

2. D. Bellucci, G. Bolelli, V. Cannillo, **A. Cattini** and A. Sola. In situ Raman spectroscopy investigation of bioactive glass reactivity: Simulated body fluid solution vs TRIS-buffered solution. Materials Characterization, Vol. 62 (2011), 10: 1021-1028. DOI: 10.1016/j.matchar.2011.07.008. ISSN: 1044-5803

3. D. Bellucci, V. Cannillo, **A. Cattini** and A. Sola. Una nuova tipologia di scaffold per ingegneria tissutale ossea. C+CA (Ceramurgia + Ceramica acta) XXXXI (2011), 2: 141-145. ISSN: 1970-0393.

4. A. Sola, D. Bellucci, V. Cannillo, **A. Cattini**. Bioactive glass coatings: a review. Surface Engineering, Vol. 27 (2011) 8: 560-572. DOI: 10.1179/1743294410Y.0000000008. ISSN 0267-0844

5. L. Łatka, **A. Cattini**, L. Pawłowski, S. Valette, B. Pateyron, J-P. Lecompte, R. Kumar and A. Denoirjean. Thermal diffusivity and conductivity of yttria stabilized zirconia coatings obtained by suspension plasma spraying. Surface and Coatings Technology, Vol. 208 (2012) 15: 87-91. DOI: 10.1016/j.surfcoat.2012.08.014. ISSN: 0257-8972.

6. L. Łatka, D. Chicot, **A. Cattini**, L. Pawłowski and A. Ambroziak. Modeling of elastic modulus and hardness determination by indentation of porous Yttria Stabilized Zirconia coatings. Surface and Coatings Technology. 2012. IN PRESS. DOI: 10.1016/j.surfcoat.2012.07.025.

7. P. Carpio, E. Rayón, L. Pawłowski, **A. Cattini**, R. Benavente, E. Bannier, M.D. Salvador and E. Sánchez. Microstructure and Indentation Mechanical Properties of YSZ Nanostructured Coatings Obtained By Suspension Plasma Spraying. Surface and Coatings Technology. 2012. IN PRESS. DOI: 10.1016/j.surfcoat.2012.09.047.

8. **A. Cattini**, L. Łatka, D. Bellucci, G. Bolelli, A. Sola, L. Lusvarghi, L. Pawłowski, and V. Cannillo. Suspension plasma sprayed bioactive glass coatings: Effects of processing on microstructure, mechanical properties and in-vitro behaviour. Surface and Coatings Technology. 2012. IN PRESS. DOI: 10.1016/j.surfcoat.2012.10.076.

9. L. Łatka, **A. Cattini**, D. Chicot, L. Pawłowski, S. Kozerski, F. Petit, A. Denoirjean. Mechanical properties of yttria and ceria stabilized zirconia coatings obtained by suspension plasma spraying. Journal of Thermal Spray Technology. 2012. IN PRESS. DOI: 10.1007/s11666-012-9874-7.

Conference

1. D. Bellucci, V. Cannillo, **A. Cattini**, A. Sola, Shell Scaffolds for bone regeneration and repair. International Conferences on Modern Materials and Technologies, CIMTEC, 5th Forum on New Materials, Montecatini Terme (Italy), June 13-18, 2010.

   Proceeding: "A New Generation of Scaffolds for Bone Tissue Engineering". Advances in Science and Technology, 2010, Volume 76: 5th FORUM ON NEW MATERIALS PART E, pp. 48-54. Ed. by P. Vincenzini, J.A. Jansen, K. Ishihara. ISBN: 3-908158-59-1

2. A. Sola, D. Bellucci, V. Cannillo, and **A. Cattini**, Bioactive titania-hydroxyapatite functionally graded coatings: production, post-processing and characterization. 23rd European Conference on Biomaterials, the annual conference of the European Society for Biomaterials, ESB 2010, Tampere (Finland), September 11-15, 2010.

3. L. Łatka, D. Chicot, S. Kozerski, L. Pawłowski, and **A. Cattini**. Mechanical properties of suspension plasma sprayed yttria stabilized zirconia coatings. 5th Rencontres Internationales sur la Projection Thermique, 5RIPT, Limoges (France), December 7-9, 2011.

4. **A. Cattini**, L. Pawłowski, V. Cannillo, L. Łatka, A. Sola, D. Bellucci, L. Lusvarghi. Suspension plasma sprayed bioactive glass coatings: effect of processing on microstructure, mechanical properties and in-vitro behavior. 5th Rencontres Internationales sur la Projection Thermique, 5RIPT, Limoges (France), December 7-9, 2011.

5. L. Łatka, L. Pawłowski, S. Valette, B. Pateyron, J.P. Lecompte, A. Denoirjean, **A. Cattini**, and R. Kumar. Thermal Diffusivity and Conductivity of Yttria Stabilized Zirconia Coatings Obtained by Suspension Plasma Spraying. International Thermal Spray Conference 2012, ITSC 2012, Houston, Texas (USA), May 21-24, 2012.

   Proceeding: Thermal Spray 2012, Proceedings from the International Thermal Spray Conference (ASM International). 2012. pages: 800-804

6. L. Łatka, L. Pawłowski, **A. Cattini**, A. Denoirjean, D. Chicot, S. Kozerski, F. Petit. Mechanical Properties of Yttria and Ceria Stabilized Zirconia Coatings Obtained by Suspension Plasma Spraying. International Thermal Spray Conference 2012, ITSC 2012, Houston, Texas (USA). May 21-24, 2012.

   Proceeding: Thermal Spray 2012, Proceedings from the International Thermal Spray Conference (ASM International). 2012. pages: 805-809

7. Graded hydroxyapatite/ bioglass coatings. **A. Cattini**, V. Cannillo, and L. Pawłowski. Journée Matériaux du futur. Limoges (France), October 4, 2012.

Work in progress (to be submitted as journal publication)

1. A. Cattini *et al*. Production and *in vitro* characterization of hydroxyapatite coatings with and without a Suspension Plasma Sprayed bioactive glass topcoat

2. A. Cattini *et al*. Suspension Plasma Sprayed hydroxyapatite/bioactive glass composite coatings with different microstructures

3. A. Cattini *et al.* Production and characterization of a functionally graded coating hydroxyapatite/bioactive glass via Suspension Plasma Spray